Fall 1-1-2020

The Effect of Light And Dark Periods on the Growth of Chlorella Sorokiniana: Modeling & Experimentation

Farid F. Khoury
Cleveland State University

THE EFFECT OF LIGHT AND DARK PERIODS ON THE GROWTH OF CHLORELLA SOROKINIANA: MODELING & EXPERIMENTATION

FARID F. KHOURY

Bachelor of Science in Chemical Engineering

Cleveland State University

2019

submitted in partial fulfillment of requirements for the degree

MASTER OF SCIENCE IN CHEMICAL ENGINEERING

at the

CLEVELAND STATE UNIVERSITY

DECEMBER 2020

We hereby approve this thesis

for

FARID F. KHOURY

Candidate for the Master of Science in Chemical Engineering degree

for the Department of

Chemical and Biomedical Engineering

And

CLEVELAND STATE UNIVERSITY'S

College of Graduate Studies by

Thesis Chairperson, Dr. Joanne Belovich

Department of Chemical and Biomedical Engineering Date_____

Thesis Committee Member, Dr. Jorge Gatica

Department of Chemical and Biomedical Engineering Date_____

Thesis Committee Member, Dr. Chandra Kothapalli

Department of Chemical and Biomedical Engineering Date_____

Student's Date of Defense

September 11, 2020

DEDICATION

This thesis is dedicated to my grandfather,

Dr. Farid Khoury

The person who engraved in me the importance of education

and raised me to always strive for excellence.

If I have been able to reach higher, it is by standing on your shoulders

Until We Meet Again.

ACKNOWLEDGMENTS

I want to thank my mom Lina for all the sacrifices she has made for me to have a better future. From leaving everything behind and moving to a new country, to pushing me always to be better, and never letting me worry about a thing but planning my future. Everything is possible when you have a great family supporting you, and that is precisely what I have. There's no point in me listing what you have done for me. It will be much longer than this whole thesis. Let me just keep it simple, and just say that I'm fortunate that I was born a part of this family! To all my family: Farid and Rafat, Lina and Amir, Lama and Malek, Jamil, Michael, and Roula; Thank you! Additionally, I want to thank my girlfriend, Samantha, who somehow never gets tired of listening to me talk for hours about my research.

Dr. Joanne Belovich, also referred to, by my classmates, as Farid's CSU mom. There are no words to explain how appreciative I am for you. You are the most excellent teacher and advisor I have ever had and will ever have. I have learned so much from you such as how to think like an engineer and scientist, how to tackle problems, how to always strive for success, and more importantly how to be a down to earth person despite you being dean of engineering, department chair previously, and the most respected professor I have ever met. Your office door was always open for me, no matter how busy you were. You have always challenged me to do better. Your guidance has got me to where I am today. My excellence awards, leadership award, NSF fellowship, getting accepted into top schools, and much more can all be attributed to your constant support and excellent mentorship. Thank you for everything!

I want to thank my great mentors and thesis committee members Dr. Gatica and Dr. Kothapalli. I also want to thank Dr. Marvin Thrash, my academic advisor, for being a great mentor all these years at CSU. You were always there for me, boosted my confidence whenever it dropped and advised me for countless hours as I planned my future. Additionally, I want to thank all the other great professors of the Chemical Engineering Department: Dr. Tewari, Dr. Talu, Dr. Guma, Dr. Wirth, Dr. Holland, and Dr. Ao. Big thank you goes to the hidden soldiers of the ChemE Department Becky Laird and Darlene Montgomery. Finally, thank you to Cleveland State University as a whole, and all the friends that I have made along the way.

THE EFFECT OF LIGHT AND DARK PERIODS ON THE GROWTH OF CHLORELLA SOROKINIANA: MODELING & EXPERIMENTATION

FARID F. KHOURY

ABSTRACT

Microalgae are abundant unicellular photosynthetic organisms with more than 200,000 species. They are more efficient in harvesting solar energy than land-based plants with green microalgae having more than ten times higher biodiesel productivity than the next best land-based crop. Their ability to grow in harsh environments, non-agricultural lands, and make use of wastewater, and the diversity of the products that can be extracted from them, which include cosmetics, pharmaceuticals, food supplements, biofuels, and many others, gives them the potential to replace fossil fuels and revolutionize the biotech industry. In order to move onto large scale production, first, the growth rate of the cell culture must be increased, which requires screening of promising species, studying their growth kinetics, and selecting their most suitable environment. Second, microalgae use their internal energy reservoirs (lipid bodies) during dark periods; nighttime biomass loss must be prevented.

In this study, we analyzed the effect of light intensity on the growth of *Chlorella sorokiniana,* a promising species for biofuel production. We constructed a growth model that accurately predicts the growth response of the cell culture to varying irradiance conditions and photoperiods. We incorporated the concept of Monod kinetics into our model and quantified the effect of light intensity on biomass accumulation under light-limiting conditions. We determined that the empirically measured maximum growth rate

parameter has a value of 0.20 h^{-1} which is limited by the maximum photosynthetic rate. Additionally, we determined the Monod saturation constant to be 238 μmol s^{-1} m^{-2}.

We found that biomass loss rate due to respiration and other metabolic activities peaked during the day ($8.7x10^{-3}$ h^{-1}), and was constant during nighttime ($1.8x10^{-3}$ h^{-1}). We determined that 5% of the biomass gained during the 16-hour day period was lost during the following 8-hour dark period, which lead to a 16% lower biomass yield when compared to a continuously illuminated culture after nine days of cultivation at a constant temperature of 30°C in a well-mixed five-liter photobioreactor. Finally, we illustrated that illuminating the dark period with low-consumption red LEDs will prevent biomass loss and enhance cell replication.

TABLE OF CONTENT

PAGE

LIST OF TABLES

LIST OF FIGURES

CHAPTER I

INTRODUCTION

Fossil fuels are non-renewable energy reservoirs, including oil, coal, and natural gas, formed from dead plants and animals buried under layers of rocks for millions of years [1]. Fossil fuels have been the dominant source of energy in the economy. They have driven the industrial revolution, innovations, technological advancements, and economic development of our society [2]. Although fossil fuels continue to allow us to reach glorious achievements, burning them comes with disastrous consequences on the planet and all living species.

The Department of Energy (DOE) estimated that 75% of human-caused greenhouse gas (GHG) emissions are a result of burning fossil fuels for energy [1]. The solar energy absorbed on Earth's surface is radiated back as heat into outer space. GHGs are gasses that trap the heat from escaping the Earth's atmosphere [3]. Greenhouse gasses warm the Earth's surface by acting like a blanket and slowing the rate of energy escape to space [4]. Eight of the ten warmest years on record have been in the past 20 years. Studies show that the increase in the planet's temperature will lead to extreme weather conditions such as more frequent intense hurricanes and heat waves, melting of ice, and a rise in sea level putting

coastal cities at risk of regular flooding [5]. In 2018, greenhouse gas emissions were made up of 81% carbon dioxide, 10% methane, 7% nitrous oxide, and the rest include water vapor and other gasses [6]. Oceans absorb about one-third of all carbon dioxide emissions making the water more acidic. The changes in the acidity of the oceans can lead to loss of coral reefs, destruction of marine biodiversity, and life disturbance both on Earth and in the sea [7].

Additionally, pollution due to the burning of fossil fuel has catastrophic effects on human lives. Breathing problems, cancer, heart attacks, and many other health issues are linked to air and water pollution [8]. Unfortunately, because of the growing demand for energy, especially with new growing economies such as India and China, greenhouse emissions will continue to rise and lead to environmental damage [7]. The emitted gasses stay in the atmosphere long enough to be well mixed. Therefore, regardless of the emission source, the effect will be felt all over the world [6]. For that reason, global efforts to cut down on the use of fossil fuels and move onto renewable, carbon-neutral energy sources is vital.

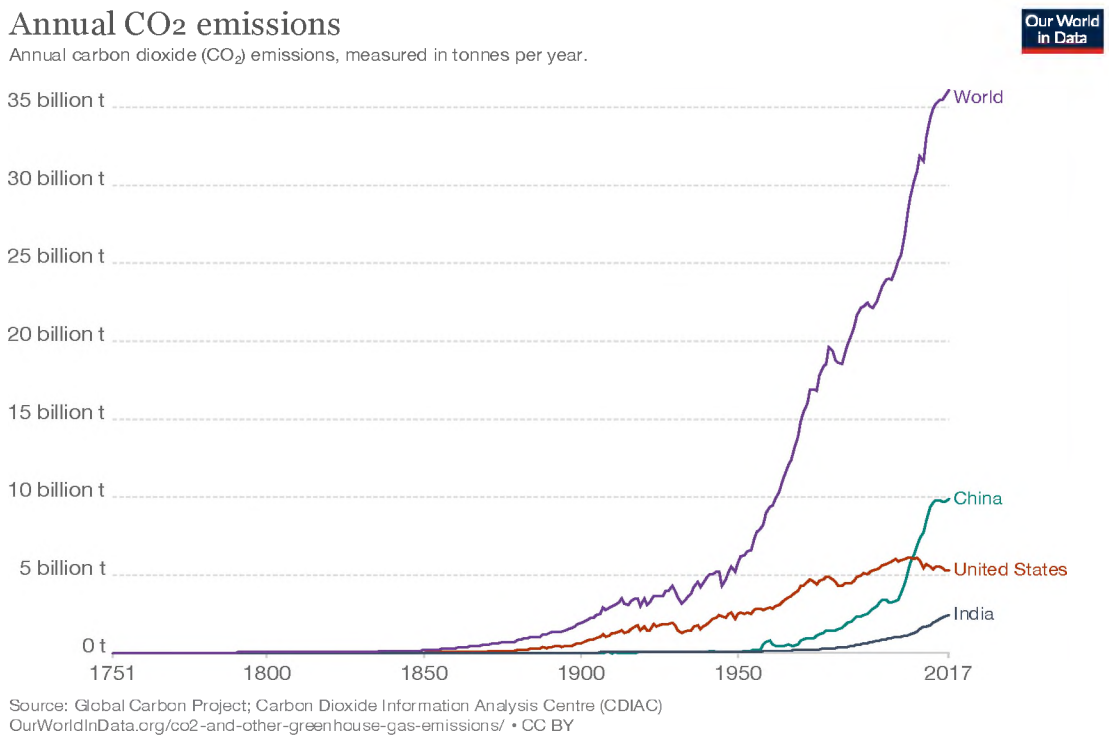

Figure 1-1: Annual carbon dioxide emissions. The graph shows a continued increase in greenhouse emissions **[2]**.

Clean energy can be harvested from renewable energy resources such as solar, wind, geothermal, hydroelectric, and biomass [8]. Energy from clean, renewable resources can have many advantages. First, it will reduce GHG emissions, which could prevent, or at least mitigate, consequences of climate change such as extreme weather conditions, drought, and coastal flooding [8] [9]. Second, better quality air and water, due to reduced pollutants emission, can improve public health, preserve natural biosystems, and save thousands of species from extinction [8]. Third, renewable energy will allow for far more stable energy prices, and it will ensure the nation's energy security by reducing the need for imported fuels [8] [9]. Finally, renewable energy induces economic growth and creates hundreds of thousands of new jobs. For instance, in 2016, the entire coal industry employed 160,000 employees, while the solar sector of the renewable energy employed over 260,000 people alone [8].

Biofuels have generated more electricity than solar or wind up until now [10]. Besides the quantity of the generated power, biofuels have a couple of advantages over solar or wind. First, they are a more reliable source, as storage of the harvested energy from solar or wind is still a significant issue. Second, biofuels can be used with already existing engines and require little to no modification [10]. A major limitation to the first generation of biofuels is that they are derived from biomass that is also a food source. The second generation of biofuels, although they come from non-food biomass sources, competes with food crops for land use [11]. The limitations of the first two generations have led to spot the light on an alternative; microalgae derived fuels, also known as third-generation biofuels.

Microalgae are abundant unicellular photosynthetic organisms with more than 200,000 species. They are more efficient in harvesting solar energy than land-based plants due to their simple structure and being submerged in water where carbon dioxide and other nutrients are readily available [12]. Microalgae can be grown in harsh environments, non-agricultural lands, and make use of saline water, wastewater, and sewage [12]. Additionally, green microalgae have more than ten times higher biodiesel productivity than the next best crop [7]. Microalgae-derived products include cosmetics, pharmaceuticals, food supplements, biofuels, and many others. The diversity of the products extracted from microalgae gives them the potential to replace fossil fuels and revolutionize the biotech industry [7].

Current challenges with the third generation of biofuels must be overcome to reach economic feasibility. In order to move onto large scale production, first, the growth rate of the cell culture must be increased, as well as that of lipid productivity, which requires

screening of promising species, studying their growth kinetics, and selecting their most suitable environment [13]. Second, microalgae use their internal energy reservoirs (lipid bodies) during dark periods; thus, nighttime biomass loss must be prevented [14]. Third, the dewatering of microalgae must be efficient and economical [13]. Intensive research in all areas is undergoing. Light intensity and light cycle are the most critical parameters in photosynthesis. Therefore, they are also the most critical parameters for microalgae growth. The data available in the literature is far from complete; for that reason, we seek to understand *Chlorella sorokiniana's* ability to grow, replicate, and accumulate lipids under varying irradiance conditions and compare it to other promising species for biofuel production. In this study, we analyze the effect of light intensity on the growth of *Chlorella sorokiniana,* a promising species for biofuel production. We determine the growth kinetics using mathematical models such as the logistic model and the Monod equation. We study the effect of varying light-dark periods on the overall productivity, analyze the impact of the dark period on biomass loss, and learn whether prolonged cultivation will yield the same biomass and cell concentrations as per continuously illuminated cultures without intervention. Finally, we evaluate the results of nighttime supplementation with low-consumption artificial red LEDs on preventing nighttime biomass loss and enhancing productivity. The results of this research illustrate the effect of the light and dark periods on the growth of *C. sorokiniana*. The models that were constructed and validated in this work are useful for designing cultivation systems that utilize the most of incident light, which in turn maximizes biomass productivity.

CHAPTER II

BACKGROUND

2.1 The Microalgae Cell

"We could replace up to 17 percent of the oil we import for transportation with this fuel that we can grow right here in the United States. That means greater energy security, more jobs, and a stronger economy" - President Obama on algae-derived fuels based on a study by the Department of Energy

2.1.1 What are green microalgae?

Green microalgae are abundant eukaryotic photosynthetic unicellular organisms that can fix carbon dioxide into carbohydrates [12]. Microalgae have enormous diversity, with estimates of 200,000 to more than one million species. AlgaeBase, a global algal database of taxonomic, nomenclatural, and distributional information, had processed more than 33,000 of these species as of June 2012 [15]. Microalgae have high growth rates and can grow in harsh environments due to their unicellular structure and their ability to shift from one metabolic pathway to another in response to the environmental conditions. Microalgae can grow photoautotrophically, where food is primarily produced through photosynthesis, and heterotrophically, where algae depend on organic compounds such as sugars.

Microalgae can execute both metabolic pathways simultaneously, which is known as mixotrophic growth [16]. They have two categories of nutrients: 1) micronutrients, which are elements needed in trace amounts, such as calcium, magnesium, sodium, potassium, iron, and others, all present as salts; and 2) macronutrients that are required in higher concentrations, such as nitrogen and phosphorus. Sufficient light and moderate temperatures are also required [12]. The rapid growth of microalgal cultures, their high tolerance to extreme environmental conditions, and the variety of high-value biological derivatives give rise to their potential to revolutionize the biotech industry. Some of the microalgae-derived products include biofuels, cosmetics, pharmaceuticals, health supplements, and food additives [7]. The lipids produced in algae can be extracted and converted to biodiesel and other fuels. Microalgae with low oil content can have more than ten times higher biodiesel productivity compared to the next best renewable feedstock, and up to 25 higher yields when using high oil content microalgae. Other advantages of using microalgae as a feedstock for biofuel include the removal of CO_2 from the atmosphere and the reduction of the nutrient load from wastewater [7].

2.1.2 Microalgae Strain Selection: Why Chlorella sorokiniana?

The different microalgae species and strains vary in terms of productivity, tolerance to harsh conditions, and the ability to accumulate different high-value compounds. For that reason, the first step should be to find a microalgae species that can handle the environmental settings in which it will be cultivated [17]. Regarding biofuel production, because of the enormous amounts needed, microalgae must be grown on a large scale. A major drawback, in large scale production, is most strains' inability to achieve high growth and high concentration due to biological contaminant, variations in temperature, and light's

inability to penetrate the entire thickness of the pond [16]. Therefore, resistance to predation, and salinity and temperature tolerance are essential in a strain being screened for biofuel production in addition to high biomass productivity and lipid content [12]. Two genera have been identified as major contenders for biofuel production: *Chlorella* and *Spirullina* [16]. Environmental conditions that favor high lipid content often result in lower biomass productivity, which yields a decrease in overall lipid productivity. Therefore, when screening microalgae for biofuel production, lipid productivity is a more critical selection parameter than lipid content or growth rate individually [18]. The NAABB, National Alliance For Advanced Biofuels and Bio-products, has identified *Chlorella sorokiniana (DOE 1412)* as a promising species for biofuel production [19]. It has a high tolerance for harsh conditions and has high lipid productivity, as shown in Figure 2-1. For that reason, we selected to study the effect of irradiance and other environmental conditions on the growth of *Chlorella sorokiniana*.

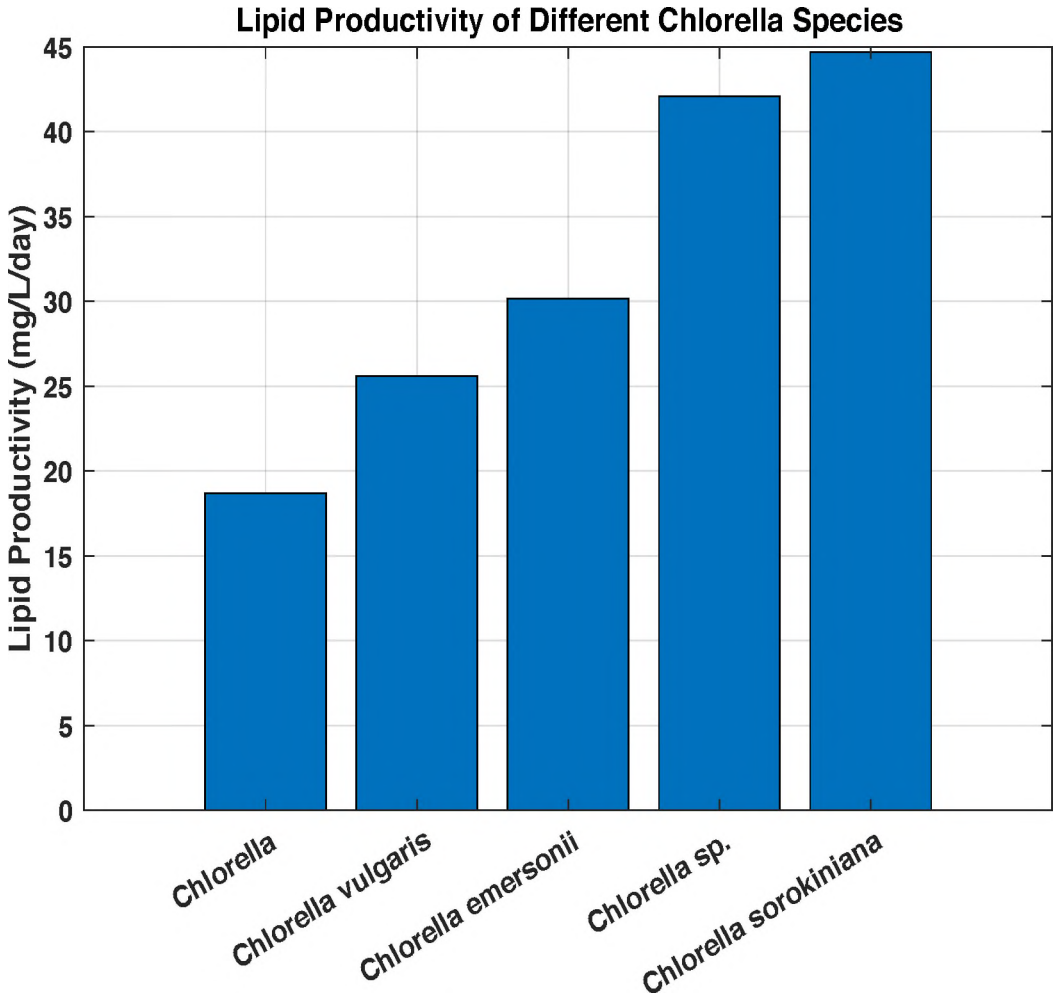

Figure 2-1: Lipid productivity, on average, of five different *Chlorella* species [7]. The figure illustrates the high lipid productivity of *Chlorella sorokiniana*. Lipid productivity data for *Chlorella Protothecoides*, about 1214 (mg/L/day), was omitted because the species can only be grown heterotrophically, which does not align with the scope of this project (effect of light on growth). The data available in the literature are far from complete and rigorous comparison across experiments carried out under different conditions is not possible. However, the collated information provides a framework for decision-making and a starting point for further investigation of species selection. **[18]**

Chlorella sorokiniana (DOE 1412) emerged as one of the most promising species for biofuel production with remarkable growth rates. The productivity of (DOE 1412) was estimated by a recent study to be almost double the productivity of the DOE's 2015 State of Technology annual cultivation productivity at 15 g m^{-2} day^{-1}. However, it is still short of the productivity needed for economic production at 25 g m^{-2} day^{-1} [20]. The study indicates the necessity for more research to reach the DOE's projected target of 2022.

2.2 Photosynthesis in Microalgae

"It's not love or money that makes the world go round, it's photosynthesis." - *Richmond*

All life on Earth is either directly or indirectly dependent on a single unique process known as photosynthesis. Oxygenic photosynthesis is the process by which photoautotrophs harvest light energy and utilize the harvested energy to produce complex organic molecules and oxygen [21]. Photoautotrophs (plants, algae, and cyanobacteria) are the only organisms capable of performing photosynthesis [22]. The process is divided into a light-dependent and light-independent reactions. In the overall process, carbon dioxide and water are converted into carbohydrates and oxygen [21]. The overall reaction is:

$$CO_2 + H_2O \xrightarrow{Light\ Energy} CH_2O + O_2$$

The products of photosynthesis, carbohydrate molecules, enter other metabolic pathways in the cell and are converted to amino acids, lipids, and sugars. Lipids can be harvested and converted to carbon-neutral fuels.

2.2.1 Light Absorption in Photosynthetic Pigments

Light is a critical parameter in microalgae cultivation for biofuels and other high-value products. To study and analyze the effect of irradiance on the growth of microalgae, we must understand the mechanism by which light energy is harvested in photoautotrophs and its role in catalyzing photosynthetic reactions. In the chloroplast, shown in Figure 2-2, small stacked disk-shaped membranes called thylakoids contain light-harvesting complexes (LHCs) [23]. The light-harvesting complexes are membrane proteins non-covalently bonded to chlorophylls and other light-absorbing pigments. The chemical structure of chlorophyll, shown in Figure 2-3, has an alternating single and double carbon-carbon bonds, which allow for light absorption by exciting the π-electrons [21].

Chlorophyll absorbs the energy of a red photon (600-700 nm), and one of its π-electrons gets promoted from a ground energy state S_0 to an excited state S_1. Chlorophyll molecules can also absorb energy from a blue photon (400-500 nm), and its π-electron jumps to an even higher energy state S_2. On a picosecond time scale, the electron in S_2 gets downgraded to S_1 due to energy loss as heat (molecular vibrations). The electrons in S_1 have less energy hence more stable. For the electron to return to the ground state S_0, the electron gives up its energy in one of three ways. First, electron return to S_0 by losing the energy as heat due to molecular vibrations. Second, it could lose energy by emission of a photon, also known as fluorescence. Third, if another chlorophyll molecule is oriented in a specific way and within 7 nm of the excited pigment, energy can be exchanged between the two molecules in a process called excitation energy transfer (EET) [21]. The absorbed energy is transferred from one chlorophyll molecule to another until it reaches the reaction center (RC) where the light-dependent reaction takes place, as shown in Figure 2-4.

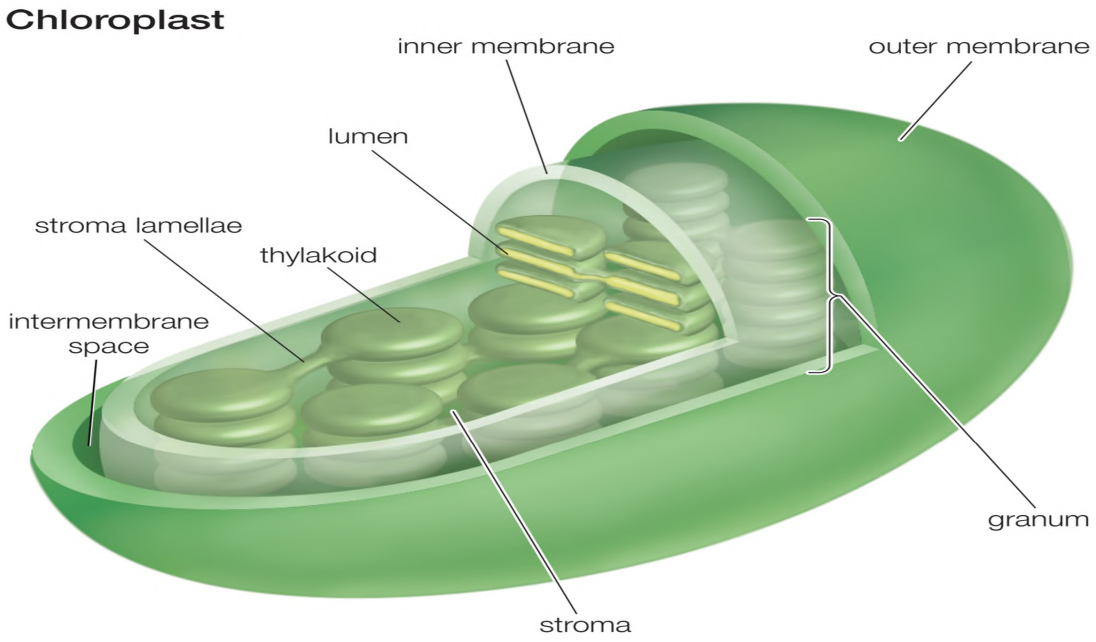

Figure 2-2: Chloroplast is an organelle in the cells of plants and green algae that is the site of photosynthesis **[23]**.

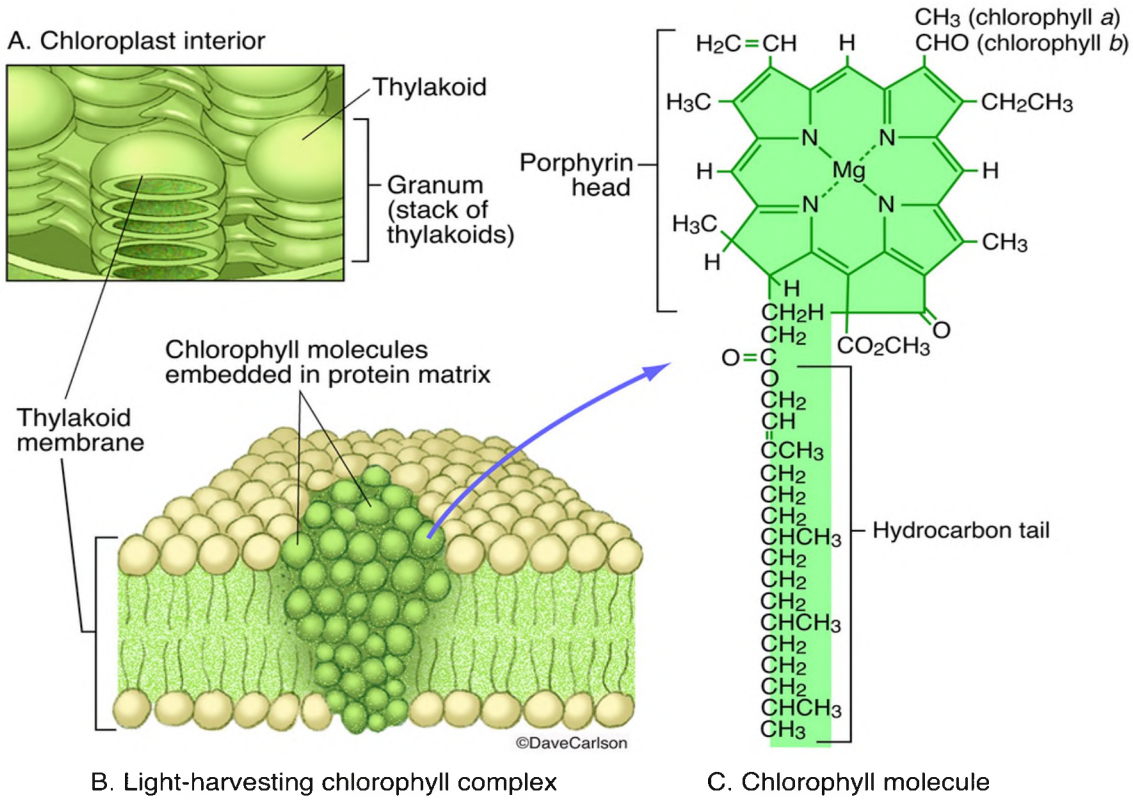

Figure 2-3: Chlorophylls are the primary light-harvesting pigments. Chlorophyll binds non-covalently to embedded membrane proteins forming the light-harvesting complexes (LHCs). The unique chemical structure of chlorophyll a and b, which features conjugate C-C double bonds, give rise to their ability to absorb light.

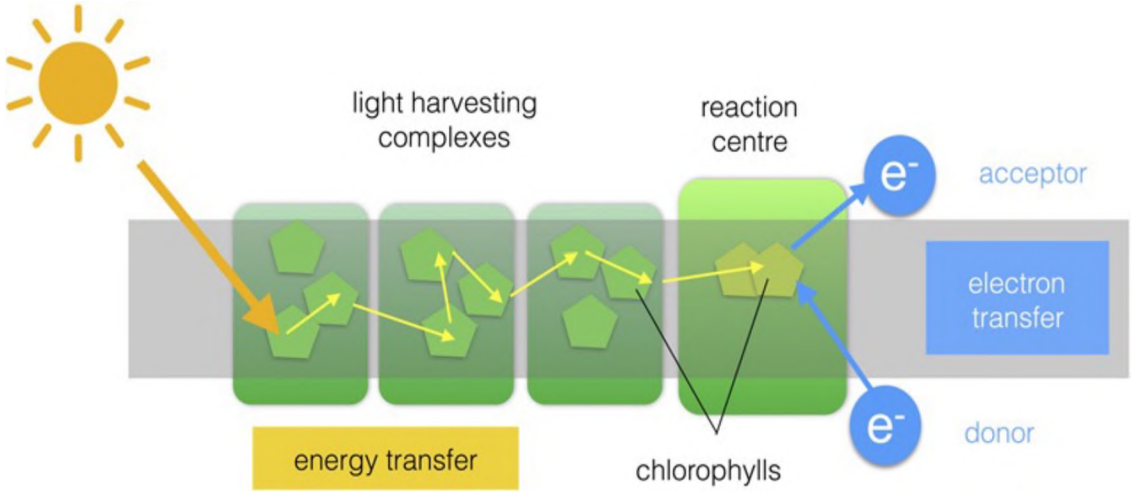

Figure 2-4: Chlorophylls absorb the energy of a blue or a red photon and excite one of their π-electrons. Excited pigment exchanges the energy with a nearby pigment in a process called excitation energy transfer (EET). The process is repeated until the energy reaches the reaction center (RC), where it catalyzes the light-dependent reactions of photosynthesis **[21]**.

2.2.2 The Light-Dependent Reactions

The primary purpose of the light-dependent reactions is to store light energy in a chemical form (NADPH and ATP). Photosystems I (PSI) and photosystem II (PSII) are where the light-dependent reactions of photosynthesis take place. PSI and PSII have the same structure, including a reaction center (RC) that is surrounded by light-harvesting complexes [24]. The two photosystems differ in what they oxidize and reduce. The energy harvested by the LHCs is delivered to the reaction center, where it excites a special pair of chlorophyll molecules that are redox-active. The excited chlorophyll pair donates an electron to the electron transport chain, and replaces it by the splitting of water according to the following reaction [21]:

$$2H_2O \xrightarrow{light} O_2 + 4H^+ + 4e^-$$

The electron travels through the electron transport chain, where it loses its energy, and gets delivered to PSI. PSI absorbs light photons exciting its reaction center, and sends a high-energy electron to $NADP^+$ to form NADPH (nicotinamide adenine dinucleotide phosphate hydrogen). Due to the splitting of water molecules, proton concentration increases inside the thylakoid reducing the pH and creating a pH gradient due to high pH in the stroma (space outside the thylakoid). ATP synthase utilizes the pH gradient to make ATP (Adenosine triphosphate) from ADP (Adenosine diphosphate). The energy carriers ATP and NADPH are used in the 'dark' reactions of photosynthesis to fix carbon dioxide into carbohydrates [24].

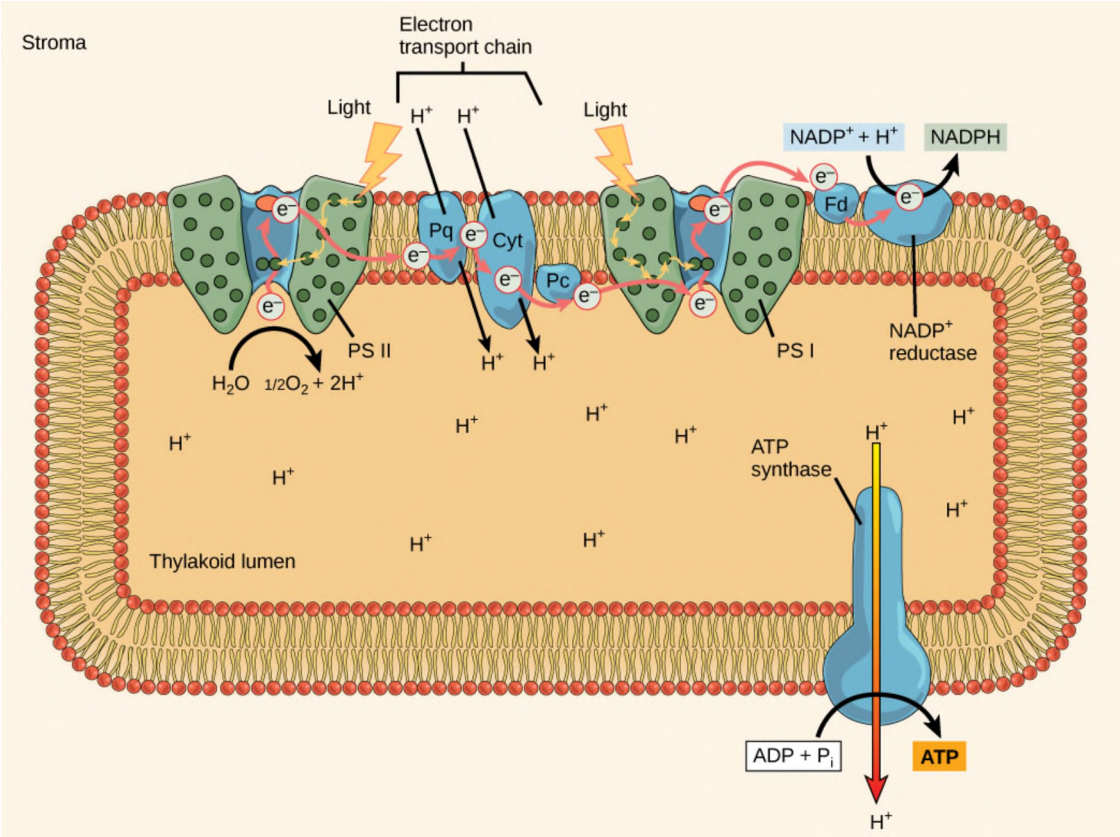

Figure 2-5: Light-dependent reactions of photosynthesis **[24]**.

2.2.3 The Light-Independent Reactions

The stroma of the chloroplast is where the 'dark' (more correctly called "light-independent") reactions take place, resulting in carbon dioxide being fixed into carbohydrates. Carbon dioxide diffuses into the cell and then into the chloroplast, reaching the stroma. ATP and NADPH, products of the light-dependent reactions, which were manufactured in the stroma, can only survive for millionths of a second. The 'dark' reactions, also known as the Calvin cycle, convert the 'unstable' energy of ATP and NADPH into a long term energy storage in the form of carbohydrates by the fixation of CO_2. The Calvin cycle is a three-stage process, as shown in Figure 2-6. The first stage is carbon fixation. Three molecules of CO_2 react with three molecules of RuBP, a five-carbon biphosphate molecule, catalyzed by the enzyme RuBisCO. The products are six three-

carbon molecules called 3-PGA. The second stage of the Calvin cycle is the reduction of 3-PGA. Six molecules of 3-PGA are reduced to six molecules of G3P, another three-carbon molecule, by the oxidation of six ATP and NADPH molecules. Five of the six G3Ps are used to regenerate three RuBP molecules in the third stage of the Calvin cycle [25]. The leftover G3P enters other metabolic pathways in the cell and gets converted into amino acids, lipids, or sugars [21]. In the overall process of the Calvin cycle, three carbon dioxide molecules are fixed into one molecule of G3P that is later used to make amino acids, lipids, or sugars.

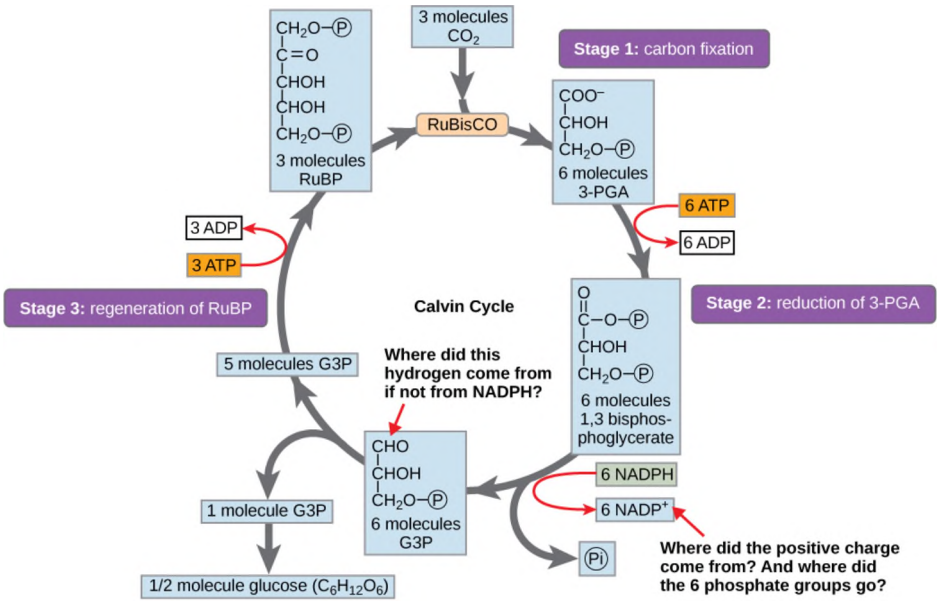

Figure 2-6: The Calvin-Benson Cycle The biochemical pathway for the fixation of CO_2 into carbohydrates in photoautotrophs **[25]**.

2.3 Photoautotrophic Cultivation of Chlorella Sorokiniana

Photoautotrophic growth refers to the process in which microalgae utilizes photosynthesis to convert carbon dioxide into complex organic molecules in order to grow and replicate in the presence of light. Microalgae accumulate lipid bodies, including triglycerides, an essential component in biodiesel production, in significant amounts. Maximizing lipid productivity of the microalgae culture is crucial for biofuel production,

which requires optimizing both lipid content and growth rates. Fortunately, considerable lipid accumulation in *Chlorella sorokiniana* can be easily achieved by applying lipid induction techniques, such as nutrient deprivation, towards the end of the growth phase [26]. However, low biomass productivity, in photoautotrophic culture, remains a significant challenge in making the process economically feasible. The main environmental factors that affect the growth rate are light cycle and intensity, pH, CO_2 availability, and temperature [7]. *C. sorokiniana* can be cultivated in both open ponds and closed photobioreactors (PBRs). Although closed systems are accompanied by significantly (3-10 times) higher initial and operating costs compared to raceway ponds, many advantages make them more attractive than open ponds [7] [27]. For instance, PBRs allow about 16 times higher cell concentration, prevent evaporation, reduce CO_2 losses, and reduce vulnerability for outside influence such as biological contaminants. Additionally, PBRs offer control over culture conditions such as temperature, pH, and mixing and better light usage efficiency [7], [27].

2.3.1 Theoretical Limits of Photoautotrophic Cultivation

Examining the thermodynamic limits of any process can help us understand the potential of the proposed solution, set a frame of reference to evaluate current systems, and guide process design efforts toward optimization. The maximum theoretical growth rate of a photoautotrophic algae culture should be limited by the maximum rate of photosynthesis. The maximum rate of photosynthesis is calculated by Richmond based on the following assumption [28]. In the reaction center (RC), up to 50 carbon atoms per second can be fixed when considering an electron transfer turnover rate of 2 ms, and ten electrons transferred per carbon atom fixed. The turnover rate can reach 2 ms in a fast-growing culture adapted

to high irradiance. Assuming photosystem II (PSII) contains about 300 chlorophyll molecules, the photosynthesis rate can reach 7.9 grams of carbon fixed per gram of chlorophyll per hour. At this rate, the theoretical maximum growth rate of the photoautotrophic algae culture (μ) is about 0.2 h^{-1}, which corresponds to a doubling time of 3.5 hours [28]. Many factors affect the growth rate and can keep it from reaching the theoretical maximum, such as average irradiance per cell, temperature, pH, gas exchange rate, and mixing. In a photobioreactor, a steep light gradient forms resulting in an overexposure of the outer layer, which could inhibit growth due to photoinhibition and lead to low light-energy conversion efficiency. In order to maximize efficiency, the light-dependent growth kinetics must be well understood.

2.3.2 Common Growth Patterns in Batch Culture

Batch culture is a technique used to grow microorganisms and cells and applies to most single-cell organisms. In the process, the cells are provided with a limited amount of nutrients. When deprivation of nutrients become limiting to growth, the cell culture is harvested, and the desired product is extracted [29]. A batch process has twice the triglyceride yield compared to continuous culture, making it more attractive for biofuel production [30, 31]. A typical batch growth curve includes five phases: lag phase, exponential growth phase, deceleration phase, stationary phase, and death phase [32].

The lag phase occurs immediately after inoculation. In this period, the cells are adapted to their new environment. This phase is characterized by a slight increase in biomass concentration and no increase in cell number. The length of the lag phase is dependent on factors such as the age of the inoculum and nutrients concentration. To minimize the length of the lag phase, the inoculum should be adapted to the growth medium, cells should be

relatively young and active (in the exponential growth phase), and the size of the inoculum should be significant in the range of 5% to 10% by volume [33].

After the cells have adapted to their new environment, they enter the exponential growth phase. During this period, cells grow and replicate quickly, and cell mass and number increase rapidly with time. Also, the composition of the cells in this period remains roughly constant. Since nutrients are still abundant in this phase, the growth is independent of the nutrient concentrations. In this phase, the growth rate can be calculated using either biomass or cell number data and should yield the same results. The exponential growth rate is first-order given by Eq. 2.1: [33]

$$\frac{dX}{dt} = \mu_{net}\, X, \qquad X(t_o) = X_o \qquad \textbf{Eq. 2.1}$$

where,

X: biomass concentration [g/L] or cell concentration [cells/mL].

μ_{net}: the specific growth rate [h^{-1}].

The deceleration phase follows the exponential growth phase. The deceleration in the growth rate may be due to the accumulation of toxic products or the depletion of critical nutrients, with light being considered as a crucial 'nutrient' for microalgae growth. The rapidly changing environmental conditions in the deceleration phase forces stressed cells to restructure to survive in a hostile environment. In this phase, the cell composition and size vary significantly, and lipids start to accumulate [33].

The stationary phase, which follows the deceleration phase, is characterized by a net-zero growth rate, which results from the death rate equaling the growth rate. During this phase, the cells are still metabolically active, and some cells produce secondary

metabolites, also known as non-growth-related metabolites. The production of some products, such as antibiotics, is enhanced during this period. Following the stationary phase is the death phase. During the death phase, the death rate, another first-order kinetics, is higher than the growth rate, which leads to a rapid decline in the cell numbers [33].

Understanding and quantifying the growth kinetics of *C. sorokiniana* is essential for the comparison with other candidates for biofuel production and vital for proper process design and economical scaleup. Microbial growth refers to both the increase in cell numbers due to cell division and the increase in cell size [34]. Microorganisms, including green microalgae, extract nutrients from their growth medium and convert it to biological compounds. Cells use these compounds as an energy source, as building blocks, and for other functions that are essential to growth and maintenance. The uptake of nutrients can lead to a change in cell size and replication rate [33]. The growth rate of microbes is usually proportional to the cell concentration, and can be modeled by the equations below [33]:

$$\frac{dX}{dt} = \mu_{net} X \qquad \textbf{Eq. 2.1}$$

$$\mu_{net} = \mu_g - k_l \qquad \textbf{Eq. 2.2}$$

where,

X: biomass concentration [g/L] or cell concentration [cells/mL].

μ_{net}: the net specific growth rate [h^{-1}].

μ_g: the gross specific growth rate [h^{-1}].

k_l: the rate of biomass loss due to respiration and other metabolic activities [h^{-1}]. During cellular respiration, cells use the carbohydrates manufactured during photosynthesis for energy.

Eq. 2.1 is widely accepted as an adequate model for microbial growth. Models for μ_g and k_l are plentiful. In this study, we use the logistic model, the Monod model, and derivatives of the two to evaluate the growth kinetics of *C. sorokiniana* under light-limited conditions and varying light:dark cycle ratios.

2.3.3 The Effect of Light/Dark Cycle on Productivity and Nighttime Biomass Loss

Since photosynthesis consists of both light and light-independent reactions, an essential consideration in optimal design is the length of the light to dark cycle during algae cultivation. If we build an algae plant at the equator, the culture will receive about 12 hours of light and 12 hours of dark year-round [35]. If the plant were in Cleveland, Ohio, the city in which this study is taking place, the culture would receive as little as nine hours of light in December and up to 15 hours in the summer [36]. Much research has gone into studying whether 24:0, 16:8, 12:12, or other combination is the optimal light: dark cycle (L:D cycle) for microalgae growth. It turns out that the answer maybe none of the above. To select the optimal L:D cycle to maximize lipid productivity, we must review our understanding of photosynthesis in microalgae. As discussed in *Section 2.3.1,* the maximum specific growth rate is limited by the rate of photosynthesis. When a cell is illuminated, photosystem II (PSII) is continually damaged and repaired [37]. The turnover rate of PSII ranges from 2-15 milliseconds. The L:D cycle should be only long enough to allow for the light-dependent reaction of photosynthesis to take place and PSII to process the absorbed energy. One study attributes growth enhancement under flashing light to a lower rate of high-light induced non-photochemical quenching when compared to a continuously illuminated culture [38]. Therefore, the optimal L:D cycle is on the order of milliseconds, not hours.

Pulsed light can inhibit growth rather than promote it if the light and dark alternation are not established carefully [37]. One study confirms this finding by comparing pulsed light at specific intervals to continuously provided light in a tubular photobioreactor (TPBR). The research shows that a light:dark duration of 250:250 (ms:ms) inhibits the growth of *Chlorella pyrenoidosa* and results in 25% lower biomass productivity when compared to a continuously illuminated TPBR. However, at a light: dark duration of 5:5 (ms:ms), biomass productivity increased over 21% when compared to a continuously illuminated reactor [39]. Therefore, the light: dark period must be carefully established and controlled for each unique system.

Three methods have been proposed as solutions capable of forming such short photoperiods. First, flashing lamps are very accurate and precise equipment for this purpose. On a lab bench scale, using artificial lights to control the photoperiods is simple. However, on a large scale, we seek to utilize sunlight to power algae plants. Unfortunately, the sun is a continuous illumination source, thus failing the first solution to scale-up. Second, mixing in photobioreactors is the most commonly used parameter to optimize photoperiods. The outer layer of the algae culture absorbs light energy and forms a steep light profile in PBRs. The algae cells in the inner layer are shaded from light by the outer layer in a phenomenon known as auto-shading. As mixing continues, cells occupying the inner layer eventually reach the outer layer and vice versa. The effect of mixing will create a light: dark period alternation in the presence of a continuous illumination source. However, it is impossible to precisely control the light: dark periods using mixing due to the random movement of cells in such systems. For that reason, optimization of the photoperiods using mixing is based on experiments, and the solution is unique to the system

in study. However, we must note that mixing does not only affect the period of light exposure; it also plays a role in parameters that affect cell growth, such as CO_2 concentration and shear stress. Finally, a novel design of a TPBR is done by shading the reactor periodically and controlling the flow rate to achieve the desired light:dark periods in a continuously illuminated culture [39]. Additionally, the tube diameter of the photobioreactor must be selected to prevent the formation of steep light profiles. Figure 2-7 illustrates a schematic of a periodically shaded TPBR.

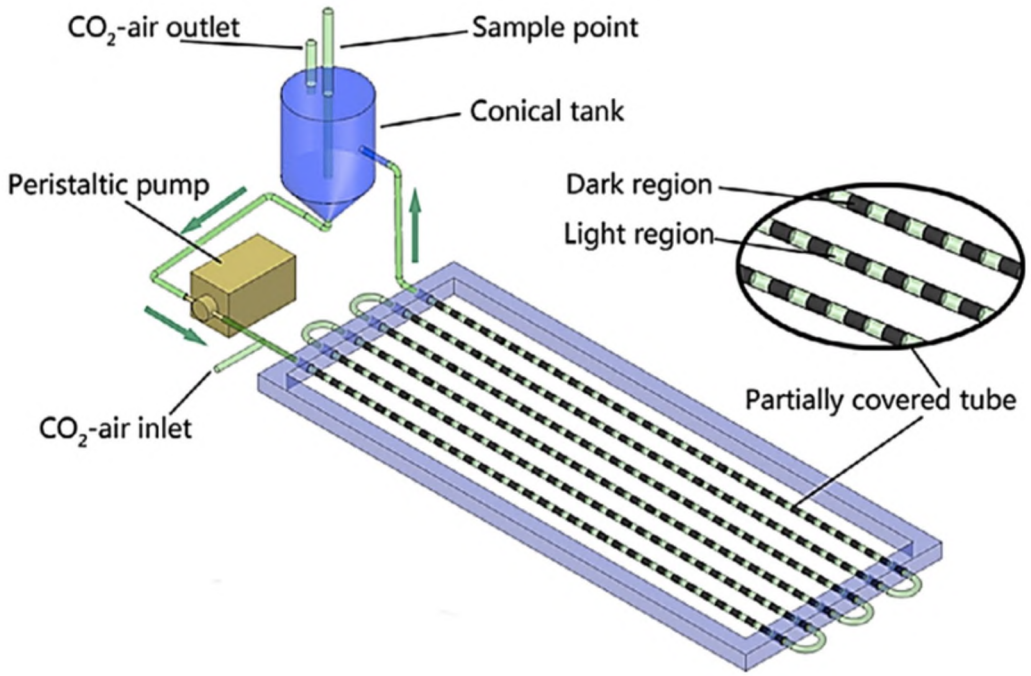

Figure 2-7: Schematic of a periodically shaded tubular photobioreactor (TPBR) **[39]**.

Much more research is still needed to make these methods for millisecond light/dark cycles economically feasible. However, what happens during nighttime is another issue to consider. As the sun sets, microalgae turn to internal energy reservoirs to survive the night in a process known as photorespiration. Some studies have reported up to 17% biomass loss during nighttime, while others reported up to 35% in losses [40]. A study-specific to

Chlorella sorokiniana reported varying biomass losses from 4% (10ºC) to 15% (25-30ºC) in a 10-hour dark period [14]. Nighttime biomass loss can be attributed to photorespiration; it slows growth and delays lipid accumulation [41] [42]. Artificial light and nighttime organic carbon supplementation are two techniques that can be used to prevent losses. Nighttime carbon supplementation increases the risk of contamination. Organic carbon sources include glucose, acetate, and ethanol with corresponding uptake rates of 0.11, 0.12, and 0.09 (g/ g cell/ h) for *Chlorella sorokiniana* [40].

Additionally, the dark period is not entirely detrimental when algae is grown using wastewater. Two main components that need removal from sewage are nitrate and phosphorus. Although nitrate uptake rates are highest during the daytime, phosphorus uptake rates are much higher during the nighttime and almost non-existent in the light period. For that reason, the dark period proves essential for wastewater [43]. In Table 2-1**,** we tabulated some of the growth rates reported in literature for *C. sorokiniana* and other *Chlorella* species. The different studies all showed that longer light periods lead to higher biomass productivity and higher specific growth rates.

Table 2-1: A summary of growth rates and productivities of microalgae Chlorella sorokiniana under a different light:dark periods, as reported in the literature. Although direct comparison is not possible due to different cultivation systems and illumination sources used in each study, the summary provides an adequate frame of reference.

Species Chlorella	*Light: Dark Cycle*	*Light Intensity*		*Cultivation System*	*Parameter Measured*	*Specific Growth Rate [h^{-1}]*	*Biomass Productivity [$g\ L^{-1}\ h^{-1}$]*	*Reference*
sorokiniana	Natural	300-1200	µmol $m^{-2}\ s^{-1}$	180L Hybrid PBR	Cell Conc. [cells/mL]	0.046	-	[44]
sorokiniana	24:0	250	µmol $m^{-2}\ s^{-1}$	1.5L Roux Flasks	Biomass Conc. [g/L]	-	0.042	[40]
sorokiniana	10:14	250	µmol $m^{-2}\ s^{-1}$	1.5L Roux Flasks	Biomass Conc. [g/L]	-	0.011	[40]
sorokiniana	24:0, 12:12	150	µmol $m^{-2}\ s^{-1}$	1L Std. Glass Bottles	Biomass Conc. [g/L]	24:0 higher than 12:12	-	[31]
sorokiniana	-	-		-	Biomass Conc. [g/L]	0.016	-	[45]
vulgaris	-	-		-	Biomass Conc. [g/L]	0.019	-	[45]
pyrenoidosa	12:12	8000	lux	1L PBR	Biomass Conc. [g/L]	0.019	-	[45]
pyrenoidosa	12:12	8000	lux	1L PBR	Biomass Conc. [g/L]	0.015	-	[45]

2.4 The Effect of Irradiance on Photoautotrophic Growth

2.4.1 The Nature of Light

Light is electromagnetic radiation, travels at a speed of $3x10^8$ m s^{-1}, with wavelengths ranging from 1 pm to more than 100 m. Based on the wavelengths, it can be divided into several components, including Gamma rays, X-rays, UV light, visible light, infrared, microwaves, and radio waves. The visible portion of the light spectrum has a wavelength ranging from 380 nm (violet) to 750 nm (far red) [46]. The visible light corresponds to the photosynthetically active radiation (PAR), the portion of the light that photosynthetic organisms can utilize. Light energy is quantized and therefore delivered in separated packages known as photons. Chlorophyll pigments absorb the energy of a photon of blue or red light and transfer it to the reaction center [28].

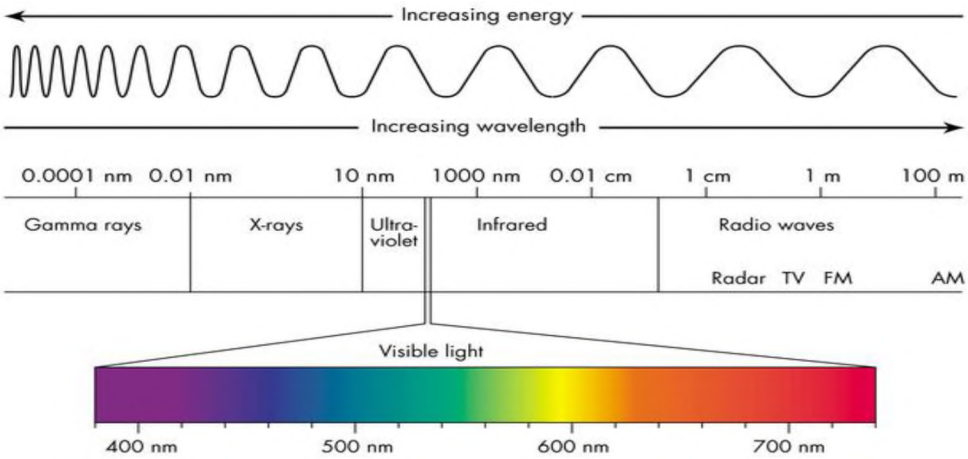

Figure 2-8: Spectrum of light **[46]**. The visible component of the light spectrum, 380 nm - 750 nm, corresponds to the photosynthetically active radiation (PAR).

2.4.2 The Effect of Light Quality on Growth

The most abundant light-absorbing photosynthetic pigments, chlorophyll, absorb photons of blue and red light. Chlorophyll molecule's π-electron gets promoted from ground energy state S_o to a higher energy state S_1 when it absorbs a photon of red light. The absorbed energy is then transferred to the reaction center. Since blue light corresponds to a shorter wavelength, a photon of blue light possesses higher energy and excites the chlorophyll π-electron to an even higher energy level S_2. Only the energy of a red photon is transferred to the reaction center, and the excess energy of the blue photon is lost as heat due to molecular vibrations, refer to *Section 2.2.1*.

Since the energy of a red photon is all that is needed for the microalgae to carry out the photosynthetic reactions, it has been hypothesized that red light promotes cell replication, and the excess energy from the blue photon stresses the algae cell and causes biomass accumulation and higher production of lipids. Therefore, white light, which contains both blue and red, would yield the highest lipid productivity as it would combine both the high growth with the lipid accumulation. A study on *Chlorella vulgaris* reported maximum lipid content when cultivated under blue light, and highest lipid productivity under white light

confirming the hypothesis [47]. Additionally, another study concluded that growing microalgae cultures under red light yielded double the cell numbers produced as compared to white light, and that exposing the culture to white light towards the end of the growth phase promoted biomass accumulation [48]. Lastly, another study on *Chlorella pyrenoidosa* reported a higher growth rate, based on biomass measurements, under blue cultivation, that was 1.33 times the growth rate under red light [49]. Mathematical modeling and statistical analysis suggested white light as the preferred choice for cultivation [50]. Most of these studies are either reporting biomass concentration or cell concentration, but not both. Studies reporting biomass concentration conclude that blue light is better for growth since it induces biomass accumulation [49]. On the contrary, studies reporting cell concentration find that red light is far better than blue light [47] [48]. To observe the full effect of light wavelengths on growth, both measurements need to be collected.

Proposed methods of optimization by cultivating microalgae using red light and introducing white light towards the end of the cultivation cycle will never be scaled up to outdoor systems due to our inability to control the wavelength of sunlight. In our study, assuming that red light promotes the replication of cells, and because red LEDs have lower consumption of energy compared to other wavelengths, we utilized artificial illumination, in the form of red LEDs, to mitigate the effect of nighttime on *C. sorokiniana's* productivity.

2.4.3 The Effect of Light Intensity on Growth

Light intensity is often attributed as the most significant parameter affecting growth rates in photoautotrophic cultures. The intensity of light is measured in lux, lumens per

square meter, and it is used as the measure of light intensity as perceived by the human eye. In more relatable terms, solar irradiance reaching Earth's surface, on a sunny day, is about 100,000 lux, which is equivalent to a 1000 W/m^2. The photosynthetically active radiation (PAR) represents around 40% of the solar radiation incident on the Earth's surface. Chlorophyll molecules are excited by harvesting the energy of photons. Therefore, it is more logical to express light intensity in terms of the number of photons incident on a surface rather than in lux. In microalgae related literature, the most common unit of expressing light intensity is µmol photon per square meter per second. A 100 lux quantity of sunlight is equivalent to 4.5 µmol photon m^{-2} s^{-1} [28]. Additionally, 100 lux quantity of white light LED is equivalent to 1.5 µmol photon m^{-2} s^{-1} [51]. The reason for the different conversion factors results from the different spectrum of each light source.

Research has shown increasing growth rates and biomass productivity with increasing light intensity. One study tested four different species, including *C. vulgaris*, at 50, 150, and 300 µmol photon m^{-2} s^{-1} surface intensity. The results of the study showed higher productivity at higher intensities for all species [52]. However, at even higher intensities, photoinhibition of microalgae occurred, and growth was inhibited [53]. Light intensity also affects the composition of the cells, and it can be optimized to yield better quality fuels. Fuels rich with polyunsaturated fatty acids are prone to oxidation-dependent degradation, which were the most abundant at low irradiance. Monounsaturated fatty acids became the most abundant with increasing light intensities. Fuels with a high content of monounsaturated fatty acids are not susceptible to oxidation, have better flow properties, and reduced solidification temperature [52].

2.4.4 Current Models of Light Effect on Microalgae Growth

Current models of the effect of light intensity on biomass productivity fit data poorly and do not scale up effectively due to the complexity of the task. Some of the complexities facing modeling efforts include photoinhibition, self-shading, and photoacclimation [54]. Photoacclimation is the process used by photosynthetic organisms to respond to frequent changes in irradiance by changing the number of photosynthetic units and or the size of the light-harvesting antenna [28]. The effect of photoinhibition can be ignored under light limiting conditions [55].

The logistic model is a simple widely used population model. It postulates that a limit exists on the population that can be sustained in any environment, also known as the carrying capacity, and the growth rate decreases as the population approaches that limit [56] [57]. The logistic model provides insights on how the cultivation environment as a whole affects the growth, but it fails to give any information on the effect of a specific parameter on growth. Additionally, the rate of mass loss (k_l) is neglected in the logistic model. Some of the logistic model parameters found in literature are summarized in Table 2-2. The specific growth rate is given by the following equation [33]:

$$\mu_{net} = \mu_g = k\left(1 - \frac{X}{X_\infty}\right) \qquad \textbf{Eq. 2.3}$$

where,

X: cell mass concentration [g/L] or cell concentration [cells/mL].

k: the maximum growth rate [h^{-1}].

X_∞: carrying capacity [g/L] or [cells/mL].

Table 2-2: Summary of growth kinetics that are found in literature using the logistic model.

Species	*k (h^{-1})*	*X_∞ (g/L)*	*Reference*
S. dimorphus	0.039 ± 0.001	1.49 ± 0.05	[58]
C. vulgaris	0.012	-	[59]
C. salina	0.444	-	[60]
N. oculata	0.447	-	[60]
Chlorella Sp.	0.005	0.76	[61]

The Monod equation is a simple unstructured model yet powerful as it captures the effect of a single substrate on growth. It assumes that the substrate is growth-rate limiting, and other nutrients, ordinarily present in excess, have no influence on the growth rate. In literature, the Monod equation has been used to study the effect of light, nitrogen source, organic carbon source, and others on the growth of microalgae. The specific growth rate given by the Monod equation in light-limited conditions is:

$$\mu_g = \mu_m \left(\frac{I_{avg}}{K_g + I_{avg}} \right) \qquad \textbf{Eq. 2.4}$$

where,

μ_m: the maximum specific growth rate [h^{-1}].

I_{avg}: the average light intensity in the PBR [µmol s^{-1} m^{-2}].

K_g: saturation or half-velocity constant [µmol s^{-1} m^{-2}].

The Monod kinetics that relate growth to light intensity are commonly used when considering photoautotrophic growth of microalgae. The reported values in literature ranged from 0.02 - 0.15 h^{-1} for the maximum specific growth rate (μ_m). The half-velocity constant (K_g) ranged from 100-300 [µmol s^{-1} m^{-2}] [62]. Some of the light dependent kinetics, using the Monod model, are summarized in Table 2-3. These models did not account for biomass loss, which is commonly overlooked. In this study, The Monod

equation is coupled with biomass loss terms to better represent the varying photoperiods, see *Section 3.3.2*.

Table 2-3: Summary of growth kinetics that are found in literature using the Monod model

Species	μ_m *(h^{-1})*	K_g *(µmol s^{-1} m^{-2})*	*Reference*
Spirulina	0.047	238	[63]
Synechocystis Sp.	0.50	380	[64]
C. vulgaris	0.022	275	[64]

One of the problems that face modeling efforts is the steep light profile that forms inside the PBR. The light profile formed has been modeled using Beer's law as a function of biomass concentration and depth [65]:

$$I(z,X) = I_o \, e^{-k_a \cdot X \cdot z} \qquad \textbf{Eq. 2.5}$$

where,

$I(z,X)$: the light intensity at a depth z and biomass concentration X [lux or µmol m^{-2} s^{-1}]

I_o: the light intensity at the surface of the PBR [lux or µmol m^{-2} s^{-1}]

k_a: biomass light absorption coefficient [lenght^2/mass]

Using the mean value theorem [66], the average irradiance per cell in a PBR can be given by Eq. 2.6:

$$I_{avg} = I_o \cdot \left[\frac{1 - e^{-k_a \cdot X \cdot d}}{k_a \cdot X \cdot d} \right] \qquad \textbf{Eq. 2.6}$$

where d is the depth of the culture. k_a is determined experimentally for each species by comparing light transmittance of a blank to that in algae samples of different biomass concentrations [67], See *Section 3.3.4*.

CHAPTER III

MATERIALS AND METHODS

3.1 Growth Medium, Inoculum Preparation, and PBR Cultivation System

3.1.1 Microalgae Strain and Growth Medium

The culture of *UTEX B 3016 Chlorella sorokiniana (DOE 1412),* used in this study, was isolated in Brooklyn, NY, USA by professor Juergen Polle, and acquired from the UTEX Culture Collection of Algae at The University of Texas at Austin. The Culture was grown in BG-11 medium per the recommendation of UTEX [68]. One liter of BG-11 medium contains 17.6 mmol $NaNO_3$, 0.23 mmol K_2HPO_4, 0.30 mmol $MgSO_4 \cdot 7H_2O$, 0.24 mmol $CaCl_2 \cdot 2H_2O$, 0.03 mmol $C_6H_8O_7 \cdot H_2O$, 0.02 mmol $(NH_4)_5[Fe(C_6H_4O_7)_2]$, 0.0027 mmol $Na_2EDTA \cdot 2H_2O$, 0.19 mmol Na_2CO_3, 0.46 mmol H_3BO_3, 0.09 $MnCl_2 \cdot 4H_2O$, 0.0077 mmol $ZnSO_4 \cdot 7H_2O$, 0.016 mmol $Na_2MoO_4 \cdot 2H_2O$, 0.003 mmol $CuSO_4 \cdot 5H_2O$, and 0.0017 mmol $Co(NO_3)_2 \cdot 6H_2O$. A detailed procedure for medium preparation can be found in Appendix A.

3.1.2 Inoculum Preparation

Inoculum is a group of cells used in an inoculation, i.e., the cells added to start a culture [69]. Inoculation is the process of adding microorganisms into a culture medium [70]. To

properly inoculate the photobioreactor, the inoculum must be in an active state (exponential growth phase) and be of a significant size (5%-10%) of the culture medium [71]. In our study, the inoculum size ranged from 300 to 500 mL (6%-10% of the PBR working volume) and a cell concentration of 2-5x10^7 cells per mL. The inoculum cell culture was grown in 2L glass bottles under white fluorescent light and 12:12 light: dark cycle. The light intensity at the surface of the bottles was measured to be about 3,000 lux with a Fisherbrand™ Traceable™ Dual-Range Light Meter. The gas flow rate to each bottle was maintained at 0.5 LPM (10% CO_2 in air). The containers were placed in a Microprocessor Shaker Bath, where they were continuously shaking in an elliptical orbit at 96 rpm. The water bath temperature was constant at 30°C ± 0.2°C. The cultivation setup is illustrated in Figure 3-1.

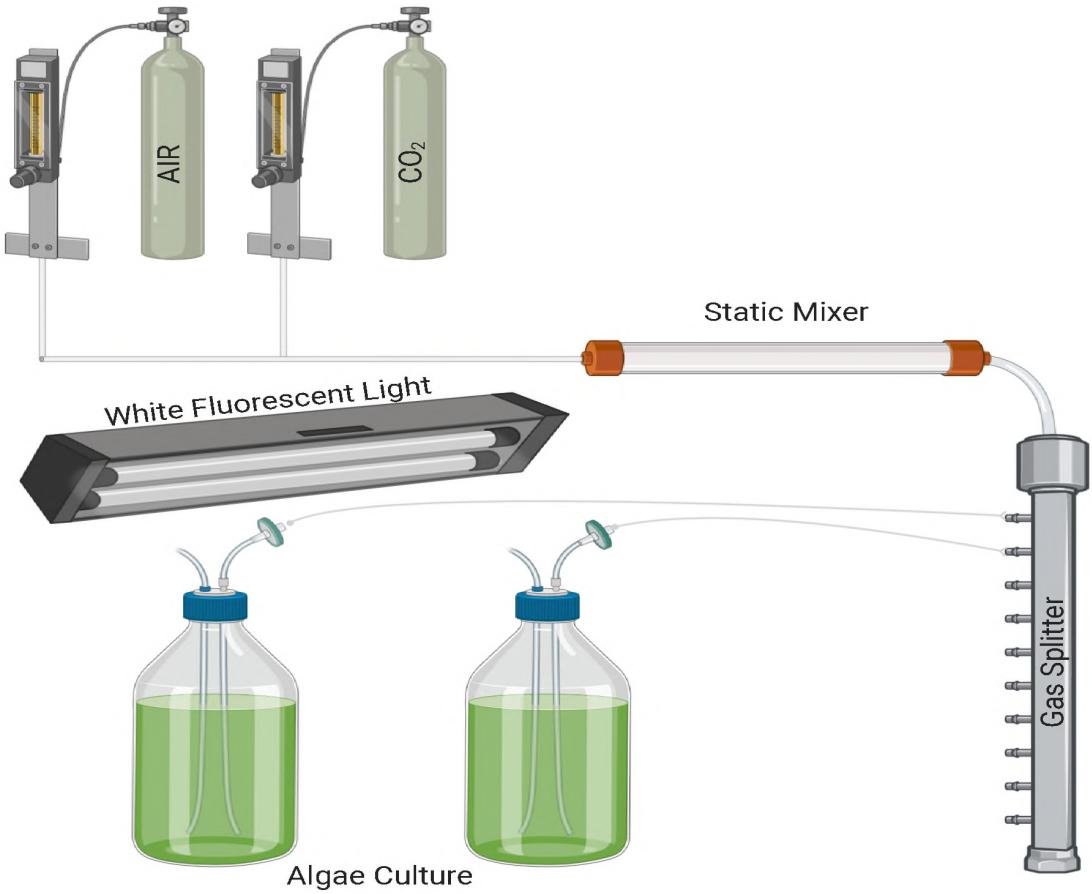

Figure 3-1: Inoculum cell culture cultivation system.

3.1.3 Photobioreactor Cultivation System

Experiments were carried out in a 7.5L Benchtop Eppendorf BioFlo®/CelliGen® 115 bioreactor. The working volume of the bioreactor ranges from 2.0 L to 5.6 L. A total volume of 5 L was used in all experiments. The liquid level was maintained constant by assigning a built-in peristaltic pump to turn on and deliver sterile water when the "Wet/Dry" level sensor reads "Dry." A direct drive Rushton-style impeller was used at a 200 rpm agitation rate, and removable 316L stainless steel baffles were used to improve mixing. The temperature was set to 30°C and maintained using a water jacket heater and a cooling water circulation loop. A pH probe was used to measure pH, which ranged from 5.5-8.4. The aeration rate was set to 1.1 LPM (10% CO_2 in air) and was sent into the reactor through

a ring sparger after passing a 0.2 µm inlet filter. The exhaust gas was led into a vent after passing through a co-current water-cooled (9°C) stainless steel condenser and a 0.2 µm hydrophobic filter. The inoculation procedure (Appendix D) was followed to initiate the cultivation in the PBR with an initial cell concentration ranging from $2x10^6$ to $5x10^6$ cells/ml. Finally, the bioreactor was illuminated by an RGB LED light jacket. The surface intensity was constant, and a light meter was used to measure the light intensity inside the reactor and at the surface (described in *Section 3.2.1)*. Three types of light schedules were used: 1) the 24:0 signifies 24 hours/day of constant light; 2) 16:8 signifies 16 hours of light, followed by 8 hours of dark each day; 3) 16:8red signifies 16 hours of light, followed by 8 hours of red light each day. For the 24:0 light:dark cycle experiments, one sample was collected every 24 hours. For the 16:8 and 16:8red experiments, two samples were collected daily, one each at the start and end of each light period. The sampling procedure is presented in Appendix E.

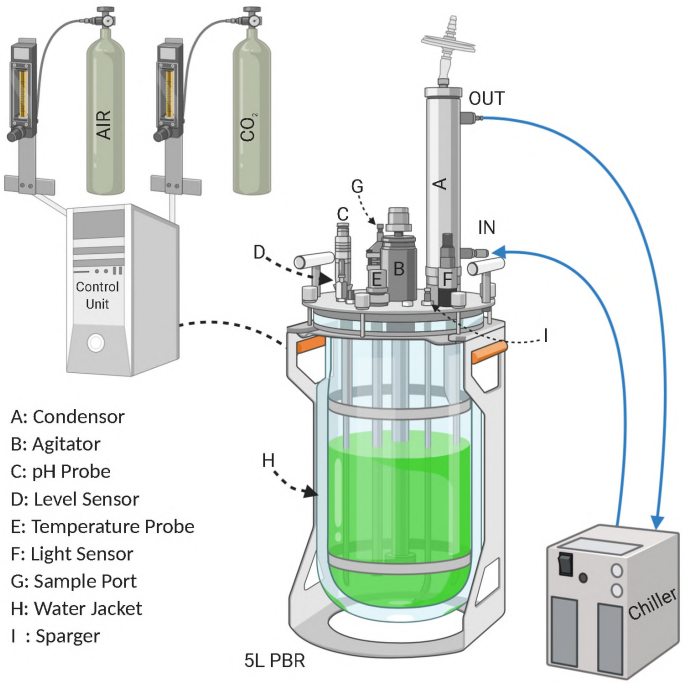

Figure 3-2: Photobioreactor Cultivation System.

3.2 Measurements

3.2.1 Light Intensity

A photoconductive cell (Luna Optoelectronics NSL-6510) was used to measure light intensity inside the bioreactor. The photocell is 6 mm in diameter, made from type 6 CdSe, and has a spectral peak at 690 nm, which is similar to the 680 nm absorption peak of chlorophyll. The light sensor was calibrated with a Fisherbrand™ Traceable™ Dual-Range Light Meter. The calibration curve is shown in Figure 3-3. The light sensor was housed in a clear glass tube and inserted into the bioreactor, 2.3 cm from the surface. The wiring diagram and Arduino code are presented in Appendix F.

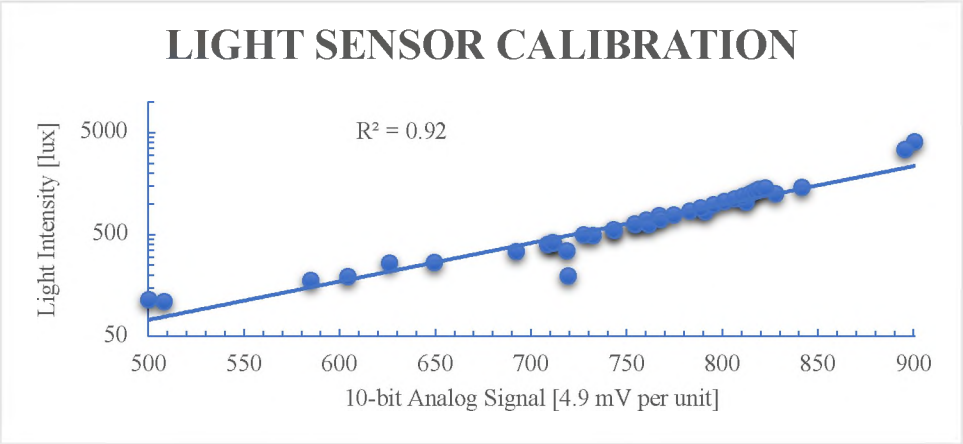

Figure 3-3: Light sensor calibration curve. The photocell was calibrated under a white LED light using Fisherbrand™ Traceable™ Dual-Range Light Meter. The conversion equation is $I = 0.94*\exp(8.69x10^{-3} * signal)$.

3.2.2 Nitrate Ion NO_3^-

The initial nitrate ion concentration in the media was about 1200 ppm (mg/L). The procedure used to measure the nitrate ion concentration is summarized in Figure 3-4. 10 mL of the sampled cell suspension was centrifuged at 1500 rpm (450 g) for 10 minutes. One milliliter of the sample retentate was collected to measure the nitrate ion concentration using a HORIBA LAQUAtwin Model NO3-11 Compact Nitrate Ion Meter. The nitrate ion

meter has a measuring range from 6 ppm to 9900 ppm, with a 10% inaccuracy in the reading [72].

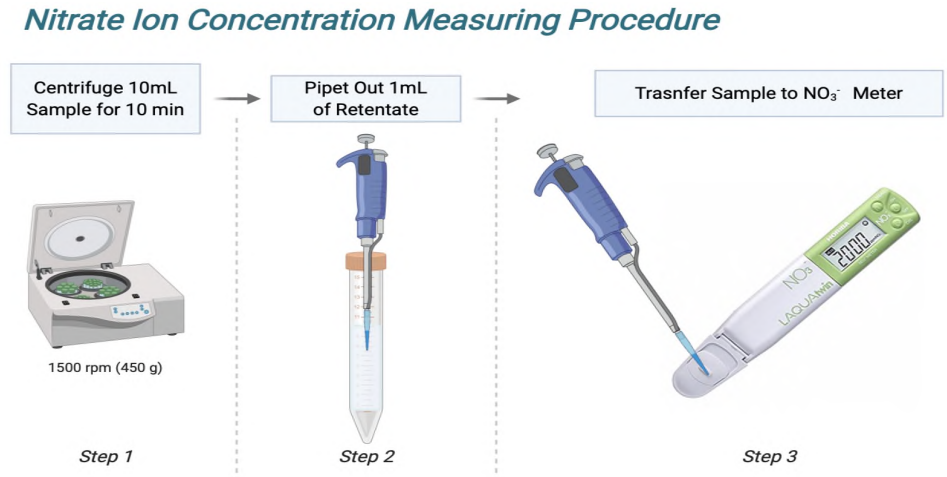

Figure 3-4: Nitrate ion concentration measurement procedure.

3.2.3 Biomass Concentration

A simple illustration of the procedure used to calculate the biomass concentration is shown in Figure 3-5. A fresh cell suspension sample was transferred to four wells of a transparent 96-well plate (200 µL sample in each well), and a BioTek® SYNERGY H1 microplate reader was used to measure the absorbance of the four repeats at 430 nm and 680 nm. Initially, the two wavelengths were selected because they correspond to chlorophyll absorption peaks. Calibration curves, for both wavelengths, were constructed and used to convert absorption data into dry weight biomass concentration (Appendix G). The dry weight biomass concentration was measured by drying 50 mL of the cell suspension sample in an oven at 60°C. The weight of the sample was recorded after ensuring all the water content had evaporated (constant weight for three consecutive days). Linear relationships between the optical density of a cell suspension sample and its dry weight were obtained at both wavelengths. The averages of the four measurements at 430

nm and the four measurements at 680 nm were converted to biomass concentrations (X_{430nm} *and* X_{680nm}) [g/L]. The average of the calculated biomass concentrations was reported as the average biomass concentration of the cell suspension X, with the corresponding standard deviation as the error bar.

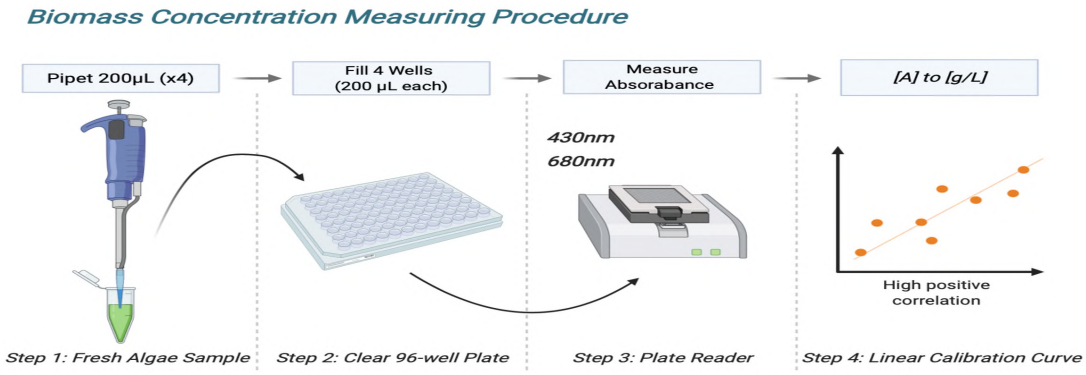

Figure 3-5: Biomass concentration measurement procedure.

3.2.4 Cell Concentration and Size Distribution Curve

Cell concentration was measured by counting cells using a hemocytometer, as illustrated in Figure 3-7. Five of the 25 (0.04 mm^2) grids were imaged under the microscope (20X magnification, phase contrast filter). The locations of the grids imaged were top left, top right, bottom right, bottom left, and center, as highlighted in Figure 3-6. The images are exported to a custom MATLAB code, which counts the number of cells per grid, calculates the corresponding cell concentration (given that the 0.04 mm^2 grid holds a volume of 4 nL at 0.1 mm depth), and produce size distribution curves. MATLAB identifies the cells as circles with a corresponding diameter and draws a blue border line around the identified cell. Visual inspection of the processed imaged is required to ensure that the program did not over or underestimate the number or the size of the identified cells.

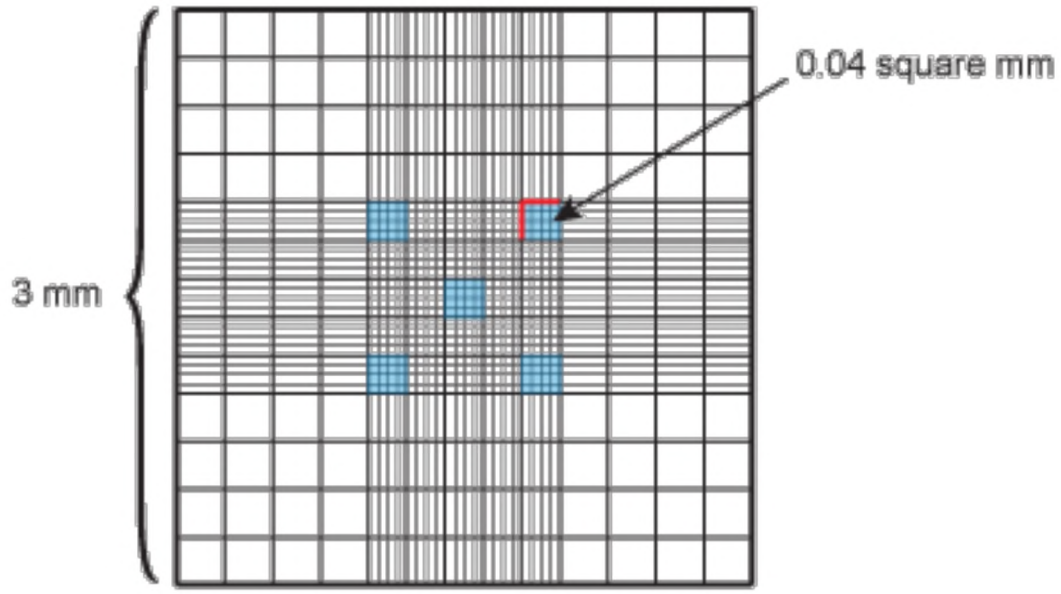

Figure 3-6: Hemocytometer grids imaged for cell concentration measurements

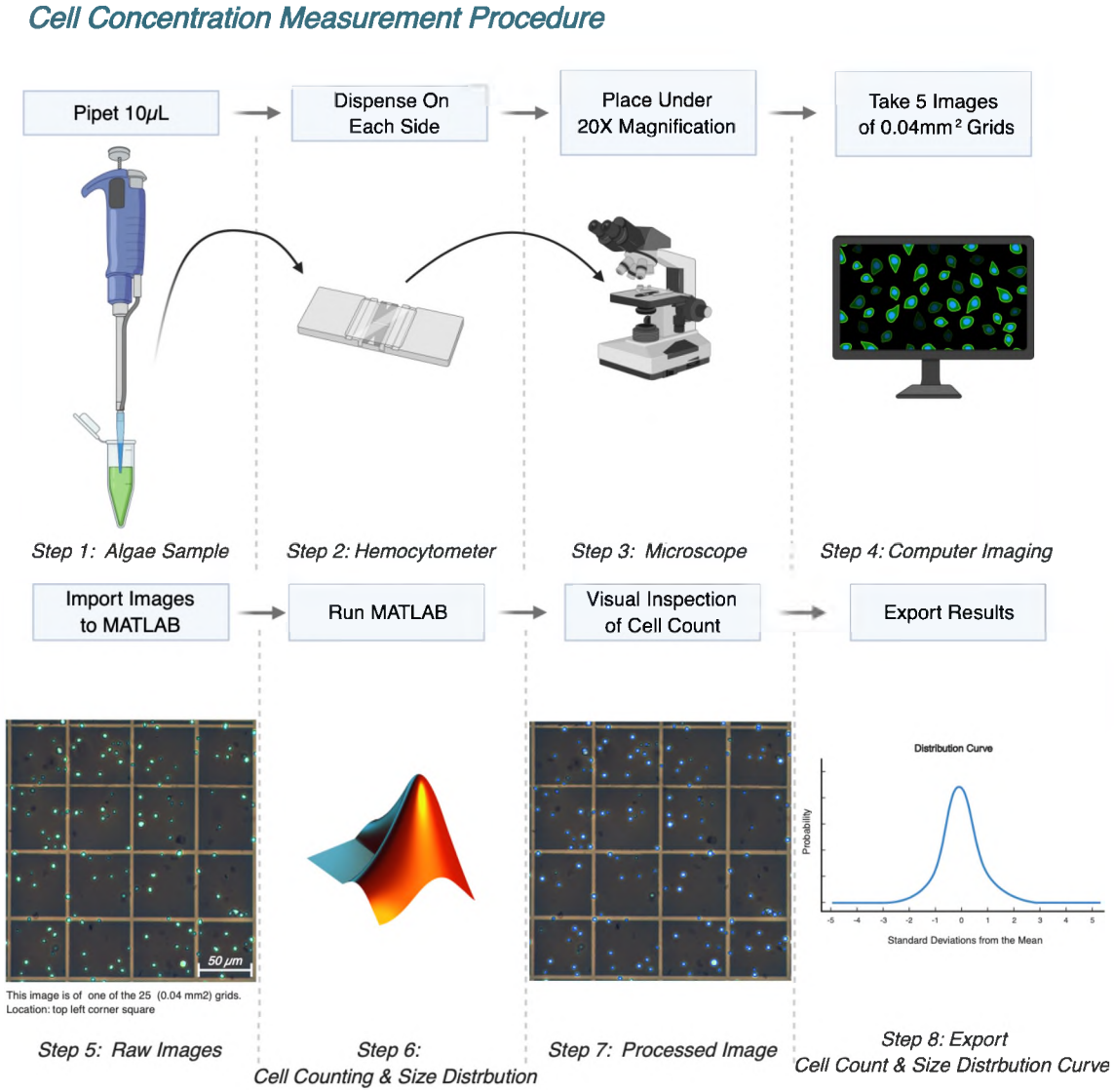

Figure 3-7: Cell concentration measurement procedure.

3.3 Growth Models and Parameter Estimation

3.3.1 The Logistic Equation

The logistic model is a widely used model of population growth. It postulates that a limit exists on the population that can be sustained in any environment. The maximum sustainable population is known as the carrying capacity. Additionally, the model posits that the growth rate of the population will decrease as the population approaches the

carrying capacity [56] [57]. The rate of mass loss (k_l) is neglected in the logistic model, and the growth specific growth rate is given by the following equation [33]:

$$\mu_{net} = \mu_g = k\left(1 - \frac{X}{X_\infty}\right) \quad \textbf{Eq. 3.1}$$

where,

X: cell mass concentration [g/L] or cell concentration [cells/mL].

k: the maximum growth rate [h^{-1}].

X_∞: carrying capacity [g/L] or [cells/mL].

3.3.2 Light-limited Growth with Constant k_l: The Monod Equation

The Monod equation is a simple unstructured model yet powerful as it captures the effect of a single substrate on growth. It assumes that the substrate is growth-rate limiting, and other nutrients, ordinarily present in excess, have no influence on growth rate. In this model, we assume that the mass-loss rate due to cell death and endogenous metabolism is constant. Additionally, under light-limiting conditions, we assume that the gross specific growth rate can be described by the Monod equation [33]:

$$\mu_g = \mu_m\left(\frac{I_{avg}}{K_g + I_{avg}}\right) \quad \textbf{Eq. 3.2}$$

where,

μ_m: the maximum specific growth rate [h^{-1}].

I_{avg}: the average light intensity in the PBR [µmol s^{-1} m^{-2}].

K_g: saturation or half-velocity constant [µmol s^{-1} m^{-2}].

Combining equations Eq. 2.1, Eq. 2.2, and Eq. 3.2 yields the substrate-limited growth model with constant k_l:

$$\frac{dX}{dt} = \left[\mu_m \left(\frac{I_{avg}}{K_g + I_{avg}} \right) - k_l \right] X \qquad \textbf{Eq. 3.3}$$

Studies have shown that the respiration rate is related to the growth rate; it peaks during the light period and stays relatively constant during the nighttime [73]. For that reason, we segregated the biomass loss rate due to respiration into two terms: 1) $k_{l,light}$ is the biomass loss rate during the light period [h^{-1}]. 2) $k_{l,night}$ is the biomass loss rate during nighttime [h^{-1}]. Eq. 3.3 expands to:

$$\frac{dX}{dt} = \left[\mu_m \left(\frac{I_{avg}}{K_g + I_{avg}} \right) - \alpha \bullet k_{l,light} - (1 - \alpha) \bullet k_{l,night} \right] X \qquad \textbf{Eq. 3.4}$$

where,

α: a dimensionless constant that is equal to one during the light period and zero during the dark period.

3.3.3 Light-limited Growth with Variable $k_{l,light}$: The Monod Equation

Under alternating light-dark periods, the assumption of constant $k_{l,light}$ is likely not valid, since respiratory activities are known to be related to the growth rate [74]. Respiration rate of *C. sorokiniana* was observed highest at the beginning of a batch culture when the growth rate was highest [74]. Since biomass loss due to respiration is related to growth, and the growth rate is a function of light intensity, we can postulate a Monod relation between mass-loss rate and light intensity:

$$k_{l,light} = k_{l,max} \left(\frac{I_{avg}}{K_l + I_{avg}} \right) \qquad \textbf{Eq. 3.5}$$

where,

$k_{l,max}$: the maximum mass loss rate during the light period [h^{-1}].

K_l: saturation constant for the effect of light intensity on biomass loss [µmol s^{-1} m^{-2}].

Combining Eq. 3.3 and Eq. 3.5 yields:

$$\frac{dX}{dt} = \left[\mu_m \left(\frac{I_{avg}}{K_g + I_{avg}} \right) - \alpha \, k_{l,max} \left(\frac{I_{avg}}{K_l + I_{avg}} \right) - (1 - \alpha) \bullet k_{l,night} \right] X \qquad \textbf{Eq. 3.6}$$

3.3.4 Modeling I_{avg}: Measurement of The Biomass Light Absorption Coefficient

The light intensity inside the reactor was measured using a light sensor 2.3 cm from the surface, and thus not representative of the average intensity within the reactor. Mathematical expressions such as Beer's law can be used to model the steep light profile in the PBR and predict the average light intensity by using Eq. 2.5 and Eq. 2.6. To measure the light absorption coefficient, five algae samples (0.33, 0.49, 0.66, 0.92, and 1.30 g/L) were transferred to transparent cuvettes. The five cuvettes, plus one cuvette filled with DI water as blank, were placed in a Styrofoam frame and illuminated from the front using a multicolor LED (iPhone X flashlight). The light intensity was measured behind the cuvette using a Fisherbrand™ Traceable™ Dual-Range Light Meter. Each sample was illuminated with four incident light intensities, including 75, 150, 238, and 250 µmol s^{-1} m^{-2} as measured with the light meter at the front surface of the cuvette. Finally, the biomass light absorption coefficient was calculated using the rearrangement of Beer's Law, Eq. 3.7 [65].

$$k_a = -\frac{1}{X \bullet L} \ln\left(\frac{I}{I_o}\right) \qquad \textbf{Eq. 3.7}$$

where,

k_a: the biomass light absorption coefficient [dm^2/g].

X: biomass concentration [g/L].

L: the light path length [dm]. The light path length is equal to 0.123 dm for this setup.

I: the light intensity measure behind the cuvette for the sample [μmol s^{-1} m^{-2}].

I_o: the light intensity measured behind the cuvette for the blank [μmol s^{-1} m^{-2}].

The results, shown in Figure 3-8, illustrate that k_a is independent of the incident light intensity. p-values of unpaired two-tailed t-tests that compare the three data sets at higher light intensity to the lowest light intensity data set, in a sequential order, have the values 0.76, 0.61, and 0.98. All p-values show that k_a is independent of light intensity.

On the contrary, Figure 3-9 shows a trend between the coefficient and biomass concentration. The actual median of measurements at 0.33 g/L does significantly differ from measurements at 0.66 g/L (p-value = 0.07), which in turn does significantly differ from measurements at 1.30 g/L (p-value = 0.01). Although it may introduce an error component into modeling and overestimate the light profile, as shown in Figure 3-10, we assume that using an average value for the coefficient is still satisfactory. The mean value for the biomass light absorption coefficient was calculated to be 17.1 ± 3.88 [dm^2/g] from the 20 data points.

In summary, I_{avg} was calculated at each time point, in each experiment, by means of Eq. 2.6, using the predicted biomass concentration X(t), the depth of the culture (d=9 cm), the light absorption coefficient (k_a=17.1 dm^2/g), and the measured surface intensity (I_o=300 μmol s^{-1} m^{-2}). So, although the light intensity was measured and recorded at 2.3 cm for the duration of each experiment, the data were only used from one of the experiments to validate the use of the model for the average intensity and the k_a value.

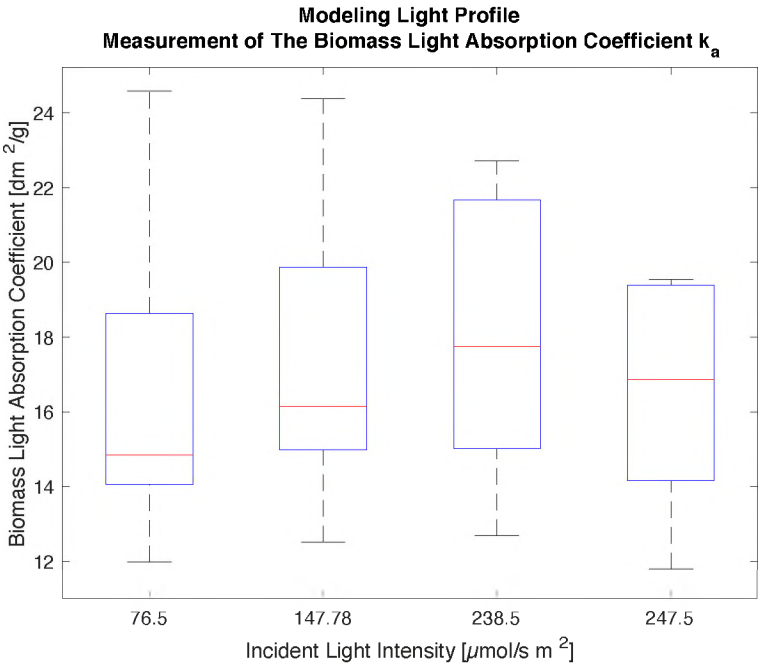

Figure 3-8: Biomass light absorption coefficient vs. incident light intensity. The average value of the factor was calculated to be 17.1 ± 3.88 [dm^2/g] for *C. sorokiniana* (DOE 1412). On each box, the central mark indicates the median, and the bottom and top edges of the box indicate the 25th and 75th percentiles, respectively. The plotted whisker extends to the most extreme data value. Each data set consists of five measurements, one measurement at each biomass concentration. The medians do not differ from one another, therefore, the biomass light absorption coefficient, k_a, is independent of light intensity.

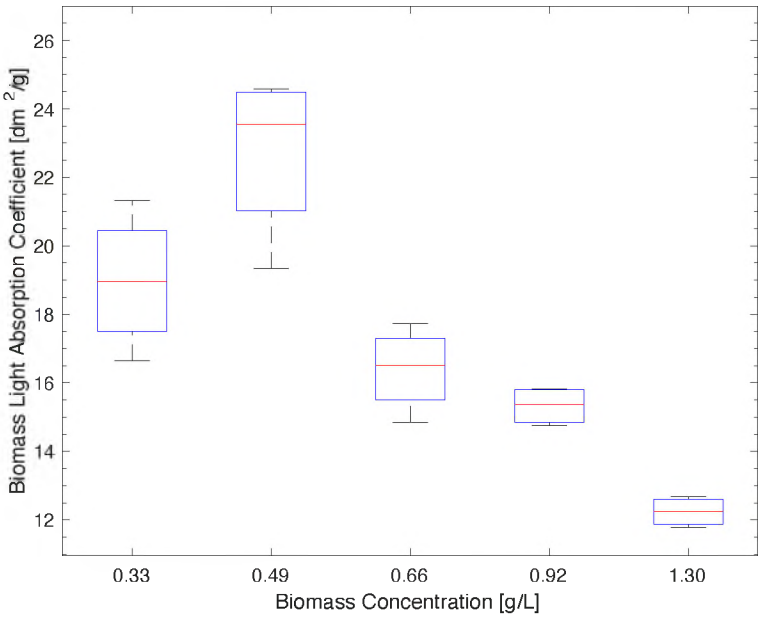

Figure 3-9: Biomass light absorption coefficient vs. biomass concentration. The average value of the factor was calculated to be 17.1 ± 3.88 [dm^2/g] for *C. sorokiniana* (DOE 1412). On each box, the central mark indicates the median, and the bottom and top edges of the box indicate the 25th and 75th percentiles, respectively. The plotted whisker extends to the most extreme data value. Each data set consists of five measurements, one measurement at each light intensity.

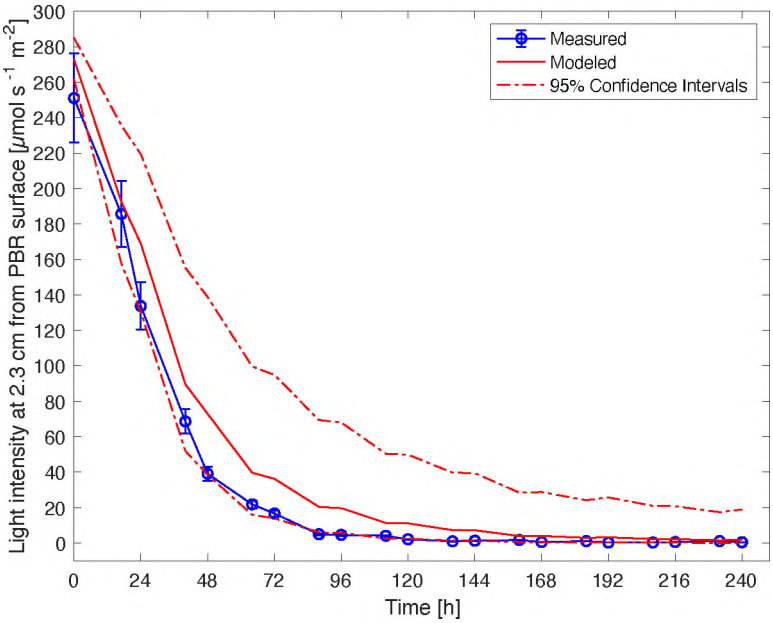

Figure 3-10: Validation of the light profile model. The figure illustrates a comparison between the measured light intensity using a calibrated photoresistor 2.3 cm from the PBR's surface during one of the growth experiments (16:8red, trial 1) and the predicted light intensity at the same distance from the surface, using **Eq. 2.5**, the measured biomass concentration X at each time point, and the k_a of 17.1 dm^2/g, and a surface intensity of 300 µmol s^{-1} m^{-2}. The error bars in the light intensity measurements reflect a 10% measuring error of the photoresistor.

3.3.5 Parameter Estimation

We used Simulink interactive blocks to create our mathematical models. Simulink Design Optimization™ was then used to analyze models' sensitivity, increase accuracy, and estimate parameters. The chosen estimated parameters are the combination of parameters that minimize the optimization cost function, which we selected to be the sum of the squared error (SSE). The optimization efforts to find the combination of parameters used nonlinear least squares optimization method, which used the 'Trust-Region-Reflective' algorithm. For the logistic model parameter estimation, the parameters were estimated for each experiment independently. In other words, each trial has its own set of estimated parameters. The initial guess for X_o was the first measured data point, the initial guess for the carrying capacity was the maximum value observed for biomass or cell

concentration, and the initial guess for the specific growth rate was the maximum observed specific growth rate between any two consecutive data points ($k = \frac{\ln\left(\frac{x_2}{x_1}\right)}{t_2 - t_1}$). Additionally, unpaired two-tailed t-tests were used, in Excel, to quantify whether parameters estimated from one data set statistically differ from other data sets.

Parameters of the light-limited models were estimated using a different technique from the logistic model parameters. First, the Monod equation parameters (μ_m and K_g) and light related biomass loss parameters ($k_{l,light}, k_{l,max}, and\ K_l$) from Eq. 3.4 and Eq. 3.6 were estimated from the second trial of the 24:0 experiment. Second, the second trial of the 16:8, along with already estimated parameters, were used to determine the dark period biomass loss rate ($k_{l,night}$). Finally, the constructed model was validated with the other trials of both experiments.

3.4 Summary of Experiments

The operating parameters and the initial and final cultivation conditions are summarized for each experiment in Table 3-1.

Table 3-1: Summary of experiments and cultivation conditions. In the table, M stands for *measured*, while NM stands for *not measured.*

Experiment	*24:0 (h:h)*	*24:0 (h:h)*	*16:8 (h:h)*	*16:8 (h:h)*	*16:8red (h:h)*	*16:8red (h:h)*
Trial no	1	2	1	2	1	2
Total Time [h]	216	216	258	267	240	240
Intensity at surface [$\mu mol\ s^{-1}m^{-2}$], M	300	300	330	300	300	300
Aeration rate [lpm]	1.1 ± 0.1	1.1 ± 0.1	1.1 ± 0.1	1.1 ± 0.1	1.1 ± 0.1	1.1 ± 0.1
CO_2:air ratio	1:10	1:10	1:10	1:10	1:10	1:10
Temperature [ºC]	30.0 ± 1.0	30.0 ± 1.0	30.0 ± 1.0	30.0 ± 1.0	30.0 ± 1.0	30.0 ± 1.0
Mixing rate [rpm]	200 ± 15	200 ± 15	200 ± 15	200 ± 15	200 ± 15	200 ± 15
pH (range for exp), M	6.41-7.84	5.97-8.42	5.81-5.85	5.94-7.11	5.36-7.21	6.28-6.68
NO_3^- (range for exp)[ppm]	NM	NM	NM	NM	1100-400	930-410
Biomass Conc. [g/L]	M	M	M	M	M	M
Initial [g/L], M	0.02	0.05	0.04	0.02	0.02	0.02
Final [g/L], M	1.340	1.401	1.306	1.251	1.286	1.220
Cell Conc. [cells/ml]	M	M	M	M	M	M
Initial [cells/mL], M	$3.4x10^6$	$7.5x10^6$	$5.5x10^6$	$5.1x10^6$	$2.2x10^6$	$2.3x10^6$
Final [cells/mL], M	$1.8x10^8$	$2.0x10^8$	$1.5x10^8$	$1.6x10^8$	$1.6x10^8$	$1.8x10^8$
Cell Size Distribution	M	M	M	M	M	M

CHAPTER IV

RESULTS AND DISCUSSION

4.1 Growth Curves

Repeatability of test results is critical in any study to ensure that the results are not mere artifacts and of an actual scientific significance. Repeatability is defined as "the closeness of agreement" between independent trials of the same experiment (same equipment, method, material, and observer) [75]. Additionally, repeatable results are critical and reliable for producing accurate, scalable models that define a system such as microbial growth models. In this study, the experiments, based on light availability, are divided into three categories:

1. 24:0 (h:h) light:dark cycle (continuously illuminated).
2. 16:8 (h:h) light:dark cycle.
3. 16:8 (h:h) white:red light cycle (nighttime supplementation with red LEDs).

Two repeats were performed per experiment. We concluded that the performed tests are repeatable by visually assessing the closeness of agreement between the trials' growth curves. The growth curves are presented in *Section 4.1.1* and *Section 4.1.2*. Measured

properties of light intensity, pH, nitrate concentration are presented in *Appendices I, J, and K.*

4.1.1 Biomass Based Growth Curves

Growth curves based on biomass concentration measurements are shown in Figure 4-1 to Figure 4-3. The biomass concentration was calculated by measuring the absorbance at 430 nm and 680 nm. Four measurements at each wavelength were converted to dry weight using a calibration curve. The average of eight biomass concentration measurements (four at each wavelength) was reported along with the standard deviation as the error bar for each data point (see procedure in *Section 3.2.3)*. In the 24:0 experiment, both trials of the experiment underwent exponential growth in the first two days, followed by a linear growth phase of about five days. The culture reached its carrying capacity, about 1.3 g/L, after nine days of cultivation. In the 16:8 experiment, shown in Figure 4-2, the carrying capacity approached the same carrying capacity as the continuously illuminated culture. However, due to biomass losses during the dark period, they required 11 cultivation days to reach the stationary phase, about 48 hours longer than the 24:0 experiments.

The observed nighttime biomass losses show signs of a relation to the biomass concentration. It starts with minute losses at the beginning of the batch and become more pronounced with time. When the ordinarily dark period is illuminated with low-intensity red light, as shown in Figure 4-3, the small biomass losses are often replaced with biomass gain. As biomass concentration increases and the low-intensity red light fails to penetrate deep into the culture, although no net gain in biomass is observed, the supplementation with red light seems to prevent biomass loss. Additionally, in the 16:8red experiment, the carrying capacity was reached in 232 cultivation hours, which saved more than one

cultivation day when compared to the 16:8 experiment. An economic analysis is needed to determine whether illuminating the culture with low-consumption red LEDs at low surface intensity (150 µmol s^{-1} m^{-2}) for nine consecutive dark periods (72 hours) is more economical than operating the entire cultivation system for an additional day. Operating the system would include temperature control, mixing, aeration, computer systems, labor, and other expenses. In all three experimental setups, the data were very reproducible among the replicate trials.

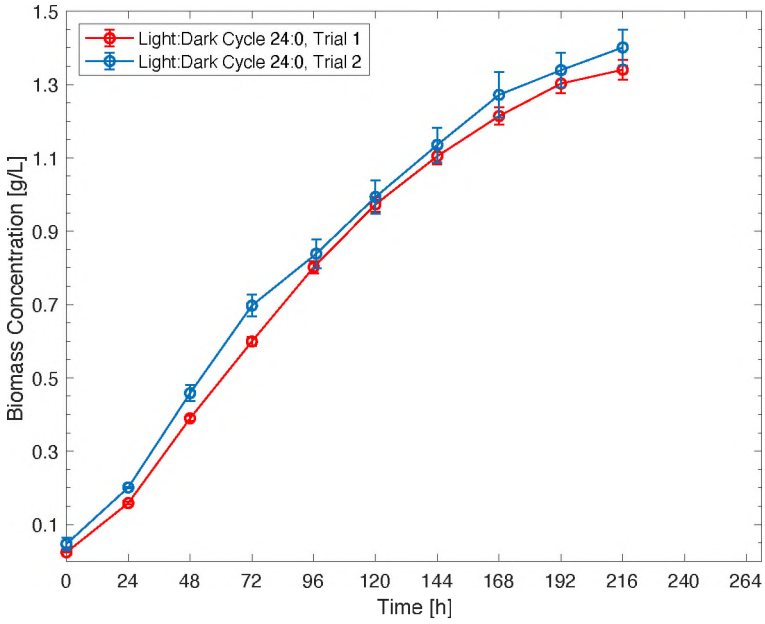

Figure 4-1: Biomass growth curves for 24:0 (h:h) light:dark cycle. Each data point reflects the mean biomass concentration [g/L], which is calculated by converting absorbance results of four measurements at 430 nm and 680 nm to biomass concentration using a calibration curve. The average of the total eight measurements is reported as the biomass concentration, and the error bars represent the standard deviations of the measurements.

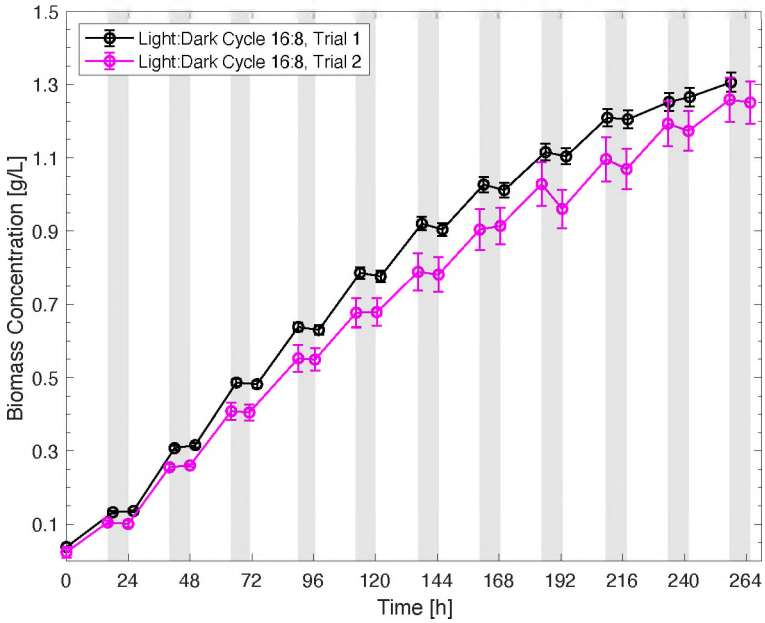

Figure 4-2: Biomass growth curves for 16:8 (h:h) light:dark cycle. The shaded area represents the dark period. Each data point reflects the mean biomass concentration [g/L], which is calculated by converting absorbance results of four measurements at 430 nm and 680 nm to biomass concentration using a calibration curve. The average of the total eight measurements is reported as the biomass concentration, and the error bars represent the standard deviations of the measurements.

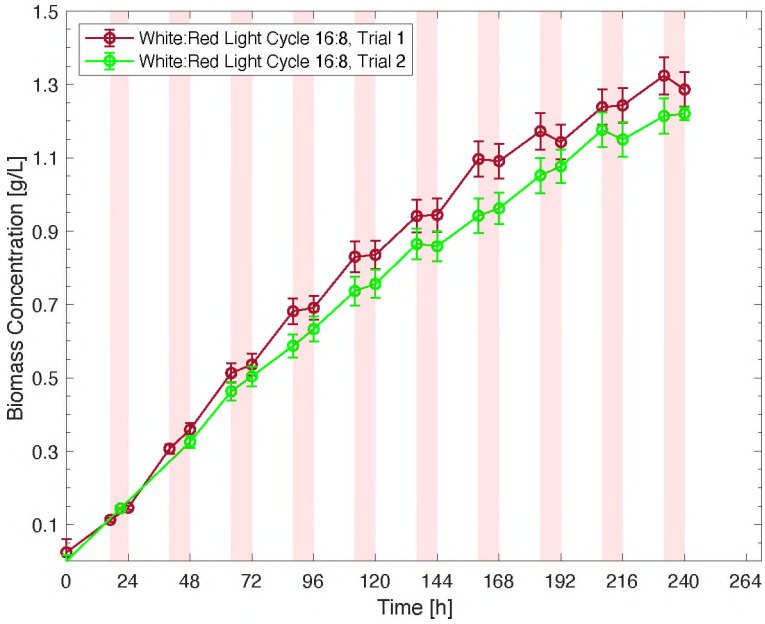

Figure 4-3: Biomass growth curves for 16:8 (h:h) white:red light cycle. The shaded area represents the period of red light. Each data point reflects the mean biomass concentration [g/L], which is calculated by converting absorbance results of four measurements at 430 nm and 680 nm to biomass concentration using a calibration curve. The average of the total eight measurements is reported as the biomass concentration, and the error bars represent the standard deviations of the measurements.

4.1.2 Cell Concentration Based Growth Curves

Cell concentration growth curves are presented in Figure 4-4 and Figure 4-6. Unlike biomass concentration growth curves, cell concentration data show much greater scatter, making it harder to extract information on the effect of the dark period on cell replication. Similar to the biomass growth curves, the cell culture, under continuous illumination with white light, required about nine days to reach the stationary phase with a carrying capacity of about $2.0x10^8$ cells/mL, as shown in Figure 4-4. On the contrary, the cell cultures that experienced an 8-hour daily dark period, shown in Figure 4-5, had a maximum cell concentration of about $1.6x10^8$ cells/mL after 11 cultivation days. The results indicate a much lower cell replication rate under the latter cultivation conditions. Figure 4-6 demonstrates that illuminating the dark period with red light significantly enhances cell replication. The culture reached its carrying capacity in as little as 6-7 days. The results are significant because they may imply that illumination with red light is only needed for the first 6 nights. The findings open the question of whether illuminating the remaining nights with blue or white light will induce biomass accumulation in the already existing cells and further reduce the total cultivation time.

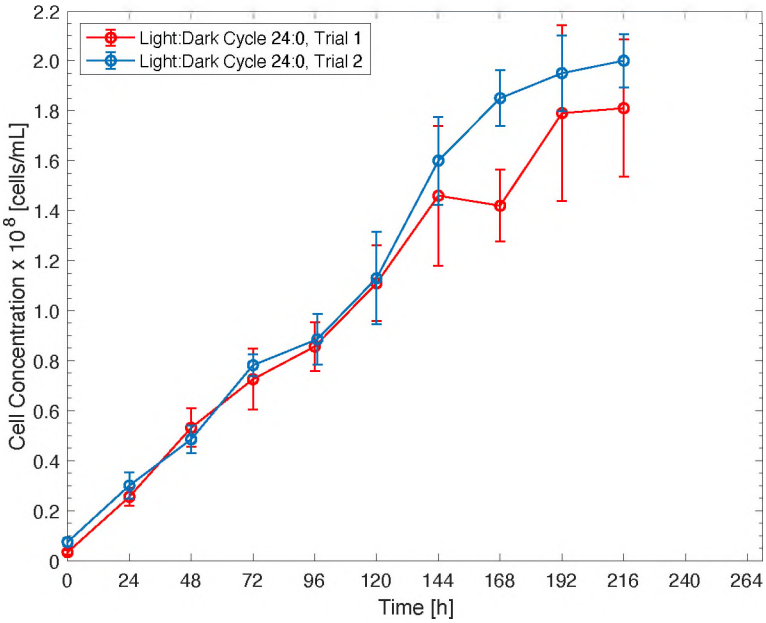

Figure 4-4: Cell concentration growth curves for 24:0 (h:h) light:dark cycle. Each data point reflects the mean cell concentration of the cell suspension. The mean cell concentration is calculated by averaging five measurements of cell concentration measured using five different 0.04 mm^2 hemocytometer grids. The error bars represent the standard deviation of the five measurements.

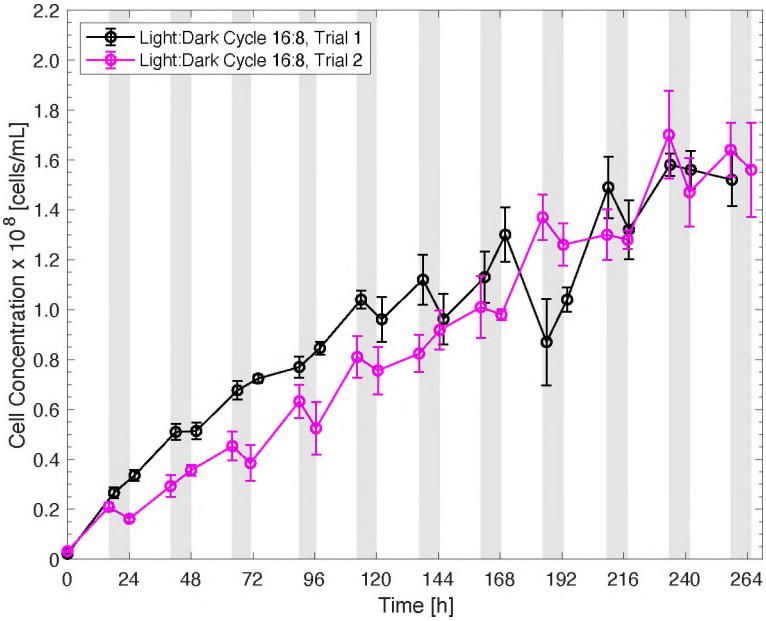

Figure 4-5: Cell concentration growth curves for 16:8 (h:h) light:dark cycle. The shaded area represents the dark period. Each data point reflects the mean cell concentration of the cell suspension. The mean cell concentration is calculated by averaging five measurements of cell concentration measured using five different 0.04 mm^2 hemocytometer grids. The error bars represent the standard deviation of the five measurements.

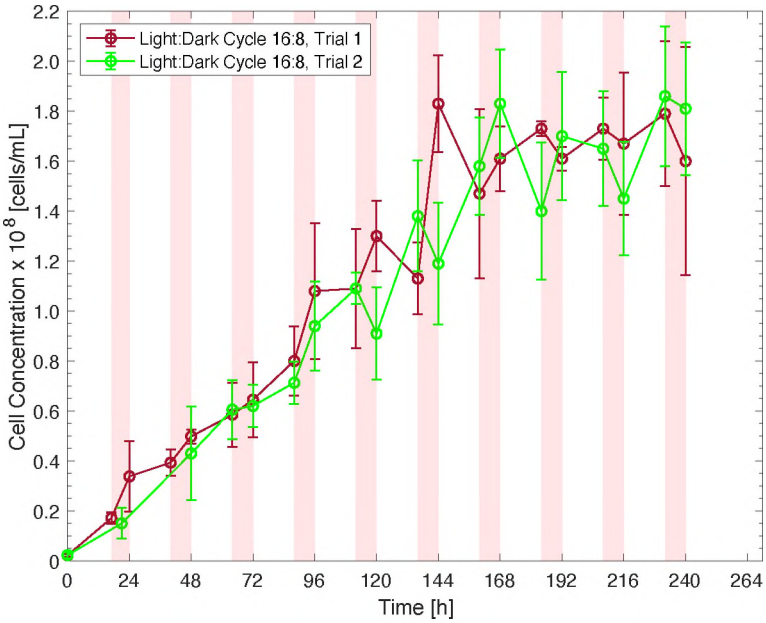

Figure 4-6: Cell concentration growth curves for 16:8 (h:h) light:red light cycle. The shaded area represents the period of red light. Each data point reflects the mean cell concentration of the cell suspension. The mean cell concentration is calculated by averaging five measurements of cell concentration measured using five different 0.04 mm^2 hemocytometer grids. The error bars represent the standard deviation of the five measurements.

4.1.3 Cell Size Distribution

The size distribution of cells as a function of time is presented by the following figures. During a 24:0 experiment (Figure 4-7), no significant change in the size distribution was observed with an average size of about 2.0-2.2 µm in diameter. On the contrary, during a 16:8 experiment (Figure 4-8), a drop in the average cell size is observed over the dark period. The reduction in cell volume is most likely due to biomass loss during nighttime. Additionally, during the first four nights, the decrease in cells' average diameter is far more significant than the drop in size in later nights of the cultivation cycle. This may be attributed to a higher replication rate during the early stage of the culture. In other words, more frequent cell division will yield to smaller cells. During a 16:8red experiment, since no biomass loss is observed from the growth curves, and cell replication happened during

both white and red light periods, we expect to see random fluctuations in average cell size around a mean value, which can observed from Figure 4-9.

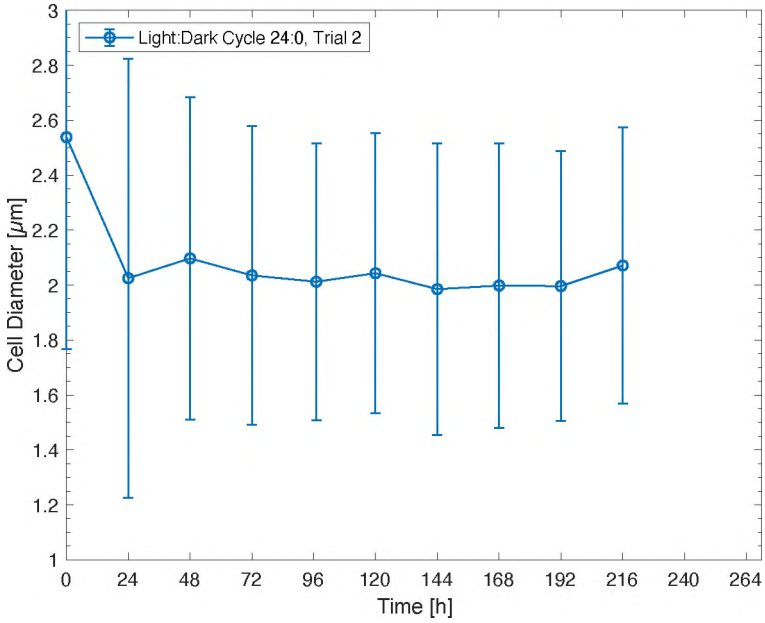

Figure 4-7: Cell size variations with time during a continuous illumination experiment.

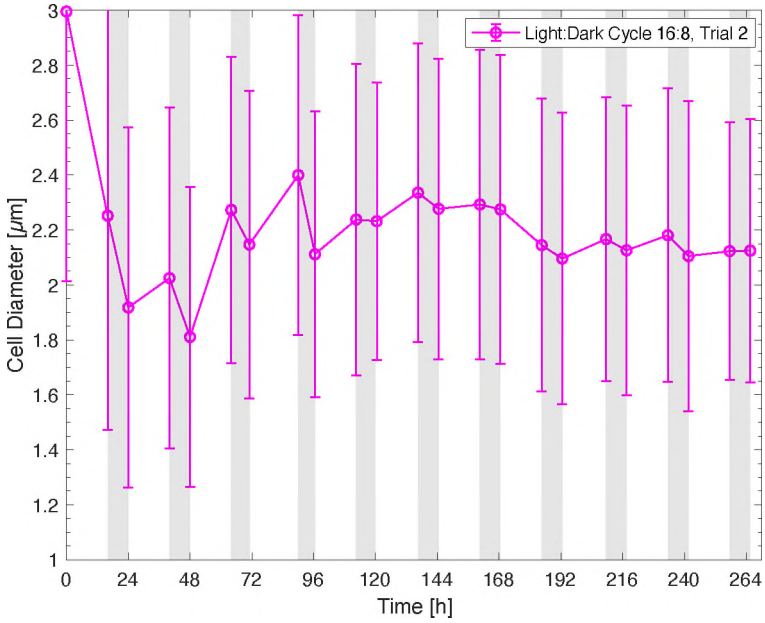

Figure 4-8: Cell size variations with time during a 16:8 experiment.

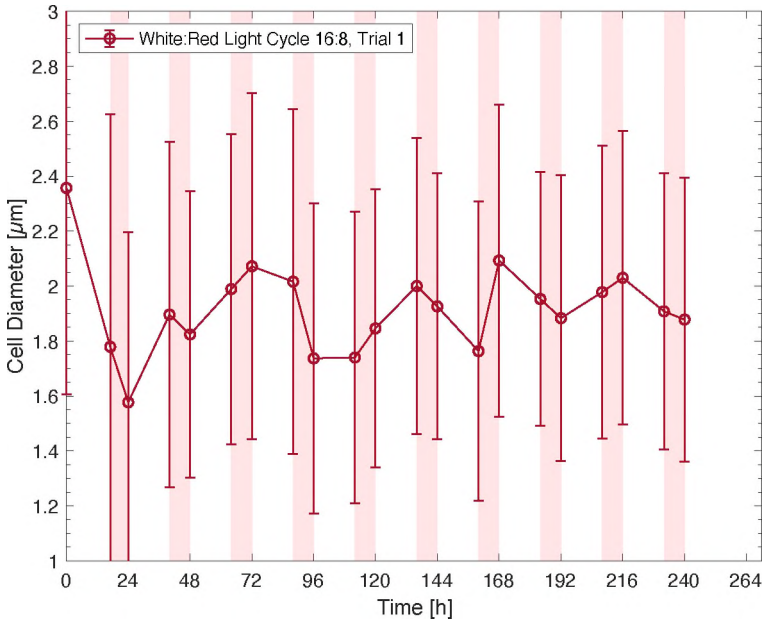

Figure 4-9: Cell size variations with time during a 16:8red experiment.

4.2 Nighttime Biomass Loss

During the nighttime, microalgae dip into their internal energy reservoirs to survive the night. The amount of biomass lost overnight increased with time, which we first inferred from Figure 4-2, and can be seen in Figure 4-10, which illustrates changes in biomass concentration during the dark period with time. The overall trend shows greater losses later in the cultivation period when compared to the first three nights. This finding indicates a relationship between biomass loss and biomass concentration. In Figure 4-11, the two boxplots represent the nighttime biomass loss as a percentage of the biomass gain in the preceding light period for both trials of the 16:8 experiment. On each box, the central mark indicates the median, and the bottom and top edges of the box indicate the 25th and 75th percentiles, respectively. The plotted whisker extends to the most extreme data value that is not an outlier. The overlapping boxes show that the reported medians for each data set do not statistically differ, and both trials yield the same finding. Since the decline appears

to be a fixed percentage of the biomass concentration, it strengthens our assumption of a constant biomass loss rate during the dark period $k_{l,night}$.

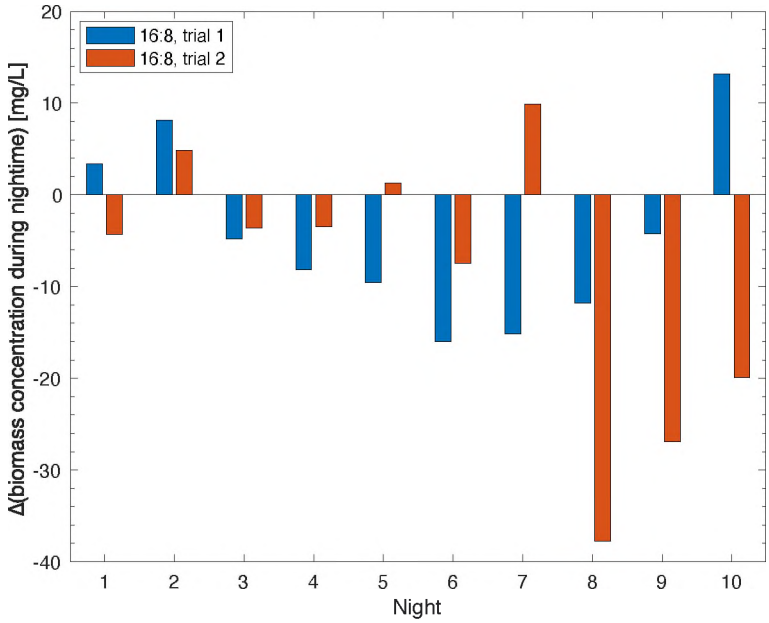

Figure 4-10: Biomass loss during nighttime. The figure illustrates changes in the biomass concentration for daily dark periods. Although a lot of discrepancy exists, the overall trend shows greater losses with time. On this figure, change in biomass concentration is illustrated, a positive value represents biomass gain, and a negative value represents biomass loss.

The results indicate that 5% ± 7% of the biomass gained during the 16-hour day period is lost due to respiration during the 8-hour night period. The results are comparable to a study that reported nighttime biomass loss ranging from 2% to 20% for *C. sorokiniana* under a 14:10 (h:h) light:dark cycle at 24°C [14]. During the dark period, the lack of light makes photosynthesis infeasible. In the growth media, there is no organic carbon source that the cells can use to build up mass. For those two reasons, the biomass concentration cannot increase overnight, yet some data suggest net gain in mass, which is shown by the negative values presented in Figure 4-11. We believe that it is due to a human or equipment error, such as pipetting from the bottom of a cuvette that contains a sample that is not well mixed. Although it is perceived as an error, the value is not far enough from the median to

be an outlier (+/- 2.7 standard deviations from the median), which is the reason why the data are included in the biomass loss figure.

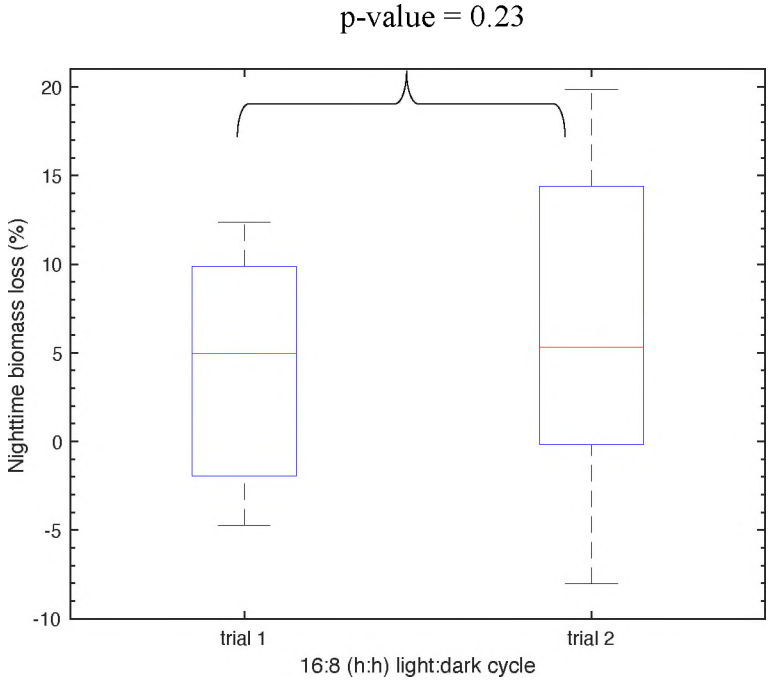

Figure 4-11: Nighttime biomass loss. The figure illustrates the biomass lost during the 8-hour dark period as a percentage of the biomass gain in the preceding 16-hour day period. The average nighttime biomass loss percentage was 5% ± 7%. On each box, the central mark indicates the median, and the bottom and top edges of the box indicate the 25th and 75th percentiles, respectively. The plotted whisker extends to the most extreme data value that is not an outlier, and the outliers are plotted individually using the '+' symbol. A data point is considered an outlier if it is more than (+/-) 2.7 standard deviations away from the median. The overlapping boxes for the two trials indicate, with 95% confidence, that the two populations do not significantly differ. The corresponding p-value of this visual test is 0.23 (p-value>0.05).

Although the percentage of losses may seem low, the losses can accumulate and have a devastating effect on the overall biomass productivity. A comparison between the growth responses of the cultures illuminated at a 16:8 (h:h) light:dark intervals and the continuously illuminated cultures, presented in Figure 4-12, show that the daily 8-hour dark period leads to a 16% ± 5% lower biomass yield over a cultivation period of nine days. We chose to compare the responses of both experiments at that specific time point because it marks the time needed for the continuously illuminated culture to reach the stationary phase in this cultivation system.

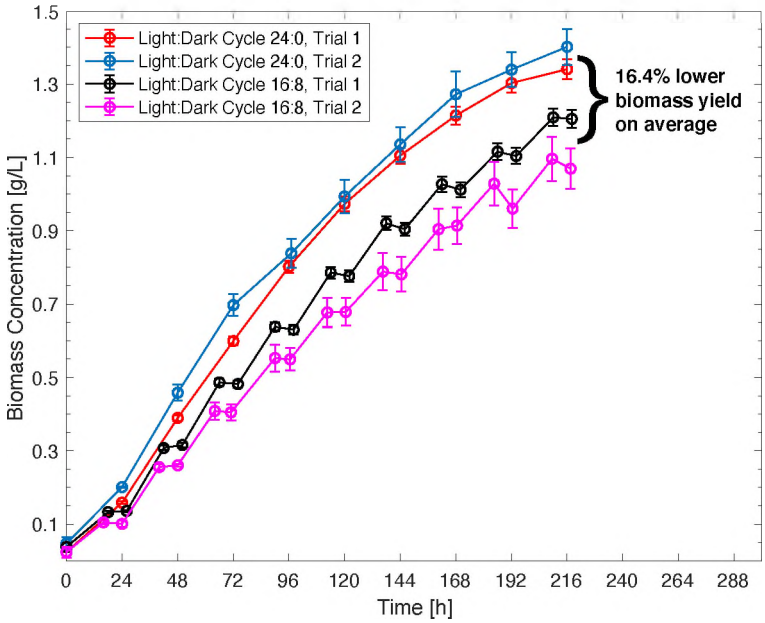

Figure 4-12: Dark period lead to lower biomass yield. 16:8 (h:h) light:dark cycle resulted in a 16.4% ± 5.3% lower biomass yield compared to a continuously illuminated culture.

4.2.1 Mitigating the effect of the dark period using artificial red LEDs

Many methods have been proposed to mitigate the effect of the dark period. The most commonly used approach consists of growing microalgae heterotrophically during nighttime by supplementing the culture with an organic carbon source. We view that method as an inadequate solution for two reasons. First, it utilizes organic carbon sources, such as glucose, which are considered food sources. Second, it exposes the microalgae culture to a higher risk of contamination, which may be more crippling than the dark period itself. In this study, we explored the possibility of preventing or at least mitigating nighttime biomass losses by artificially illuminating the culture with low consumption red LEDs at low intensities.

Figure 4-13 is a boxplot that illustrates the benefit of red light illumination during the dark period. The central mark on each box represents the median of the data set. The median has shifted from a 5% average biomass loss during the 8-hour dark period to net

gains (negative value on the plot) of -4% and -22% during the 8-hour red light illuminated periods of the two experiments (p-value=0.01). A lot of scattering is observed in the data, especially the plot that shows the results from the two trials of the 16:8 (h:h) white:red light cycle. The two populations at 16:8 (h:h) white:red light cycle do not vary, with 95% confidence, as given by an unpaired two-tail t-test (p-value = 0.11). Since both medians yielded a negative value for loss, we can conclude that artificially illuminating the 8-hour dark period with red LEDs prevents biomass loss.

Additionally, by examining the growth curves in Figure 4-3, we can conclude that red illumination did not only prevent biomass loss but promoted biomass accumulation in the early stages of the batch (Figure 4-14), where the red light can still penetrate deep into the culture. Furthermore, illuminating the dark period with red light significantly enhanced cell replication, as shown in Figure 4-6. Although the results are promising, an economic analysis must be done to prove the method feasible and less costly than prolonged cultivation.

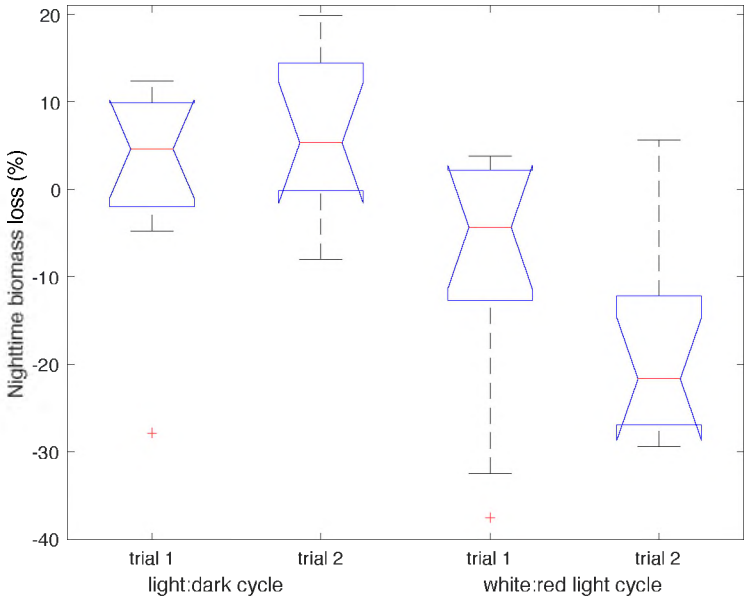

Figure 4-13: The effect of red light on nighttime biomass loss. The first two boxplots illustrate the biomass lost during the 8-hour dark period as a percentage of the biomass gain in the preceding 16-hour day period. The average nighttime biomass loss percentage was 5% ± 7%. The other two boxplots show the effect of red light on nighttime biomass loss. When illuminating the dark period with red LEDs, a net gain in biomass was observed. On each box, the central mark indicates the median, and the bottom and top edges of the box indicate the 25th and 75th percentiles, respectively. The plotted whisker extends to the most extreme data value that is not an outlier, and the outliers are plotted individually using the '+' symbol. A data point is considered an outlier if it is more than (+/-) 2.7 standard deviations away from the median.

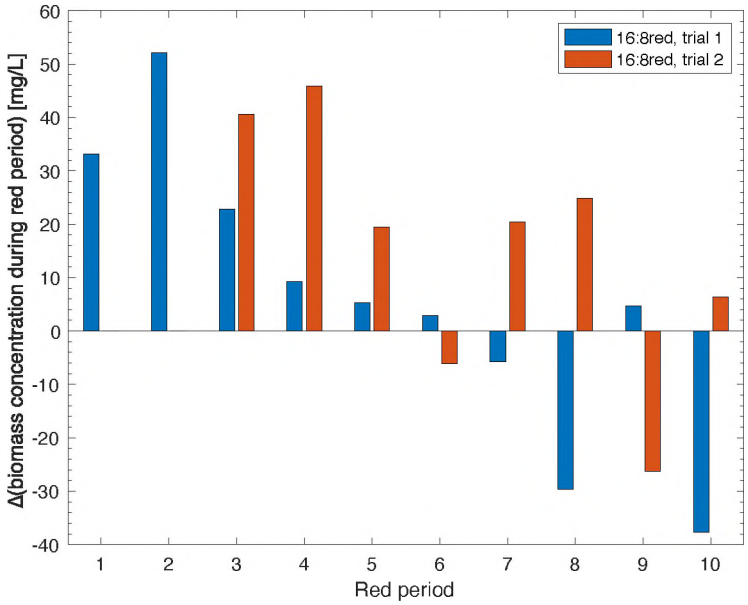

Figure 4-14: The effect of red period on biomass. The bar graph shows how the red period enhances the accumulation of biomass in the early stages of cultivation. With time, the red light fails to penetrate deep into the system, which lead to a decrease in biomass gain, and eventually losses. On this figure, a positive value represents a gain in biomass concentration.

4.2.2 The Effect of the Dark Period on Cell Concentration

The effect of the dark period on biomass is much more predictable than the impact of the dark period on cell replication. We know that the biomass concentration should either stay constant or decrease overnight due to the absence of carbon fixation by photosynthesis and the lack of organic carbon sources in the growth media. The effect of the dark period on the cell concentration, as opposed to biomass, is much more complicated. One study from the literature with *Neochloris oleoabundans*, showed that cell replication dominantly occurred during the first few hours after sunset due to processes like DNA replication and cell division being UV sensitive. However, the study reported cell replication during the day as well [76]. Another study showed an increase in cell concentration only during the dark period [77]. In our study, a significant increase in cell concentration was observed during the day, as can been seen in Figure 4-5. During the dark period, the data shows both increases and decreases in cell concentration (Figure 4-15). The two trials of the 16:8 (h:h) light:dark cycle show somewhat of a symmetric boxplot around 0%. However, due to great discrepancies in the data, we cannot infer whether a significant change in cell concentration is observed overnight. Hourly samples may be beneficial in determining how the cell concentration changes during both the day and night periods.

On the other hand, all data from the first trial of the 'red' experiment indicated gains in cell concentration, plus the median and the top 75 percentile of the second trial's data also fell in the positive region. We conclude that illuminating the dark period with red LEDs, even at low surface intensity, significantly enhances cell replication. A quantified analysis, using the logistic model, to determine the effect of light:dark photoperiods on cell replication is presented in *Section 4.3.2.*

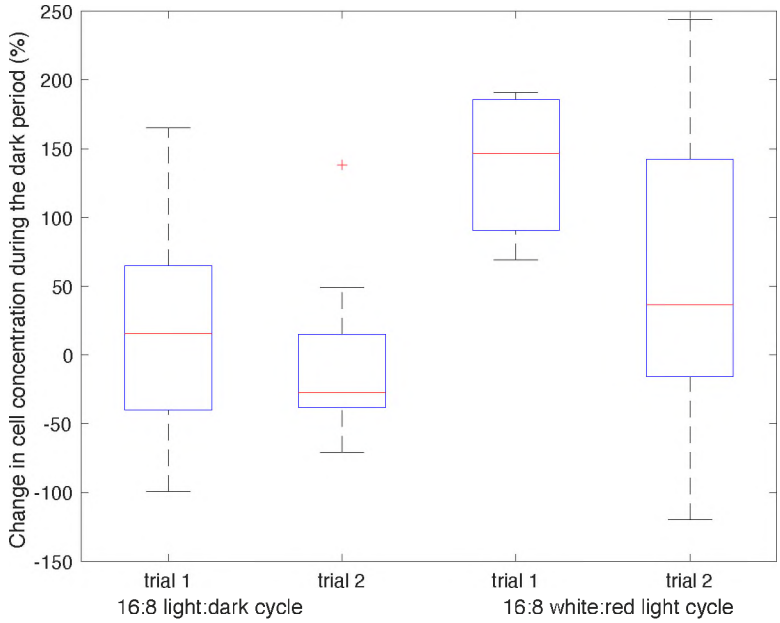

Figure 4-15: The effect of the dark period vs. red illumination on cell replication. The figure illustrates changes in cell concentration over the 8-hour dark period or the 8-hour red period as a percentage of the gain in cell concentration in the preceding day period. On each box, the central mark indicates the median, and the bottom and top edges of the box indicate the 25th and 75th percentiles, respectively. The plotted whisker extends to the most extreme data value that is not an outlier, and the outliers are plotted individually using the '+' symbol. A data point is considered an outlier if it is more than (+/-) 2.7 standard deviations away from the median.

4.3 The Logistic Model

4.3.1 Biomass Concentration

The logistic model is a simple model of population growth. Although it does not provide any information on how the light or other nutrients affect the growth of microalgae *C. sorokiniana*, it gives insight on the maximum biomass concentration a culture can sustain under specific cultivation conditions. It also provides a measure of the growth rate, which is inversely related to the time needed to reach the carrying capacity. The equation for the growth specific growth rate given by the logistic model is presented:

$$\frac{dX}{dt} = \mu_{net} X \qquad \textbf{Eq. 2.1}$$

$$\mu_{net} = \mu_g = k\left(1 - \frac{X}{X_\infty}\right) \qquad \textbf{Eq. 3.1}$$

where,

X: cell mass concentration [g/L].

k: the maximum specific growth rate [h^{-1}].

X_∞: carrying capacity [g/L].

The logistic equation was fitted to both trials of all three experiments, as shown in Figure 4-16 to Figure 4-21. The model is a good fit for the linear phase of the growth curve and well represents the carrying capacity of the system. However, the model fails to represent the exponential growth phase at the beginning of the batch. The model, using the evaluated parameters, underestimates the growth response of a system. The average estimated specific growth rates (k) are 0.020 h^{-1}, 0.022 h^{-1}, and 0.028 h^{-1} for experiments 16:8 light:dark cycle, 16:8 white:red light cycle, 24:0 light:dark cycle, respectively. The growth rate increased with increasing light availability as expected. The results also show that illuminating the dark period with low-consumption red LEDs enhances growth. An unpaired t-test shows, with 95% confidence, that the growth rates do differ from one experimental condition to the other with continuous illumination yielding the highest growth rate (p-value<0.05). The evaluated growth rates are slightly higher than what is reported in the literature (0.016 - 0.019 h^{-1}, Table 2-1). The difference is expected and can be mainly attributed to the fact that the reported data was from 12:12 (h:h) light:dark cycle experiments.

An unpaired two-tail t-test shows that the carrying capacity of a 16:8 (h:h) light:dark cycle culture does not significantly differ from the carrying capacity of a continuously

illuminated culture (p-value>0.05),see Table 4-1. We conclude that prolonged cultivation of the 16:8 (h:h) light:dark cycle culture will yield the same final biomass concentration as a 16:8 white:red light cycle and a continuously illuminated culture. In our five-liter batch reactor, operating at 30°C and 300 μmol $s^{-1}m^{-2}$ incident light intensity, the continuously illuminated culture required nine cultivation days to reach the carrying capacity while the 16:8 (h:h) light:dark cycle culture required 11 days. In reality, a continuously illuminated culture would not exist, and the availability of sunlight constrains the light:dark photoperiods. On average, sunlight is available for about 12 hours a day, year-round at the equator. If we must cultivate microalgae at a light:dark cycle of about 12:12 (h:h), we should expect even more devastating nighttime biomass losses, and prolonged cultivation becomes more critical. However, an economic analysis is needed to determine whether operating the system for a more extended period is justified for the added benefit.

Table 4-1: Biomass growth curves: the logistic model parameters, p-values, and goodness of fits

Experiment		*The Logistic Growth Model*			
L:D cycle	trial no	k [h^{-1}]	X_o [g/L]	X_∞ [g/L]	*SSE*
24:0 (h:h)	1	0.030	0.11	1.34	$8.7x10^{-3}$
24:0 (h:h)	2	0.027	0.14	1.40	$1.3x10^{-2}$
16:8 (h:h)	1	0.022	0.13	1.31	$4.2x10^{-2}$
16:8 (h:h)	2	0.019	0.13	1.28	$5.9x10^{-2}$
16:8 (red)	1	0.024	0.13	1.31	$4.7x10^{-3}$
16:8 (red)	2	0.021	0.13	1.27	$4.2x10^{-2}$
p-value (24:0, 16:8)		0.05	0.73	0.23	
p-value (24:0, red)		0.088	0.59	0.18	
p-value (16:8, red)		0.40	0.28	0.78	

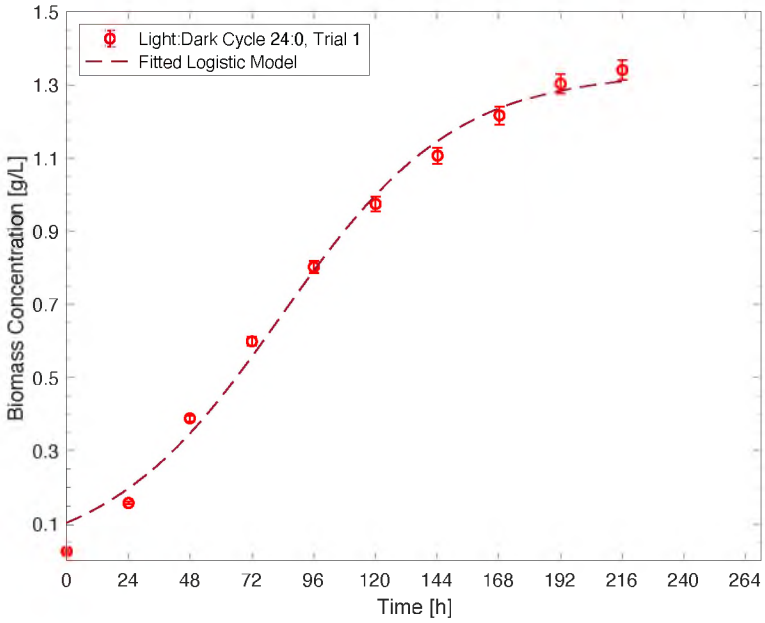

Figure 4-16: Fitted logistic model to trial 1 of the 24:0 (h:h) light:dark cycle experiment.

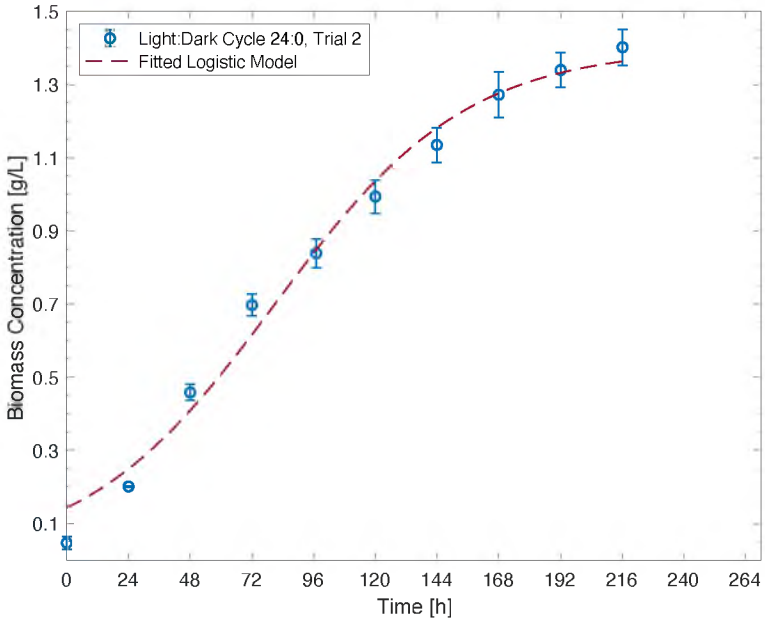

Figure 4-17: Fitted logistic model to trial 2 of the 24:0 (h:h) light:dark cycle experiment.

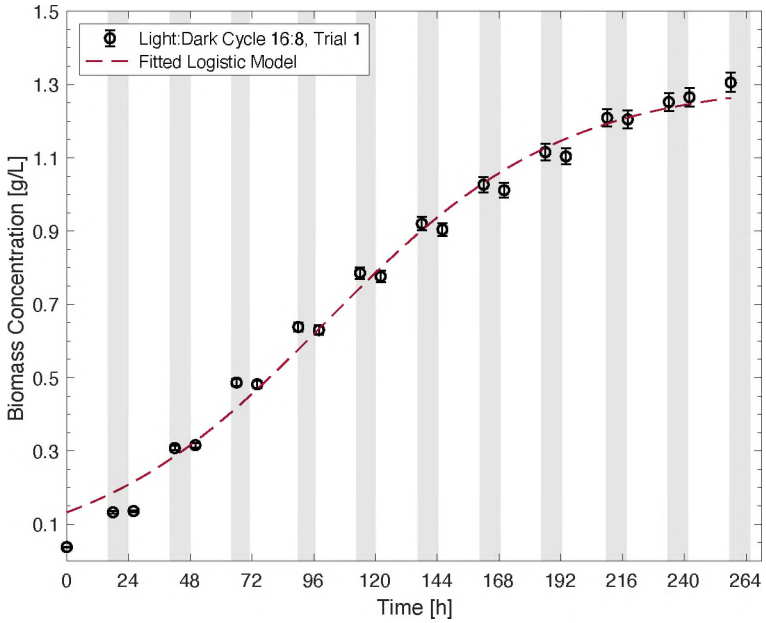

Figure 4-18: Fitted logistic model to trial 1 of the 16:8 (h:h) light:dark cycle experiment.

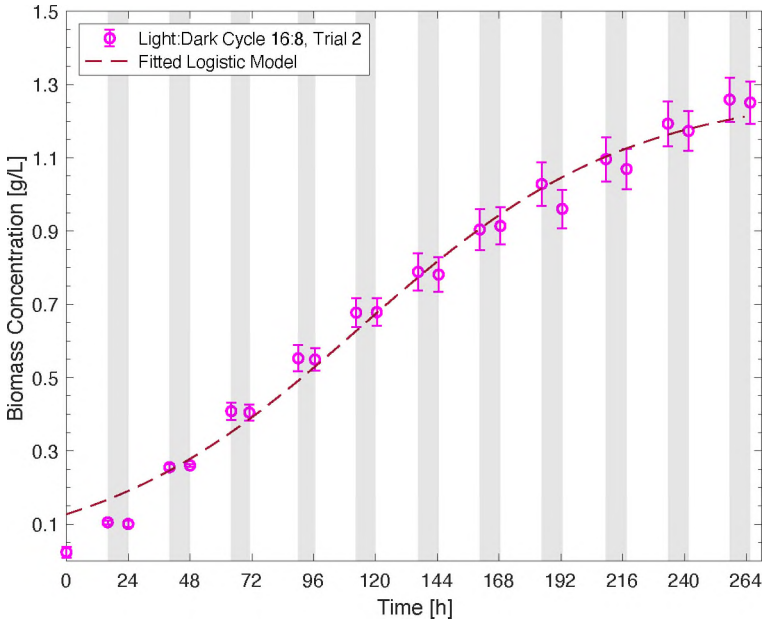

Figure 4-19: Fitted logistic model to trial 2 of the 16:8 (h:h) light:dark cycle experiment.

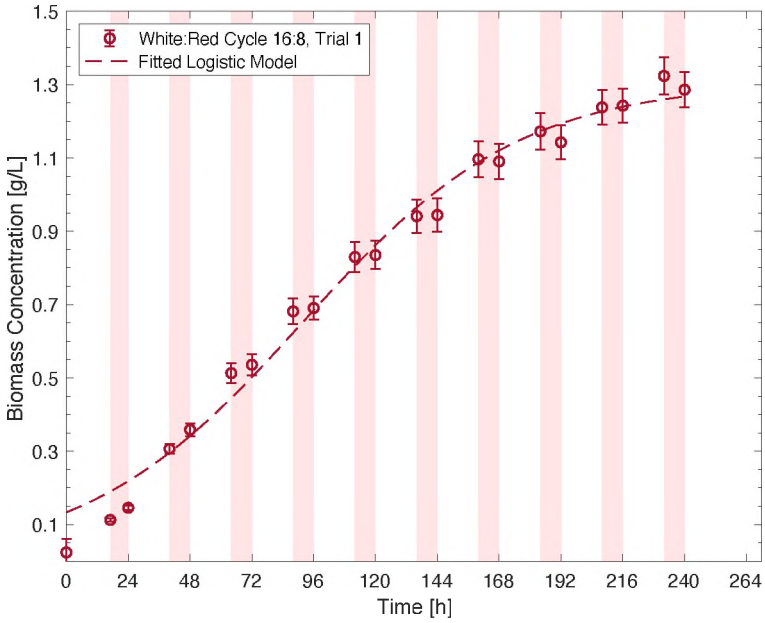

Figure 4-20: Fitted logistic model to trial 1 of the 16:8 (h:h) white:red light cycle experiment.

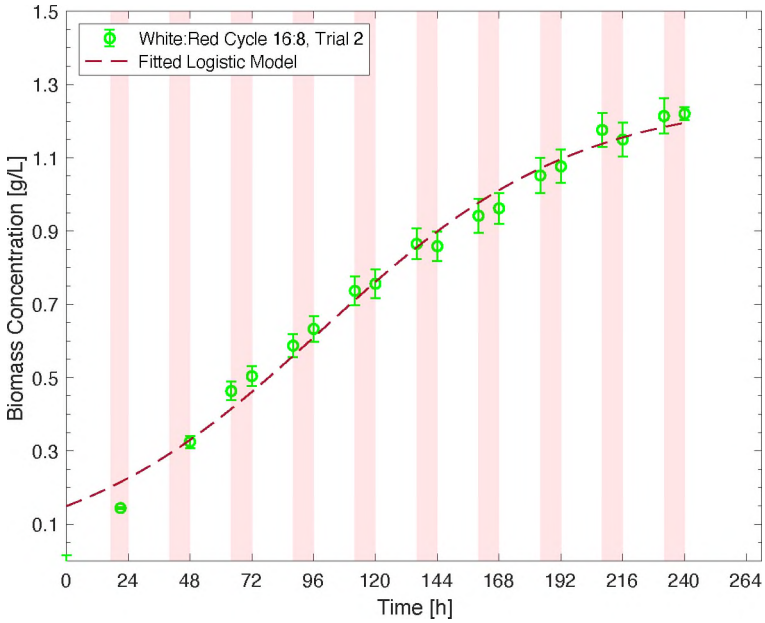

Figure 4-21: Fitted logistic model to trial 2 of the 16:8 (h:h) white:red light cycle experiment.

4.3.2 Cell Concentration

Fitting the logistic equation to the cell concentration growth curves will determine the maximum cell concentration a culture can sustain and allow us to compare the effect of

different cultivation conditions on cell replication rate. The specific replication rate can be given by an equation analogous to that used in *Section 4.3.1:*

$$\frac{dC}{dt} = \mu_{net}\, C \qquad \textbf{Eq. 2.1}$$

$$\mu_{net} = \mu_r = k\left(1 - \frac{C}{C_\infty}\right) \qquad \textbf{Eq. 3.1}$$

where,

μ_r: specific replication rate [h^{-1}].

C: cell concentration [cells/mL].

k: the maximum specific growth rate [h^{-1}].

C_∞: carrying capacity [cells/mL].

The fitted logistic model to both trials of all three experiments is shown in Figure 4-22 to Figure 4-27. Although the model well represents the majority of the data and yields a low sum squared error (Table 4-2), the logistic model fails at representing the initial period of the batch, as we have seen with biomass growth curves. For that reason, we conclude that the logistic model is inadequate for scaleup and reactor design. However, the logistic model is still useful for extracting critical information such as the carrying capacity and the growth rate of the culture. The model shows that the carrying capacity of the culture does not differ from one experimental condition to another, as shown by the p-values in Table 4-2, but how quickly the culture reaches that carrying capacity is what was affected by the different cultivation conditions. We expected that the cell replication rate would be highest when cultivated with red light, and that is precisely what the logistic model is illustrating. The estimated replication rates are 0.027 h^{-1}, 0.023 h^{-1}, and 0.015h^{-1} for 16:8 white:red light cycle, 24:0 light:dark cycle, and 16:8 light:dark cycle. The findings suggest that the dark

period crippled cell replication, and illuminating with red LEDs can almost double the cell replication rate.

The estimated parameters show that the 16:8 white:red light cycle yielded 1.2 times higher cell replication rate than a continuously illuminated culture with white light. Although illuminated for only 8-hour periods daily with a red light at a surface intensity equal to half that of the white light (150 as compared to 300 μmol s^{-1} m^{-2}), the red experiment still yielded 1.2 times higher replication rate. All in all, illuminating the dark period with red LEDs, even at a low light intensity, has proved capable of preventing nighttime biomass loss and enhancing cell replication and effectively cutting down cultivation time.

Table 4-2: Cell concentration: the logistic model parameters, p-values, and goodness of fits.

Experiment		*The Logistic Growth Model*			
L:D cycle	trial no	k [h^{-1}]	C_o [cells/mL]	C_∞ [cells/mL]	*SSE*
24:0 (h:h)	1	0.022	$1.8x10^7$	$1.95x10^8$	$2.29x10^{-2}$
24:0 (h:h)	2	0.023	$1.7x10^7$	$2.23x10^8$	$1.46x10^{-1}$
16:8 (h:h)	1	0.015	$3.0x10^7$	$1.64x10^8$	$3.25x10^{-1}$
16:8 (h:h)	2	0.016	$1.7x10^7$	$1.85x10^8$	$1.13x10^{-1}$
16:8 (red)	1	0.029	$1.4x10^7$	$1.75x10^8$	$1.79x10^{-1}$
16:8 (red)	2	0.025	$1.4x10^7$	$1.79x10^8$	$2.04x10^{-1}$
p-value (24:0, 16:8)		0.03	0.55	0.19	
p-value (24:0, red)		0.21	0.08	0.26	
p-value (16:8, red)		0.05	0.38	0.84	

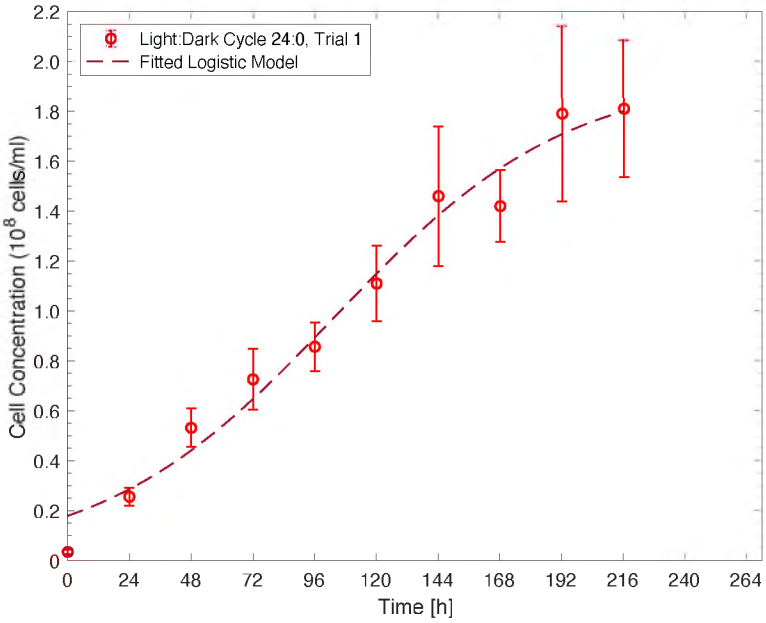

Figure 4-22: Fitted logistic model to the first trial's cell concentration curve of the 24:0 light:dark cycle experiment.

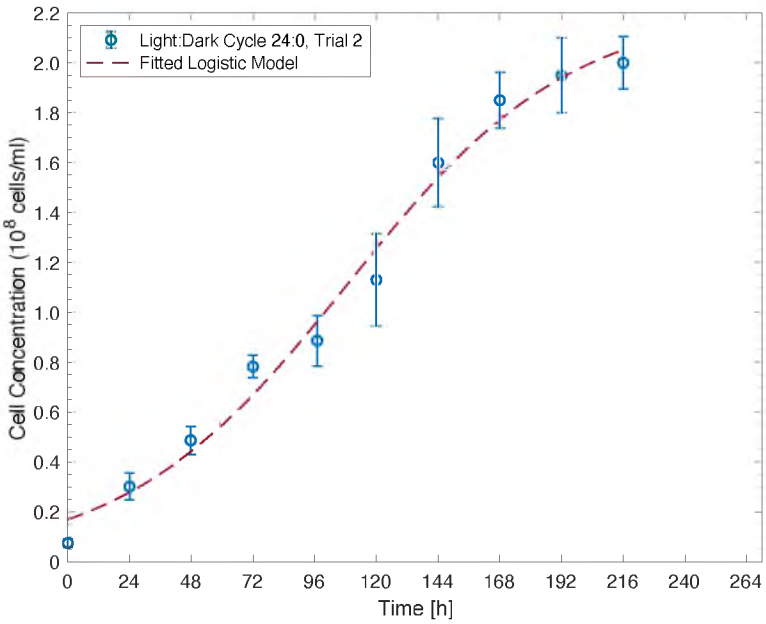

Figure 4-23: Fitted logistic model to the second trial's cell concentration curve of the 24:0 light:dark cycle experiment.

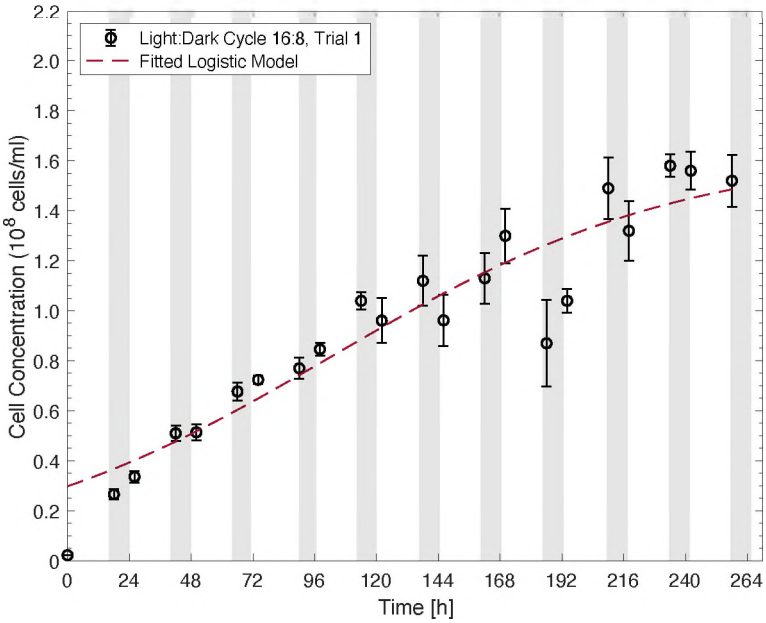

Figure 4-24: Fitted logistic model to the first trial's cell concentration curve of the 16:8 light:dark cycle experiment.

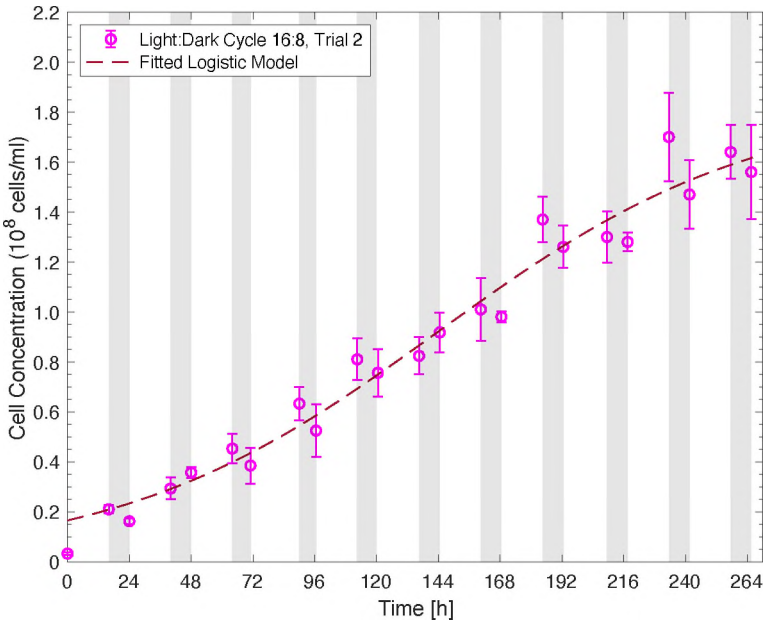

Figure 4-25: Fitted logistic model to the second trial's cell concentration curve of the 16:8 light:dark cycle experiment.

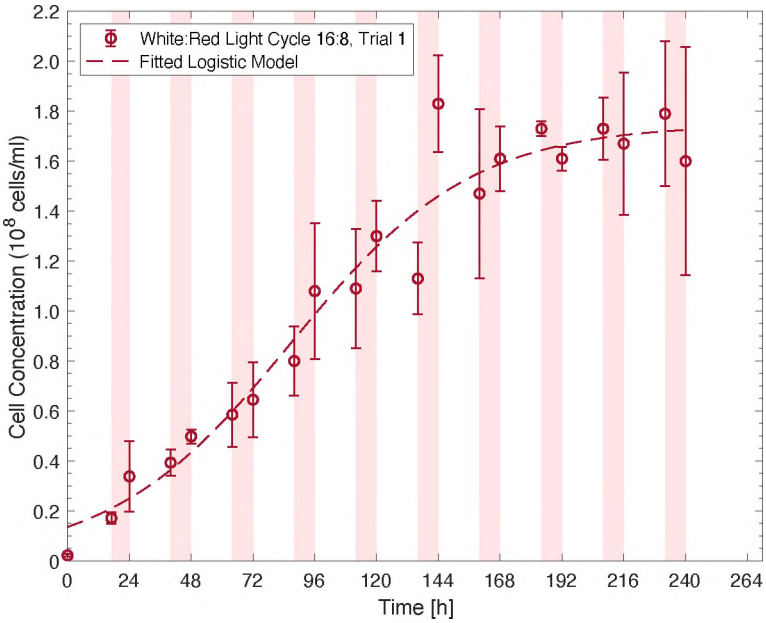

Figure 4-26: Fitted logistic model to the first trial's cell concentration curve of the 16:8 white:red light cycle experiment.

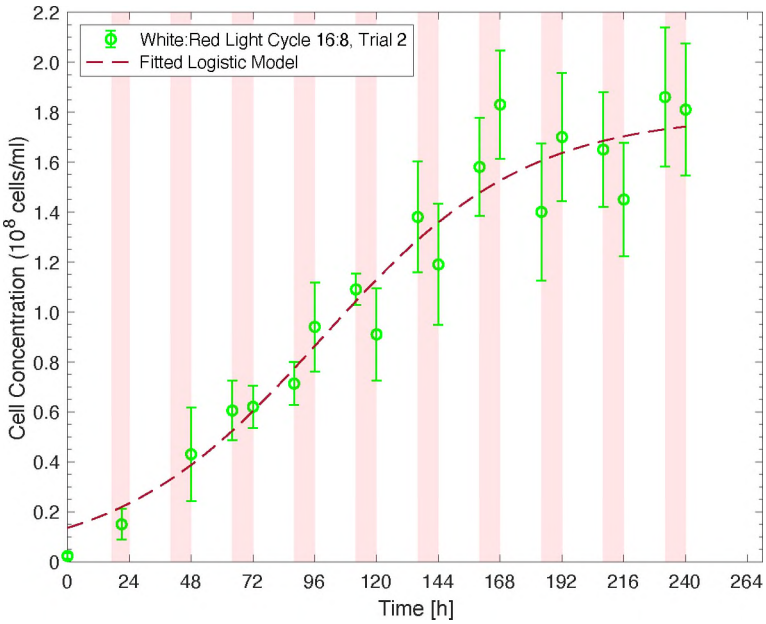

Figure 4-27: Fitted logistic model to the second trial's cell concentration curve of the 16:8 white:red light cycle experiment.

4.4 The Effect of Irradiance

Light is the most important parameter affecting microalgae growth. Higher biomass accumulation will yield more lipids that can be converted to biofuels. In this section, we utilized the Monod equation to understand the effect of light intensity on biomass accumulation in *C. sorokiniana*. Additionally, a higher cell replication rate would yield more cells in which biomass can accumulate. For that reason, we also utilized the Monod equation to study the effect of light intensity on cell replication. The estimated Monod parameters can be useful in driving design efforts to optimize the use of available sunlight. Estimated Monod parameters and model fits and validation are presented in *Sections 4.4.1* and *4.4.2*. It is important to note that this study was done under light-limiting conditions, and using the estimated parameters to model systems with light intensities above saturation limits would not account for the effect of photoinhibition. The Monod equation does not account for biomass losses due to respiration, which is commonly overlooked in literature. In our model, we added the biomass loss term as shown in Eq. 3.3:

$$\frac{dX}{dt} = \left[\mu_m \left(\frac{I_{avg}}{K_g + I_{avg}} \right) - k_l \right] X \qquad \textbf{Eq. 3.3}$$

This model assumes that the biomass loss rate is constant and the same during both light and dark periods. Studies have shown that the respiration rate peaks during the day and differs from the light period to the dark period, which in turn means that the biomass loss rate due to respiration is also different from the light to dark period. For that reason, we separated the biomass loss rate into two terms as shown in Eq. 3.4:

$$\frac{dX}{dt} = \left[\mu_m \left(\frac{I_{avg}}{K_g + I_{avg}} \right) - \alpha \bullet k_{l,light} - (1 - \alpha) \bullet k_{l,night} \right] X \qquad \textbf{Eq. 3.4}$$

Because Eq. 3.4 aligns with findings of previous studies, Eq. 3.4 was chosen to be used in our modeling efforts that are presented in the following sections. Finally, a model with a variable biomass loss rate term due to variable respiration rate during the light period was also used:

$$\frac{dX}{dt} = \left[\mu_m \left(\frac{I_{avg}}{K_g + I_{avg}} \right) - \alpha \, k_{l,max} \left(\frac{I_{avg}}{K_l + I_{avg}} \right) - (1 - \alpha) \bullet k_{l,night} \right] X \qquad \textbf{Eq. 3.6}$$

4.4.1 Effect of Irradiance on Biomass Accumulation

The second trial of the 24:0 (h:h) light:dark cycle experiment was randomly chosen (among the two trials) for parameter estimation. The growth parameters (μ_m, and K_g) and the mass-loss rate during the light period ($k_{l,light}$) were estimated using Eq. 3.4. The parameters were then used with data from the second trial of the 16:8 experiment to evaluate the nighttime biomass loss rate ($k_{l,night}$) also using Eq. 3.4. The models were then validated using the other trials of the experiments. Similarly, the data from the 2nd trial of the 24:0 experiment was used to find the parameters (μ_m K_g, $k_{l,max}$,and K_l), and then these parameters in Eq. 3.6 were fitted to the 16:8 data from the 2nd trial to find $k_{l,night}$. The models were then validated using the other trials of the experiments. See the parameter estimation procedure in *Section 3.3.5* for details. A sensitivity analysis that captures the effect of the parameters on the model's output is presented in *Appendix L*.

The results for the estimated model parameters are presented in Table 4-3. Figure 4-28 and Figure 4-29 present the growth curves that were used in calculating the parameters and the fitted models. Figure 4-30 and Figure 4-31 present the independent trials that were used to validate the models. Besides the visual confirmation and validation of the models

presented in the figures below, we also utilized a numerical statistical method to assess the goodness of the fits. The sum of squares due to error (SSE) is a measure of the deviation of the fit from the experimental values. The model can be considered more reliable, more useful for prediction, and of a smaller random error component as the value of the SSE approaches zero [78]. The SSE values for our models can be considered extremely close to zero as tabulated in Table 4-4. Based on the visual validation of the models with independent experimental trials and the low SSE values, we conclude that both models provide excellent fits for the experimental data.

Using both models, the maximum specific growth rate (μ_m) was estimated to be 0.20 h^{-1}, which is comparable to the predicted maximum specific growth rate for microalgae of about 0.2 h^{-1}, refer to *Section 2.3.1.* The half-velocity constant (K_g) was estimated at 238 µmol s^{-1} m^{-2}. The estimated parameter value is comparable to values reported for *C. vulgaris* (275 µmol s^{-1} m^{-2}) [79]. Biomass-loss rate due to respiration and other metabolic activities during the light period ($k_{l,light}$) was found equal to $8.7x10^{-3}$ h^{-1}. On the other hand, the mass-loss rate during the dark period ($k_{l,night}$) was only $1.8x10^{-3}$ h^{-1}. The results conform to studies that found the respiration rate to be significantly higher in the light period than in the dark period [74]. Additionally, we tested the robustness of the estimated model parameters by varying the initial guess. For example, the initial guess for the maximum specific growth rate (μ_m) was multiplied by 10, the model was ran, and it always converged to the same value. The process was repeated for all estimated parameters. Each parameter was multiplied by 0.01, 0.1, 10, and 100. Since the model always converged to the same results, we concluded that the model is robust and the estimated parameters are independent from one another. This process was carried out for all the models in this study.

The Monod equation with variable $k_{l,light}$ (Eq. 3.6) provides a more physical meaning to the model because the respiration rate was found to vary with the growth rate [74]. However, our results show almost no variability in the light period mass-loss rate, as indicated by the very small K_L/I_o ratio (0.08/300), which is why the model does not provide a better fit for the data.

Both of the models enhance our understand of the effect of light intensity on growth, can be used in predicting the response of other light-limited systems, and can be helpful in driving process design efforts to optimize biomass productivity.

Table 4-3: Estimated Monod Parameters.

Parameter	*Growth Model: Monod Equation with*	
	constant $k_{l,light}$, Eq. 3.4	variable $k_{l,light}$, Eq. 3.6
μ_m $[h^{-1}]$	0.197	0.197
K_g $[\mu mol\ s^{-1}m^{-2}]$	238	238
$k_{l,light}$ $[h^{-1}]$	8.73×10^{-3}	-
$k_{l,max}$ $[h^{-1}]$	-	8.77×10^{-3}
K_l $[\mu mol\ s^{-1}m^{-2}]$	-	8.01×10^{-2}
$k_{l,night}$ $[h^{-1}]$	1.83×10^{-3}	1.83×10^{-3}

Table 4-4: SSE of fits

Experiment		*SSE: Monod Equation with*	
light:dark cycle	trial no	constant $k_{l,light}$, Eq. 3.4	variable $k_{l,light}$, Eq. 3.6
24:0 (h:h)	1	1.48×10^{-3}	1.52×10^{-3}
24:0 (h:h)	2	1.35×10^{-3}	1.35×10^{-3}
16:8 (h:h)	1	3.81×10^{-3}	3.86×10^{-3}
16:8 (h:h)	2	2.76×10^{-2}	2.79×10^{-2}

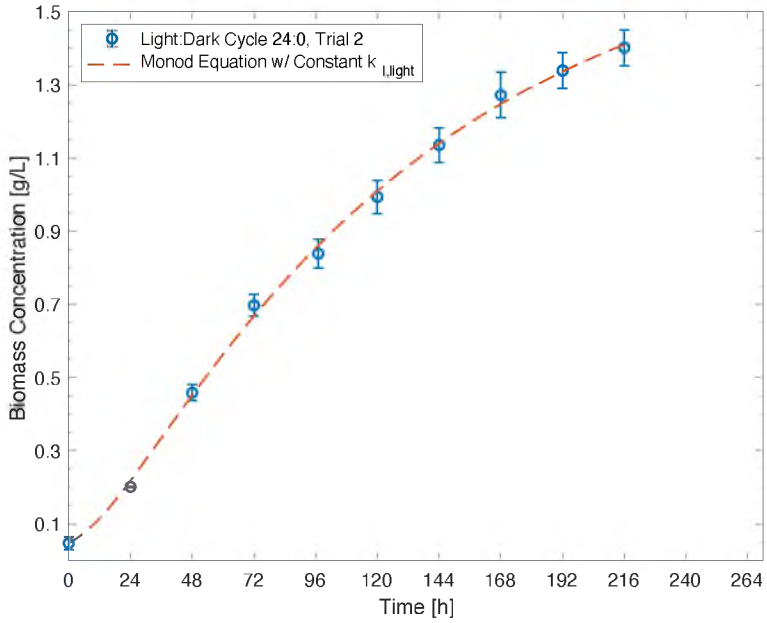

Figure 4-28: Estimation of Monod parameters. The second trial of the 24:0 (h:h) light:dark cycle experiment was randomly chosen (among the two trials) to be used for parameter estimation. The growth parameter (maximum growth rate ($\boldsymbol{\mu_m}$) and half velocity constant ($\boldsymbol{K_g}$)) and mass-loss rate during the light period ($\boldsymbol{k_{l,light}}$) were estimated based on the trial's biomass concentration growth curve. The models from **Eq. 3.4** and **Eq. 3.6** entirely overlap, for that reason, we only present the first model.

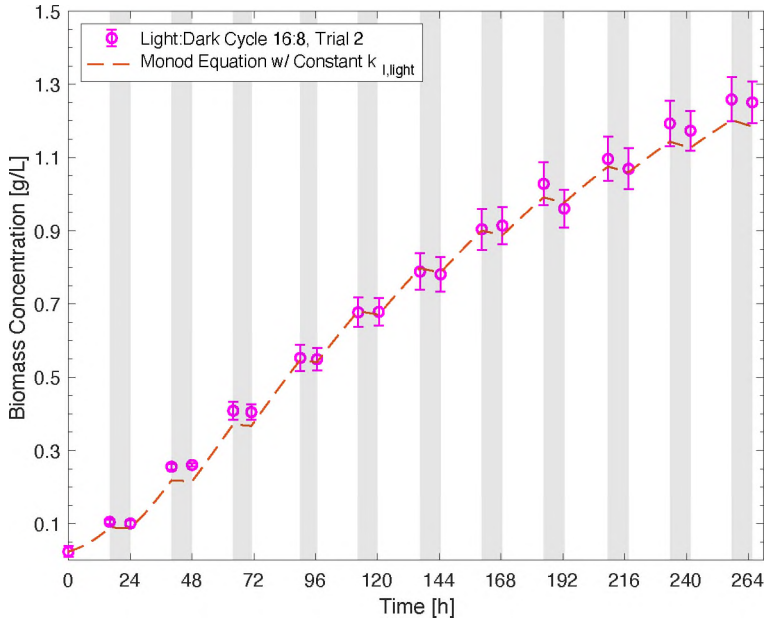

Figure 4-29: Estimation and validation of Model parameters. The second trial of the 16:8 (h:h) light:dark cycle experiment was randomly chosen to be used for parameter estimation. The growth parameter (maximum growth rate and half velocity constant) and mass-loss rate during the light period were validated. The nighttime biomass loss rate ($\boldsymbol{k_{l,night}}$) was estimated using the trial's biomass growth curve. The models from **Eq. 3.4** and **Eq. 3.6** entirely overlap.

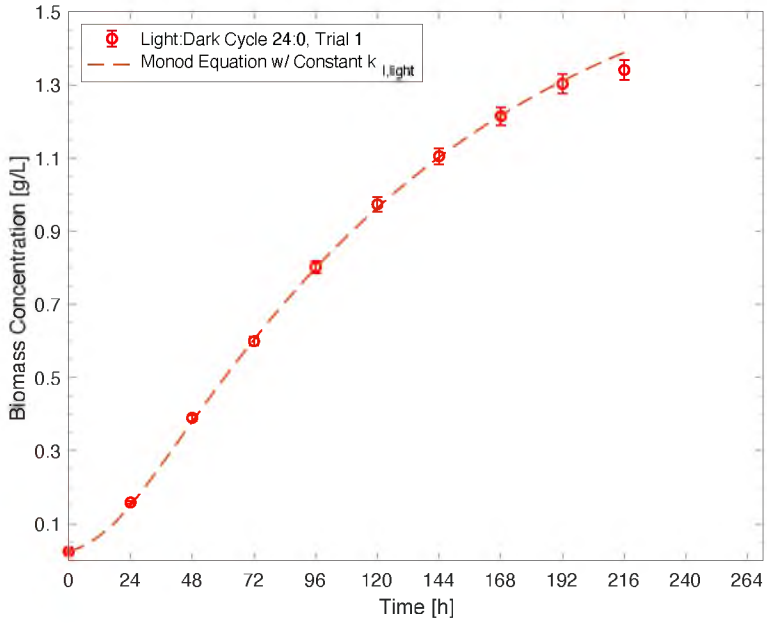

Figure 4-30: Validation of model parameters. The model parameters were validated using the first trial of the 24:0 (h:h) light:dark cycle experiment. Based on the goodness of the fit, we conclude that the model is an excellent fit of the data, and can be used to model other systems with varying light intensities and photoperiods. The models from **Eq. 3.4** and **Eq. 3.6** entirely overlap.

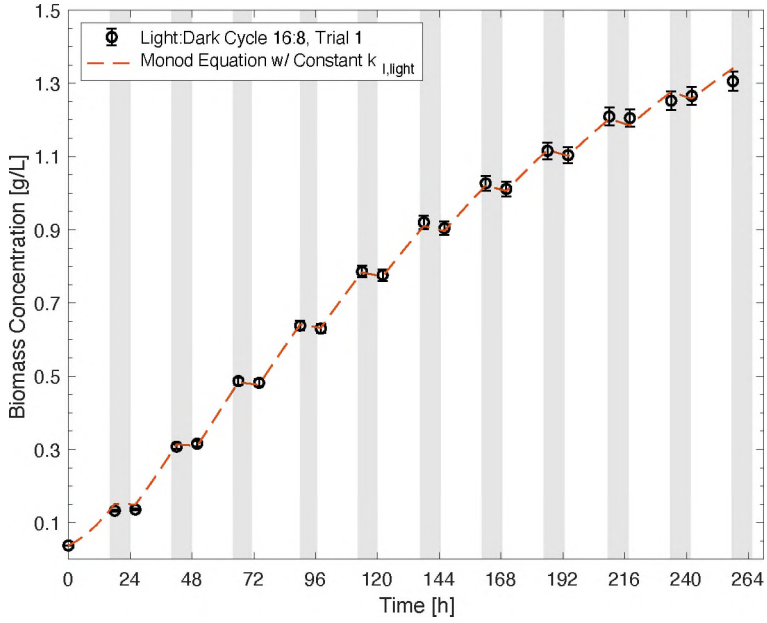

Figure 4-31: Validation of model parameters. The model parameters were validated using the first trial of the 16:8 (h:h) light:dark cycle experiment. Based on the goodness of the fit, we conclude that the model is an excellent fit of the data, and can be used to model other systems with varying light intensities and photoperiods. The models from **Eq. 3.4** and **Eq. 3.6** entirely overlap.

4.4.2 Effect of Irradiance on Cell Replication

In an analogous method to the biomass concentration Monod models, the following equation was used to quantify the effect of light intensity on cell replication:

$$\frac{dC}{dt} = \left[\mu'_m \left(\frac{I_{avg}}{K'_g + I_{avg}} \right) - \alpha \bullet k_{d,light} - (1-\alpha) \bullet k_{d,night} \right] C \qquad \textbf{Eq. 4.1}$$

where,

C: cell concentration [cells/ml].

μ'_m: maximum cell replication rate [h^{-1}].

K'_g: saturation constant [µmol s^{-1} m^{-2}].

$k_{d,light}$: cell death rate during the light period [h^{-1}].

$k_{d,night}$: : cell death rate during the dark period [h^{-1}].

α: a dimensionless constant that is equal to one during the light period and zero during the dark period.

The estimated parameters and the SSE of fits are presented in Table 4-5 and Table 4-6, respectively. The model fit, shown in Figure 4-32 and Figure 4-33, overestimates the carrying capacity of the system, which can be interpreted from the model not reaching the stationary phase at the end of the cultivation period. The maximum growth was evaluated to be 0.080 h^{-1}, the value is equal to the maximum observed replication rate between any two data points. This estimated maximum cell replication rate is far smaller than the maximum rate of biomass accumulation (≈ 0.20 h^{-1}), which contradicts our expectations, even though the net specific growth rate, at any given point in time, was comparable between the two rates. First, if this finding holds true, an increase in cell size should be observed over time because cells accumulate biomass faster than they replicate. Since cell

size does not change with time, as can be observed from Figure 4-7 - Figure 4-9, this hypothesis can be ruled out. Second, the model failed our robustness test, where the initial guesses for the parameters are varied and we look for the model to converge back to the same values. Failure of the robustness test indicates that the parameters may not be independent from one another. These two reasons cause us to lose confidence in this model.

Additionally, the model does not translate well when representing different light:dark cycle, which can be seen by the poor fits to the 16:8 (h:h) light:dark cycle experiment, see Figure 4-34 and Figure 4-35. We conclude that this model will fail at predicting cell concentration data with naturally occurring light:dark intervals. For that reason, models based on biomass concentration are far superior for prediction than those based on cell numbers.

Table 4-5: Monod parameters based on cell concentration using Eq. 4.1.

Parameter	*Growth Model: Monod Equation w/*
	constant k_d
μ_m $[h^{-1}]$	0.080
K_g $[\mu mol\ s^{-1}m^{-2}]$	28
$k_{d,light}$ $[h^{-1}]$	0.024
$k_{d,night}$ $[h^{-1}]$	0.00

Table 4-6: SSE of fits.

Experiment		*SSE: Monod Equation w/*
light:dark cycle	trial no	constant k_d
24:0 (h:h)	1	0.036
24:0 (h:h)	2	0.018
16:8 (h:h)	1	0.12
16:8 (h:h)	2	0.15

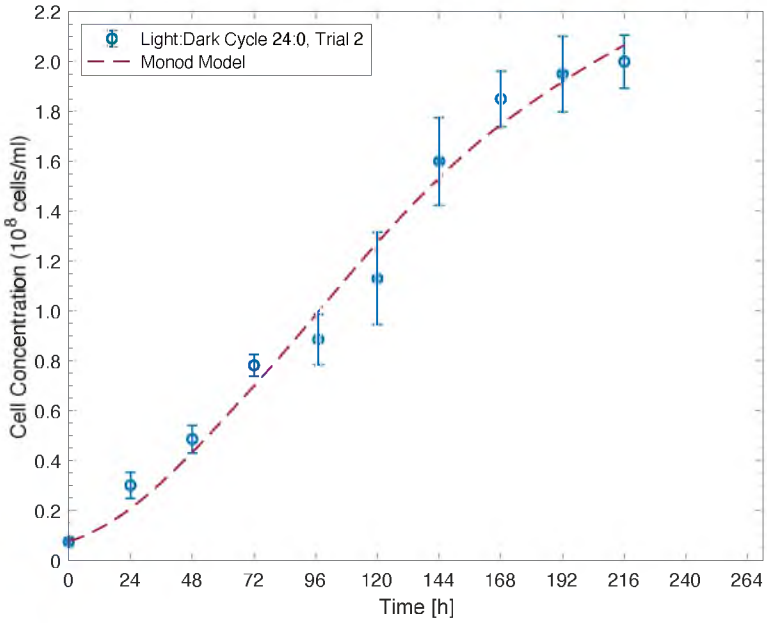

Figure 4-32: Estimation of Monod parameters. The second trial of the 24:0 (h:h) light:dark cycle experiment was randomly chosen to be used for parameter estimation based on **Eq. 4.1**.

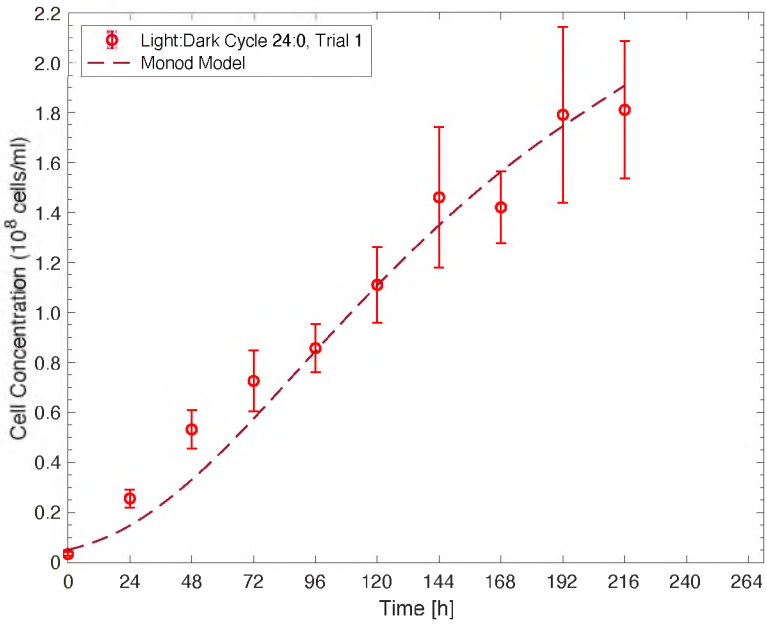

Figure 4-33: Validation of model parameters. The model parameters were validated using the first trial of the 24:0 (h:h) light:dark cycle experiment and **Eq. 4.1**.

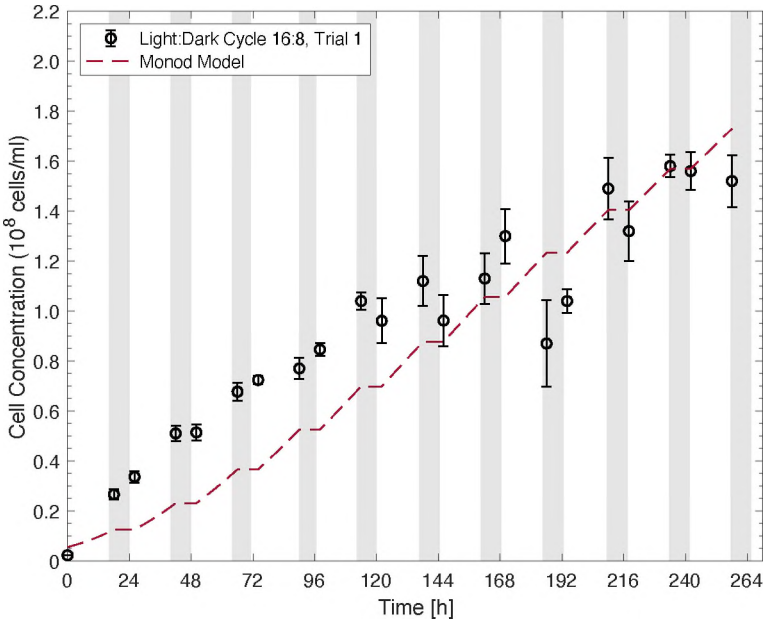

Figure 4-34: Validation of model parameters. The model parameters were validated using the first trial of the 24:0 (h:h) light:dark cycle experiment and **Eq. 4.1**.

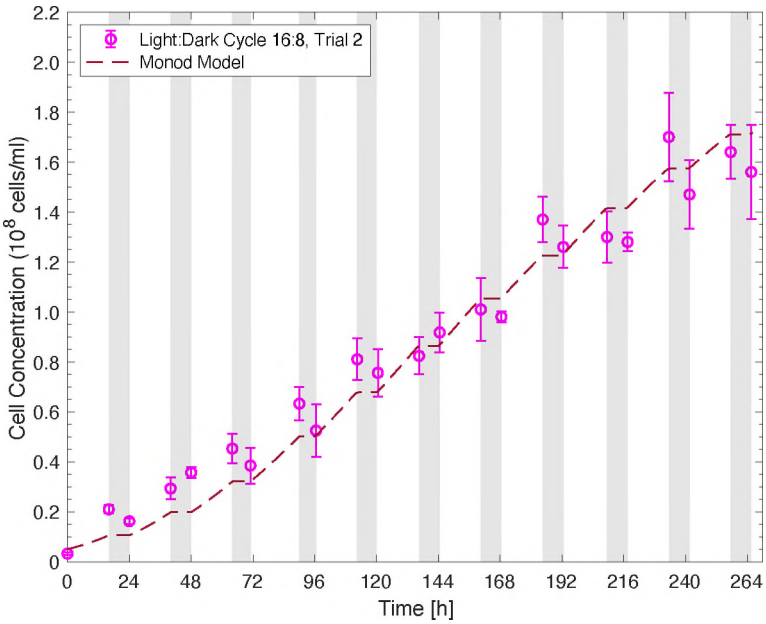

Figure 4-35: Validation of model parameters. The model parameters were validated using the first trial of the 24:0 (h:h) light:dark cycle experiment and **Eq. 4.1**.

CHAPTER V

CONCLUSIONS AND RECOMMENDATIONS

5.1 Conclusions

In this study, we analyzed the effect of light intensity and light:dark cycle on the growth of *C. sorokiniana,* and constructed models that accurately predict the growth response of the microalgae culture under light-limited conditions. We found that growth is highly dependent on light availability and intensity. Our models estimated a maximum specific growth rate, limited by the rate of photosynthesis, of about 0.2 h^{-1}. The models predicted high dependency of growth on light intensity, where the estimated Monod saturation constant (K_g= 238 µmol s^{-1} m^{-2}) was comparable to the maximum average light intensity ($K_g \approx I_{avg,maximum}$). We estimated the average biomass loss rate due to endogenous metabolism to be highest during the light period ($8.7x10^{-3}$ h^{-1}), five times higher than the biomass loss rate during the dark period ($1.8x10^{-3}$ h^{-1}).

We investigated the effect of the dark period on the biomass productivity of *C. sorokiniana*. During a daily 8-hour dark period, we estimated that the cell culture loses 5% of the biomass gained in the preceding 16-hour light period, on average. The losses accumulate and lead to a 16.4% lower biomass yield when compared to a continuously illuminated culture over nine cultivation days in a 30ºC constant temperature well-mixed

five-liter photobioreactor with an incident light intensity of 300 μmol $s^{-1}m^{-2}$. However, using the growth kinetics of a fitted logistic model, we conclude that prolonged cultivation of the cell culture at light:dark intervals of 16:8 (h:h) will yield the same final biomass and cell concentrations as per continuously illuminated culture. Finally, we utilized low consumption red LEDs to illuminate the dark period of the cultivation cycle in efforts to mitigate biomass losses. We conclude that the use of low consumption red LEDs at low illumination intensities (150 μmol s^{-1} m^{-2} incident intensity) prevents nighttime biomass loss and enhances cell replication.

5.2 Recommendations

To further the aims of this research, we make the following recommendations:

- Validate the model with other photoperiods such as 14:10, 12:12, 10:14 light:dark cycles.
- Validate the model with 'rapidly' changing light intensities. For example, vary the surface light intensity during the day analogous to what culture would experience when growing in sunlight.
- Determine how biomass losses are affected by fluctuating temperatures and incorporate that into the model.
- We have shown that prolonged cultivation will yield the same final biomass concentration. Prove that this will hold with more extended dark periods.
- Validate the model with a different reactor geometry, such as tubular photobioreactors.
- Perform an economic analysis to determine whether the use of red light to reduce nighttime biomass loss is cost-effective.

BIBLIOGRAPHY

[1] U.S. Department of Energy, "Fossil," [Online]. Available: https://www.energy.gov/science-innovation/energy-sources/fossil. [Accessed 25 July 2020]

[2] R. Hannah and M. Roser, "Our World In Data," ourworldindata.org, 2017. [Online]. Available: https://ourworldindata.org/fossil-fuels. [Accessed 25 July 2020].

[3] UCAR, "The Greenhouse Effect," 2011. [Online]. Available: https://scied.ucar.edu/longcontent/greenhouse-effect. [Accessed 25 July 2020].

[4] EPA, "Understanding Global Warming Potentials," [Online]. Available: https://www.epa.gov/ghgemissions/understanding-global-warming-potentials. [Accessed 25 July 2020].

[5] EPA, "Climate Change Indicators: Oceans," [Online]. Available: https://www.epa.gov/climate-indicators/oceans. [Accessed 25 July 2020].

[6] EPA, "Overview of Greenhouse Gases," [Online]. Available: https://www.epa.gov/ghgemissions/overview-greenhouse-gases. [Accessed 25 July 2020].

[7] T. Mata, A. Martins and N. Caetano, "Microalgae for biodiesel production and other applications: A review," *Renewable and Sustainable Energy Reviews,* vol. 14, pp. 217-232, 2010.

[8] Union of Concerned Scientists, "Benefits of Renewable Energy Use," 20 Dec 2017. [Online]. Available: https://www.ucsusa.org/resources/benefits-renewable-energy-use. [Accessed 25 July 2020].

[9] CRS, "Why Renewable Energy," [Online]. Available: https://resource-solutions.org/why-renewable-energy/. [Accessed 25 July 2020].

[10] M. Shellenberger, "With Ethanol And Biomass No Longer Viewed As 'Green,' Will Other Renewables Soon Follow?," Forbes, [Online]. Available: https://www.forbes.com/sites/michaelshellenberger/2019/03/07/with-ethanol-and-biomass-no-longer-viewed-as-green-will-other-renewables-soon-follow/#3dfaefac7fb9. [Accessed 25 July 2020].

[11] Oregon State University, "Generations of Biofuels".

[12] R. Raja, H. Shanmugam, V. Ganesan and I. S. Carvalho, "Biomass from Microalgae: An Overview," *Journal of Oceanography and Marine Research,* vol. 2, no. 1, 2014.

[13] M. I. Khan, J. H. Shin and J. D. Kim, "The promising future of microalgae: current status, challenges, and optimization of a sustainable and renewable industry for biofuels, feed, and other products," *Microbial Cell Factories,* vol. 17, no. 36, 2018.

[14] S. J. Edmundson and M. H. Huesemann, "The dark side of algae cultivation: Characterizing night biomass loss in three photosynthetic algae, Chlorella sorokiniana, Nannochloropsis salina and Picochlorum sp.," *Algal Research,* vol. 12, pp. 470-476, 2015.

[15] M. D. Guiry, "How many species of algae are there?," *Journal of Phycology,* vol. 48, no. 5, pp. 1057-1063, 2012.

[16] T. Kotasthane, "Potential of Microalgae for Sustainable Biofuel Production," *Journal of Marine Science: Research & Development,* vol. 7, no. 2, 2017.

[17] Geada, V. V, A.Vicente and B.Fernandes, "Chapter 13 - Microalgal Biomass Cultivation," in *Algal Green Chemistry*, University of Minho, Braga, Portugal, ScienceDirect, 2017, pp. 257-284.

[18] M. J. Griffiths and S. T. L. Harrison, "Lipid productivity as a key characteristic for choosing algal species for biodiesel production," *Journal of Applied Phycology,* vol. 21, p. 493–507, 2009.

[19] NAABB, "Full Final Report Section I Program Overview".

[20] M. Huesemann, A. Chavis, S. Edmundson, D. Rye, S. Hobbs, N. Sun and M. Wigmosta, "Climate-simulated raceway pond culturing: quantifying the maximum achievable annual biomass productivity of Chlorella sorokiniana in the contiguous USA," *J Appl Phycol,* vol. 30, p. 287–298, 2017.

[21] M. P. Johnson, "Photosynthesis," *Essays in Biochemistry,* vol. 60, no. 3, p. 255–273, 2016.

[22] M. Gargaud, R. Amils, J. C. Quintanilla, H. J. CleavesII, W. M. Irvine, D. L. Pinti and M. Viso, "Photoautotroph," in *Encyclopedia of Astrobiology*, Springer-Verlag Berlin Heidelberg, 2011.

[23] A. Augustyn, P. Bauer, B. Duignan, A. Eldridge, E. Gregersen, A. McKenna, M. Petruzzello, J. P. Rafferty, M. Ray, K. Rogers, A. Tikkanen, J. Wallenfeldt, A. Zeidan and A. Zelazko, "Encyclopædia Britannica," 25 November 2019. [Online]. Available: https://www.britannica.com/science/chloroplast. [Accessed 18 May 2020].

[24] M. A. Clark, M. Douglas and J. Choi, "The Light-Dependent Reactions of Photosynthesis," 28 March 2018. [Online]. Available: https://openstax.org/books/biology-2e/pages/8-2-the-light-dependent-reactions-of-photosynthesis. [Accessed 19 May 2020].

[25] M. A. Clark, M. Douglas and J. Choi, "Openstax: Using Light Energy to Make Organic Molecules," 28 March 2018. [Online]. Available: https://openstax.org/books/biology-2e/pages/8-3-using-light-energy-to-make-organic-molecules. [Accessed 20 May 2020].

[26] R. R. Narala, S. Garg, K. K. Sharma, S. R. Thomas-Hall, M. Deme, Y. Li and P. M. Schenk, "Comparison of Microalgae Cultivation in Photobioreactor, Open Raceway Pond, and a Two-Stage Hybrid System," *Frontiers in Energy Research,* vol. 4, no. 29, 2016.

[27] J. Jerney and K. Spilling, "Large Scale Cultivation of Microalgae: Open and Closed Systems," *Methods in Molecular Biology,* vol. 1980, pp. 1-8, 2018.

[28] A. Richmond, J. Masojıdek, M. Koblızek and G. Torzillo, "Photosynthesis in Microalgae," in *Handbook of Microalgal Culture*, Blackwell Science Ltd, 2004, pp. 20-39.

[29] "Batch Culture, A Dictionary of Biology," Encyclopedia.com, 11 May 2020. [Online]. Available: www.encyclopedia.com. [Accessed 8 June 2020].

[30] I. Remmers, A. Hidalgo-Ullo, B.P.Brandt, W. Evers, R. Wijffels and P. Lamers, "Continuous versus batch production of lipids in the microalgae Acutodesmus obliquus," *Bioresource Technology,* vol. 244, pp. 1384-1392, 2017.

[31] J. B. Magdaong, A. T. Ubando, A. B. Culaba, J. S. Chang and W. H. Chen, "Effect of aeration rate and light cycle on the growth characteristics of Chlorella sorokiniana in a photobioreactor," *Earth and Environmental Science,* vol. 268, 2019.

[32] K. Price and I. H. Farag, "Resources Conservation in Microalgae Biodiesel Production," *International Journal of Engineering and Technical Research,* vol. 1, no. 8, pp. 49-56, 2013.

[33] M. Shuler, F. Kargi and M. Delisa, "Chapter 6. How Cells Grow," in *Bioprocess Engineering, Basic Concepts*, Prentice Hall, 2017, pp. 175-184.

[34] nature.com, "cell growth," [Online]. Available: https://www.nature.com/subjects/cell-growth. [Accessed 15 July 2020].

[35] S. Chelsea, "WorldAtlas," Environment, 24 May 2018. [Online]. Available: https://www.worldatlas.com/articles/how-long-is-a-day-at-the-equator.html. [Accessed 20 June 2020].

[36] R. Exner, "Cleveland.com," cleveland.com, 11 March 2014. [Online]. Available: https://www.cleveland.com/datacentral/2014/03/when_are_the_longest_and_short.html. [Accessed 20 June 2020].

[37] E. Sforza, D. Simionato, G. M. Giacometti, A. Bertucco and T. Morosinotto, "Adjusted Light and Dark Cycles Can Optimize Photosynthetic Efficiency in Algae Growing in Photobioreactors," *PLoS ONE,* vol. 7, no. 6, 2012.

[38] S. Abu-Ghosh, D. Fixler, Z. Dubinsky, A. Solovchenko, M. Zigman, Y. Yehoshua and D. Iluz, "Flashing Light Enhancement Of Photosynthesis And Growth Occurs When Photochemistry And Photoprotection Are Balanced In Dunaliella Salina," *European Journal of Phycology,* vol. 50, no. 4, pp. 469-480, 2015.

[39] Q. Liao, L. Li, R. Chen and X. Zhu, "A novel photobioreactor generating the light/dark cycle to improve microalgae cultivation," *Bioresource Technology,* vol. 161, pp. 186-191, 2014.

[40] J. C. Ogbonna and H. Tanakaah, "Cyclic Autotrophic/Heterotrophic Cultivation Of Photosynthetic Cells: A Method Of Achieving Continuous Cell Growth Under Light/Dark Cycles," *Bioresource Technology,* vol. 65, pp. 65-72, 1998.

[41] H. Kamyab, M. F. M. Din, S. K. Ghoshal, C. T. Lee, A. Keyvanfar, A. A. Bavafa, S. Rezania and J. S. Lim, "Chlorella Pyrenoidosa Mediated Lipid Production Using Malaysian Agricultural Wastewater: Effects of Photon and Carbon," *Waste Biomass Valor,* vol. 7, pp. 779-788, 2016.

[42] Y. Kato, Y. Fujihara, C. J. Vavricka, J. Chang, T. Hasunuma and A. Kondo, "Light/dark cycling causes delayed lipid Open Access Biotechnology for Biofuels accumulation and increased photoperiod-based biomass yield by altering metabolic flux in oleaginous Chlamydomonas sp.," *Kato et al. Biotechnol Biofuels,* vol. 12, no. 39, 2019.

[43] F. Rezvani, M.-H. Sarrafzadeh, S.-H. Seo and H.-M. Oh, "Optimal strategies for bioremediation of nitrate-contaminated groundwater and microalgae biomass production," *Environmental Science and Pollution Research,* vol. 25, p. 27471–27482, 2018.

[44] R. N. Haneda, B. H. Vieira, S. R. Fontes, G. Ombardi, C. A. Casali and A. T. Lombardi, "Biochemical Composition of Chlorella Sorokiniana Grown in a Novel Design of Hybrid Photobioreactor," *Journal of Microbial & Biochemical Technology,* vol. 7, no. 2, pp. 76-82, 2015.

[45] T. J. Gunawan, Y. Ikhwan, F. Restuhadi and U. Pato, "Effect of light Intensity and photoperiod on growth of Chlorella pyrenoidosa and CO2 Biofixation," *E3S Web of Conferences,* vol. 31, 2018.

[46] J. Franson, "Principles of Structural Chemistry," [Online]. Available: https://sites.google.com/a/coe.edu/principles-of-structural-chemistry/relationship-between-light-and-matter/electromagnetic-spectrum. [Accessed 24 June 2020].

[47] Y. Wong, Y. Ho, K. Ho, H. Leung, K. P. Chow and K. Yung, "Effect of Different Light Sources on Algal Biomass and Lipid Production in Internal Leds-Illuminated Photobioreactor," *Journal of Marine Biology and Aquaculture,* vol. 2, no. 2, pp. 1-8, 2016.

[48] M. Al-Qasmi, N. R. Member, I. S. Talebi, S. Al-Rajhi and T. Al-Barwani, "A Review of Effect of Light on Microalgae Growth," *Proceedings of the World Congress on Engineering,* vol. 1, 2012.

[49] H. Guo and Z. Fang, "Effects of light quality on the growth characteristics and biochemical component of Chlorella pyrenoidosa," *Huan Jing Ke Xue,* vol. 35, no. 11, pp. 4212-4217, 2014.

[50] S. Satthong, K. Saego, P. Kitrungloadjanaporn, N. Nuttavut, S. Amornsamankul and W. Triampo, "Modeling the effects of light sources on the growth of algae," *AdvancesinDifferenceEquations,* vol. 170, 2019.

[51] Lighting Analysts, Inc., "Photosynthetic Photon Flux Density (PPFD) - Concepts," [Online]. Available: https://docs.agi32.com/AGi32/Content/adding_calculation_points/PPFD_Concepts.htm. [Accessed 27 June 2020].

[52] J. C. Nzayiseng, X. Farge, Sophia, L. Groll and A. Sellstedt, "Effects of light intensity on growth and lipid production in microalgae grown in wastewater," *Biotechnology for Biofuels,* vol. 13, no. 4, 2020.

[53] Y. Bazarnova, N. Lyskova, T. Kuznetsova and E. Trukhina, "Illumination Influence On Chlorella Sorokiniana Biomass Synthesis," *BIOTECHNOLOGIA ACTA,* vol. 12, no. 3, pp. 50-56, 2019.

[54] E. Barbera, A. Grandi, L. Borella, A. Bertucco and E. Sforza, "Continuous Cultivation as a Method to Assess the Maximum Specific Growth Rate of Photosynthetic Organisms," *Frontiers in Bioengineering and Biotechnology,* vol. 7, no. 274, 2019.

[55] S.-F. Han, W.-B. Jin, R.-J. Tu and W.-M. Wu, "Biofuel production from microalgae as feedstock: current status and potential," *Critical Reviews in Biotechnology,* vol. 35, no. 2, p. 255–268, 2015.

[56] Wolfram Research, Inc. , "Logistic Equation," Wolfram MathWorld, 13 July 2020. [Online]. Available: https://mathworld.wolfram.com/LogisticEquation.html. [Accessed 15 July 2020].

[57] Northwestern University, "The Logistic Equation," Northwestern.edu, [Online]. Available: https://sites.math.northwestern.edu/~mlerma/courses/math214-2-04f/notes/c2-logist.pdf. [Accessed 15 July 2020].

[58] M. Cohara, "Determination Of Growth Kinetics, Yield Coefficients And Biodiesel Properties For The Green," MS Thesis Cleveland State University, Cleveland, 2018.

[59] M. K. LAM, K. T. LEE, C. G. KHOO, Y. UEMURA and U. W. LIM, "GROWTH KINETIC STUDY OF CHLORELLA VULGARIS USING LAB-SCALE AND PILOT-SCALE PHOTOBIOREACTOR: EFFECT OF CO2 CONCENTRATION," *Journal of Engineering Science and Technology,* pp. 73-87, 2016.

[60] D. Surendhiran, M. Vijay, B. Sivaprakash and A. Sirajunnisa, "Kinetic modeling of microalgal growth and lipid synthesis for biodiesel production," *Biotech,* vol. 5, pp. 663-669, 2015.

[61] P. K, A. S, N. R and K. M, "Biochemical Responses From Biomass Of Isolated Chlorella Sp., Under Different Cultivation Modes: Non-Linear Modelling Of Growth Kinetics," *Brazilian Journal of Chemical Engineering,* vol. 35, no. 2, pp. 489-496, 2018.

[62] K. Schediwy and A. Trautmann, "Microalgal kinetics — a guideline for photobioreactor design and process development," *Engineering in Life Sciences,* vol. 19, pp. 830-843, 2019.

[63] S.-F. Han, W.-B. Jin, R.-J. Tu and W.-M. Wu, "Biofuel production from microalgae as feedstock: current status and potential," *Crit Rev Biotechnol,* vol. 35, no. 2, pp. 255-268, 2015.

[64] L. Straka, "Light-Dependent Growth Kinetics and Mathematical Modeling of Synechocystis sp. PCC 6803," Ph.D. Dissertation Arizona State University, Tempe, 2017.

[65] M. Huesemann, B. Crowe, P. Waller and M. Wigmosta, "A validated model to predict microalgae growth in outdoor pond cultures subjected to fluctuating light intensities and water temperatures," *Algal Research,* vol. 13, pp. 195-206, 2015.

[66] A. Svirin, "math24," math24.net, [Online]. Available: https://www.math24.net/average-value-function/. [Accessed 28 June 2020].

[67] M. H. Huesemann, J. V. Wagenen, T. Miller, A. Chavis, S. Hobbs and B. Crowe, "A Screening Model to Predict Microalgae Biomass Growth in Photobioreactors and Raceway Ponds," *Biotechnology and Bioengineering,* vol. 110, no. 6, 2013.

[68] UTEX at Austin, "UTEX B 3016 Chlorella sorokiniana," [Online]. Available: https://utex.org/products/utex-b-3016. [Accessed 8 July 2020].

[69] Biology Online;, "Inoculum," [Online]. Available: https://www.biologyonline.com/dictionary/inoculum. [Accessed 8 July 2020].

[70] Biology Online;, "Inoculation," [Online]. Available: https://www.biologyonline.com/dictionary/inoculation. [Accessed 8 July 2020].

[71] S. Sood and A. Kumar, Comprehensive Biotechnology (Second Edition), ScienceDirect, 2011.

[72] Horiba.com, "LAQUAtwin NO3- Sensor," HORIBA, [Online]. Available: https://www.horiba.com/en_en/products/detail/action/show/Product/laquatwin-no3-11cno3-11sno3-11-794/. [Accessed 10 July 2020].

[73] M. Shin-ya, "Day/Night Separation of Oxygenic Energy Metabolism and Nuclear DNA Replication in the Unicellular Red Alga Cyanidioschyzon merolae," *Molecular Biology and Physiology,* vol. 10, no. 4, 2019.

[74] K. Anna M. J., A. M. J. Kliphuis, M. Janssen, E. J. v. d. End, D. E. Martens and R. H. Wijffels, "Light respiration in Chlorella sorokiniana," *Journal of Applied Phycology,* vol. 23, no. 6, pp. 935-947, 2011.

[75] M. Jones and S. Marengo, "Chapter 6 - Laboratory validation, verification, and accreditation of molecular methods," in *Molecular Microbial Diagnostic Methods*, ScienceDirect, 2016, pp. 107-133.

[76] L. d. Winter, I. T. D. Cabanelas, D. E. Martens, R. H. Wijffels and M. J. Barbosa, "The influence of day length on circadian rhythms of Neochloris oleoabundans," *Algal Research,* vol. 22, pp. 31-38, 2017.

[77] L. Saiki and G. Mitsue, "The impact of day length on cell division and efficiency of light use in a starchless mutant of Tetradesmus obliquus," *Algal Research,* vol. 31, pp. 387-394, 2018.

[78] MathWorks, "Evaluating Goodness of Fit," MathWorks, [Online]. Available: https://www.mathworks.com/help/curvefit/evaluating-goodness-of-fit.html#bq_5kwr-4. [Accessed 5 August 2020].

[79] M. N. Metsoviti, G. Papapolymerou, I. T. Karapanagiotidis and N. Katsoulas, "Effect of Light Intensity and Quality on Growth Rate and Composition of Chlorella vulgaris," *plants,* vol. 9, no. 31, 2020.

[80] D. Surendhiran, M. Vijay, B. Sivaprakash and A. Sirajunnisa, "Kinetic modeling of microalgal growth and lipid synthesis for biodiesel production," *Biotech,* vol. 5, p. 663–669, 2014.

[81] H. Guo and Z. Fang, "Effect of light quality on the cultivation of chlorella pyrenoidosa," *E3S Web of Conferences,* vol. 143, 2020.

[82] M. Janssen, "Cultivation of microalgae: Effect of light/dark cycles on biomass yield," Wageningen Universiteit, 2002.

[83] J. V. Wagenen, D. D. Francisci and I. Angelidaki, "Comparison of mixotrophic to cyclic autotrophic/heterotrophic growth strategies to optimize productivity of Chlorella sorokiniana," *J Appl Phycol,* vol. 27, pp. 1775-1782, 2015.

[84] M. Cuaresma, M. Janssen, C. Vílchez and R. H. Wijffels, "Horizontal or vertical photobioreactors? How to improve microalgae photosynthetic efficiency," *Bioresource Technology,* vol. 102, p. 5129–5137, 2011.

[85] M. Ota, M. Takenaka, Y. Sato, R. L. Smith and H. Inomata, "Effects of light intensity and temperature on photoautotrophic growth of a green microalga, Chlorococcum littorale," *Biotechnology Reports,* vol. 7, pp. 24-29, 2015.

[86] M. F. Blair, B. Kokabian and V. G. Gude, "Light and growth medium effect on Chlorella vulgaris biomass production," *Journal of Environmental Chemical Engineering,* vol. 2, p. 665–674, 2013.

[87] R. Bouterfas, M. Belkoura and AlainDauta, "The effects of irradiance and photoperiod on the growth rate of three freshwater green algae isolated from a eutrophic lake," *Limnetica,* vol. 25, no. 3, pp. 646-656, 2006.

[88] S. Mohd, "The Extended Monod Model for Microalgae Growth and Nutrient Uptake in Different Wastewaters," *International Journal of Engineering & Technology,* vol. 7, pp. 200-204, 2018.

[89] A. Habibi, G. A. Nematzadeh, F. P. shariati, H. D. Amrei and A. Teymouri, "Effect of light/dark cycle on nitrate and phosphate removal from synthetic wastewater based on BG11 medium by Scenedesmus sp.," *Biotech,* vol. 9, no. 150, 2019.

[90] UTEX, "BG-11 Medium," [Online]. Available: https://utex.org/products/bg-11-medium?variant=30991786868826#recipe. [Accessed 8 July 2020].

[91] K. Kumar, S. Roy and D. Das, "Continuous mode of carbon dioxide sequestration by C. sorokiniana and subsequent use of its biomass for hydrogen production by E. cloacae IIT-BT 08," *Bioresource Technology,* vol. 145, pp. 116-122, 2013.

[92] Z. Gojkovic, I. Garbayo, T. García-Barrera and C. Vílchez, "Continuous production of selenomethionine-enriched Chlorella sorokiniana biomass in a photobioreactor," *Process Biochemistry,* vol. 48, p. 1235–1241, 2013.

[93] M. Janssen, T. Kuijpers, B. Veldhoen, M. Brik Ternbach, J. Tramper, L. Mur and R. Wijffels, "Specific growth rate of Chlamydomonas reinhardtii and Chlorella sorokiniana under medium duration light/dark cycles: 13–87 s," *Journal of Biotechnology,* vol. 70, pp. 323-333, 1999.

[94] S. Sivakaminathan, B. Hankamer, J. Wolf and J. Yarnold, "High-throughput optimisation of light-driven microalgae biotechnologies," *Scientific Reports,* vol. 8, no. 11687, 2018.

[95] P. S. Varbanov, P.-Y. Liew, J.-Y. Yong, J. J. Klemeš and H. L. Lam, "Mathematical Modelling of the Effects of Circadian Rhythm on Microalgal Growth in Phototrophic and Mixotrophic Cultures," *Chemical Engineering Transactions,* vol. 52, pp. 955-960, 2016.

APPENDICES

A. BG-11 Medium Recipe

Directions for 1L liquid media[1]:

1. Add approximately 900 mL of RO H_2O to a 1L glass bottle.
2. While stirring continuously, add the components in the order specified in Table 7-1.
3. Bring the total volume to 1L with RO H_2O.
4. Cover and autoclave medium.
5. Allow medium to cool down then store at refrigerator temperature.

Table 7-1: BG-11 medium recipe. Add the components in the order and amounts specified.

#	Component	Amount [mL]	Stock Solution Concentration	Final Concentration In Media
1	$NaNO_3$	10	75.0 g/500 mL dH_2O	17.6 mM
2	K_2HPO_4	10	2.00 g/500 mL dH_2O	0.23 mM
3	$MgSO_4 \cdot 7H_2O$	10	3.75 g/500 mL dH_2O	0.30 mM
4	$CaCl_2 \cdot 2H_2O$	10	1.80 g/500 mL dH_2O	0.24 mM
5	Citric Acid $\cdot H_2O$	10	0.30 g/500 mL dH_2O	0.03 mM
6	Ferric Ammonium Citrate	10	0.30 g/500 mL dH_2O	0.02 mM
7	$Na_2EDTA \cdot 2H_2O$	10	0.05 g/500 mL dH_2O	0.0027 mM
8	Na_2CO_3	10	1.00 g/500 mL dH_2O	0.19 mM
9	BG-11 Trace Metals Solution	1		

[1] BG-11 medium preparation procedure was adapted from UTEX Culture Collection of Algae's BG-11 Medium Recipe [90].

B. BG-11 Stock Solutions Recipe

Directions for 500 mL of stock solutions preparation:

1. Add approximately 400 mL of RO H_2O to a 500 mL volumetric flask.
2. Add the amount specified, for the stock solution of interest, according to Table 7-2.
3. Bring the total volume to 500 mL with RO H_2O.
4. Transfer to a 500 mL autoclaved glass bottle and store it at refrigerator temperature.

Table 7-2: BG-11 stock solutions recipe. Add the amount specified to 500 mL of RO H_2O and store at 4°C.

#	Stock Solution	Amount [g]	Stock Solution Concentration
1	$NaNO_3$ (Fisher BP360-500)	75.0	75.0 g/500 mL dH_2O
2	K_2HPO_4 (Sigma P 3786)	2.00	2.00 g/500 mL dH_2O
3	$MgSO_4 \cdot 7H_2O$ (Sigma 230391)	3.75	3.75 g/500 mL dH_2O
4	$CaCl_2 \cdot 2H_2O$ (Sigma C-3881)	1.80	1.80 g/500 mL dH_2O
5	Citric Acid $\cdot H_2O$ (Fisher A 104)	0.30	0.30 g/500 mL dH_2O
6	Ferric Ammonium Citrate	0.30	0.30 g/500 mL dH_2O
7	$Na_2EDTA \cdot 2H_2O$ (Sigma ED255)	0.05	0.05 g/500 mL dH_2O
8	Na_2CO_3 (Baker 3604)	1.00	1.00 g/500 mL dH_2O

C. BG-11 Trace Metals Solution Recipe

Directions for 50 mL of trace metals solution:

1. Add approximately 40 mL of RO H_2O to a 50 mL volumetric flask.
2. Add the components in the order and amounts specified in Table 7-3.
3. Bring the total volume to 50 mL with RO H_2O.
4. Transfer to a 50 mL autoclaved glass bottle and store it at refrigerator temperature.

Table 7-3: BG-11 trace metals solution recipe. Add the components in the order and amounts specified to a 50 mL RO H_2O.

#	Component	Amount [mg]	Final Concentration [mM]
1	H_3BO_3 (Baker 0084)	286	46
2	$MnCl_2 \cdot 4H_2O$ (Baker 2540)	181	9
3	$ZnSO_4 \cdot 7H_2O$ (Sigma Z 0251)	22	0.77
4	$Na_2MoO_4 \cdot 2H_2O$ (J.T. Baker 3764)	39	1.6
5	$CuSO_4 \cdot 5H_2O$ (MCIB 3M11)	7.9	0.3
6	$Co(NO_3)_2 \cdot 6H_2O$ (Mallinckroft 4544)	4.94	0.17

D. PBR Preparation and Inoculation

Reactor Preparation:

1. Wash the reactor with distilled water and soup to make sure the glass is clean.
2. Rinse the reactor multiple times with dH_2O to remove all soup.
3. Place the head plate back on the reactor and tighten it by hand.
4. Place all components back into the reactor in their dedicated holes in the head plate. The components include the condenser, level sensor, temperature probe housing tube, sparger, sample port, harvest port, make-up water port, light meter housing tube, DO meter, and pH probe (calibrate the pH probe before inserting it into the reactor).
5. Fill the reactor with four liters of media.
6. Ensure all openings are tightly closed.
7. Keep two opening only loosely wrapped with aluminum foil to avoid pressure build-up when autoclaving.
8. Fill the water jacket, half the capacity, with distilled water. Also, keep one of the openings loosely wrapped with aluminum foil.
9. Safely transfer the bioreactor to the autoclave, and start the autoclave cycle.
10. When the autoclave is done, safely remove the bioreactor and let it cool down.
11. Connect all probes to the control unit, place the light meter and temperature probe into their designated spaces, and set the motor on the agitator.
12. Start the agitator, temperature control, and set the aeration rate to 1 LPM (10% CO_2).
13. Place the light jacket around the reactor and turn on LEDs to the desired intensity.

Inoculation Procedure:

1. Measure the biomass concentration of the inoculum in the glass bottles. The inoculum should be active (during the exponential growth phase).
2. Use the following equation to calculate the required volume for inoculation:

$$V_{inoculum}C_{inoculum} = V_{PBR}C_{PBR}$$

where,

$V_{inoculum}$: the volume of inoculum needed to start the cultivation process.

V_{PBR}: the total volume of the PBR in use. It is equal to 5L in our experiments.

C_{PBR}: desired initial biomass concentration in the bioreactor.

$C_{inoculum}$: biomass concentration of the inoculum cell culture.

3. Use a peristaltic pump to transfer the algae from the growth bottle to the reactor through the make-up water port.
4. Top off the reactor to 5L with sterile media.
5. Connect the sterile make-up water to the assigned pump, and calibrate the level sensor.
6. Ensure proper connection of all ports and sensors.
7. The cultivation cycle has started—sample as needed.

E. Sampling Procedure

1. Push air through a 0.2 µm hydrophobic filter into the sampling port to remove any microalgae staggered in the sampling port. Repeat the step twice.
2. Using a sterile 50 mL syringe, withdraw 15 mL sample from the culture.
3. Push filtered air to send excess liquid into the reactor.
4. Close the sampling port, and wipe with 70% alcohol to sanitize.
5. Transfer the sample from the syringe to a 50 mL test tube.

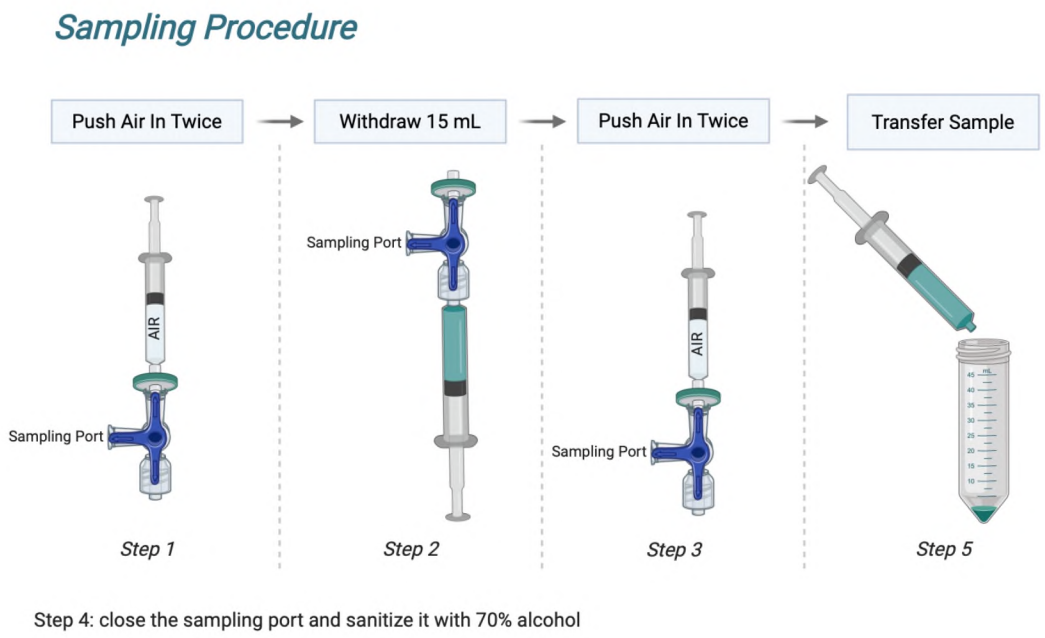

Figure 7-1: Sampling Procedure

F. Light Sensor Arduino Code and Wiring Diagram

LightSensor

```
int LS_1;
int LS_2;
void setup() {
  // put your setup code here, to run once:
Serial.begin(9600);
}

void loop() {
  // put your main code here, to run repeatedly:
LS_1 = analogRead(A1);
LS_2 = analogRead(A2);

Serial.print(LS_1);
Serial.print("    ");
Serial.println(LS_2);

delay(500);
}
```

Figure 7-2: Screenshot of Light Sensor Arduino Code.

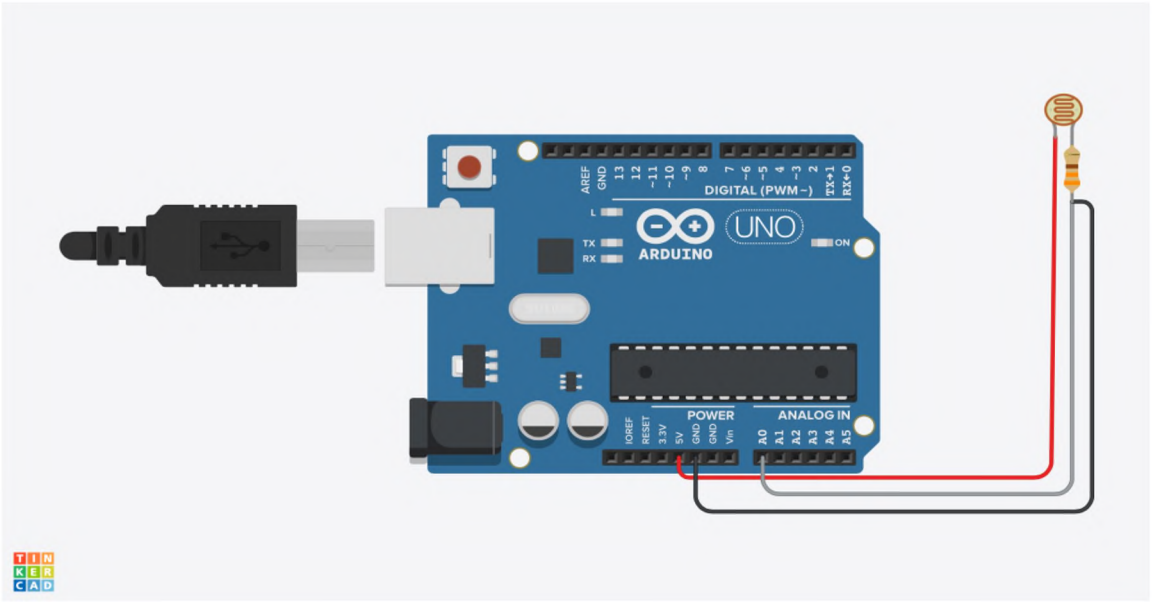

Figure 7-3: Light Sensor Wiring Diagram

G. Absorption to Biomass Concentration Calibration Curves

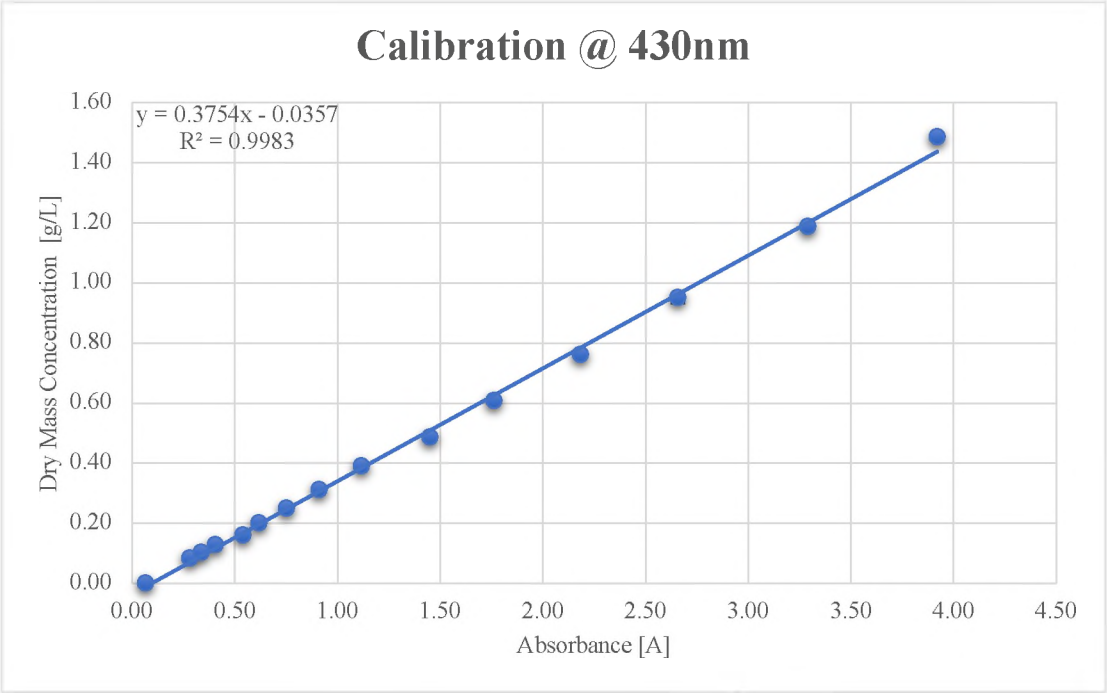

Figure 7-4: Biomass Calibration Curve @ 430nm

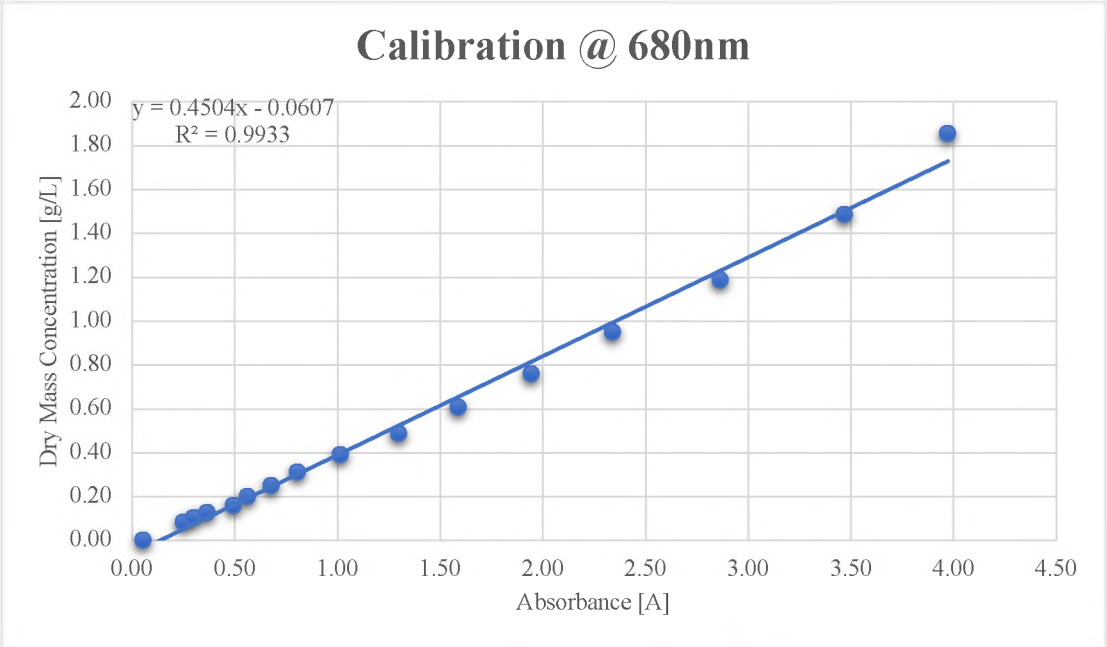

Figure 7-5: Biomass Calibration Curve @ 680nm

H. MATLAB Code: Cell Counting and Size Distribution Curves

```
1. clear,clc
2.
3. global Title
4. Title = 'PBR.LDC24-0.02.02';
5. DF = 1; % Dilution Factor
```

```
6.
7.  % Image Importing
8.  Im1 = 'PBR.LDC24-0.02.02.S1.bmp';
9.  Im2 = 'PBR.LDC24-0.02.02.S2.bmp';
10. Im3 = 'PBR.LDC24-0.02.02.S3.bmp';
11. Im4 = 'PBR.LDC24-0.02.02.S4.bmp';
12. Im5 = 'PBR.LDC24-0.02.02.S5.bmp';
13.
14. % Image Reading
15. I1 = imread(Im1);
16. I2 = imread(Im2);
17. I3 = imread(Im3);
18. I4 = imread(Im4);
19. I5 = imread(Im5);
20.
21. % Cell Counting: Circle Detection: I1
22. figure('Name',Im1,'NumberTitle','off');
23. imshow(I1);
24. imshowpair(I1,I1,'Montage')
25.
26. [centers1, radii1, metric1] = imfindcircles(I1,[2
    25],'ObjectPolarity','bright','EdgeThreshold',0.35);
27. viscircles(centers1, radii1, 'EdgeColor','b');
28.
29. % Cell Counting: Circle Detection: I2
30. figure('Name',Im2,'NumberTitle','off');
31. imshow(I2);
32. imshowpair(I2,I2,'Montage')
33.
34. [centers2, radii2, metric2] = imfindcircles(I2,[2
    25],'ObjectPolarity','bright','EdgeThreshold',0.35);
35. viscircles(centers2, radii2, 'EdgeColor','b');
36.
37. % Cell Counting: Circle Detection: I1
38. figure('Name',Im3,'NumberTitle','off');
39. imshow(I3);
40. imshowpair(I3,I3,'Montage')
41.
42. [centers3, radii3, metric3] = imfindcircles(I3,[2
    25],'ObjectPolarity','bright','EdgeThreshold',0.35);
43. viscircles(centers3, radii3, 'EdgeColor','b');
44.
45. % Cell Counting: Circle Detection: I1
46. figure('Name',Im4,'NumberTitle','off');
47. imshow(I4);
48. imshowpair(I4,I4,'Montage')
```

```
49.
50. [centers4, radii4, metric4] = imfindcircles(I4,[2
    25],'ObjectPolarity','bright','EdgeThreshold',0.35);
51. viscircles(centers4, radii4, 'EdgeColor','b');
52.
53. % Cell Counting: Circle Detection: I1
54. figure('Name',Im5,'NumberTitle','off');
55. imshow(I5);
56. imshowpair(I5,I5,'Montage')
57.
58. [centers5, radii5, metric5] = imfindcircles(I5,[2
    25],'ObjectPolarity','bright','EdgeThreshold',0.35);
59. viscircles(centers5, radii5, 'EdgeColor','b');
60.
61. figure('Name','Diameter Distribution','NumberTitle','off');
62. Diameter = 2.*[radii1;radii2;radii3;radii4;radii5] .* (50/310);
63. DistributionFit(Diameter)
64. axis([0 inf 0 inf])
65.
66.
67. % Cell Concentration
68.
69. count1 = length(centers1);
70. count2 = length(centers2);
71. count3 = length(centers3);
72. count4 = length(centers4);
73. count5 = length(centers5);
74. count = DF .* [count1 count2 count3 count4 count5];
75.
76. V_grid = 4*10^-6; %mL
77.
78. conc = count./V_grid; % Cells/mL
79.
80. Avg = mean(conc);
81. STDEV = std(conc);
82.
83. fprintf(' Cell concentration is %5.2e ± %5.2e \n',Avg,STDEV)
```

I. Light Intensity Profiles

The following figures represent the measured light intensity profiles at 2.3 cm from the PBR surface and the modeled I_{avg} using Eq. 2.6.

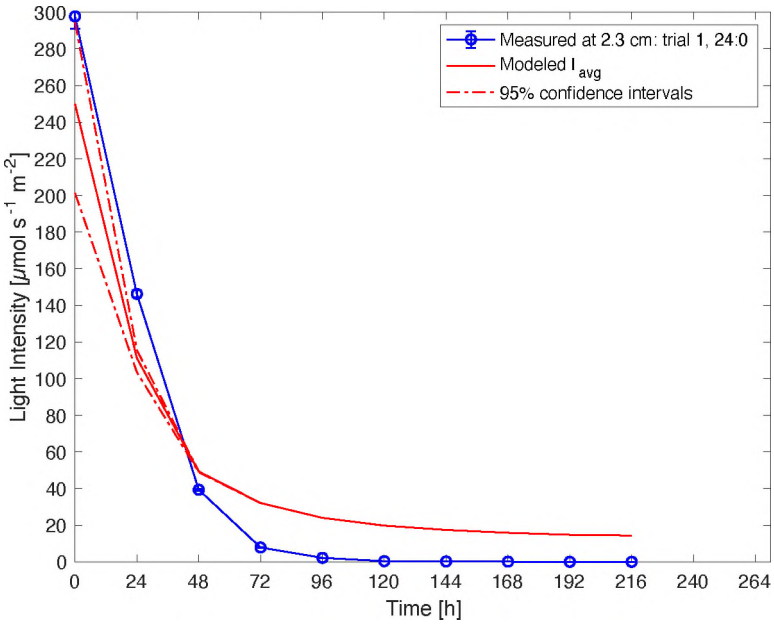

Figure 7-6: Light profile for experiment 24:0, trial 1.

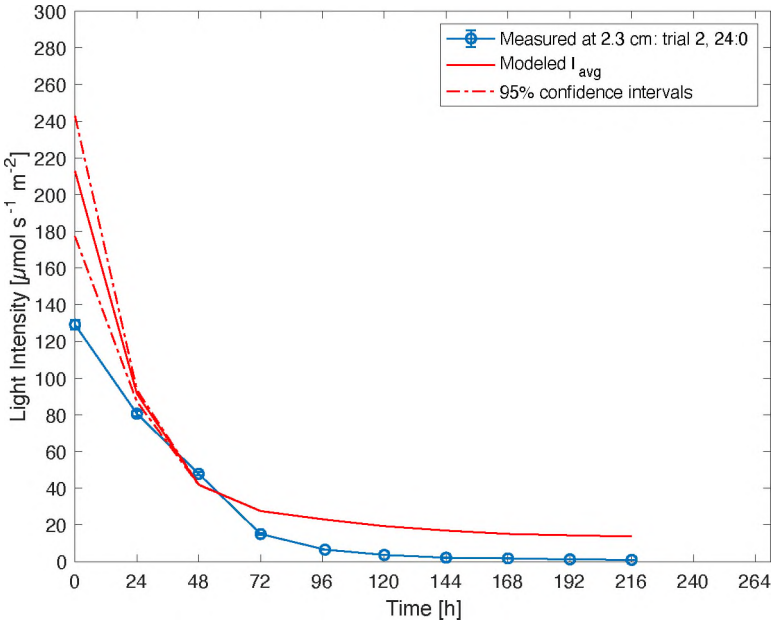

Figure 7-7: Light profile for experiment 24:0, trial 2.

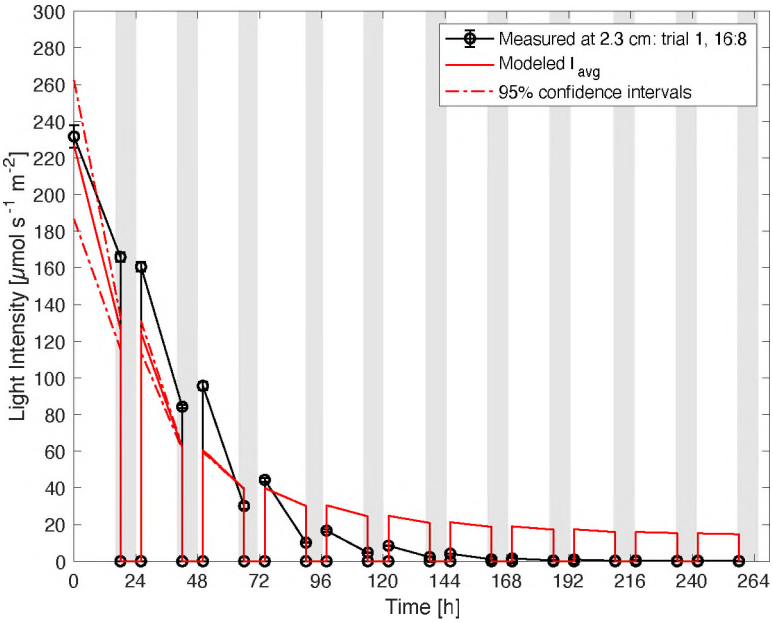

Figure 7-8: Light profile for experiment 16:8, trial 1.

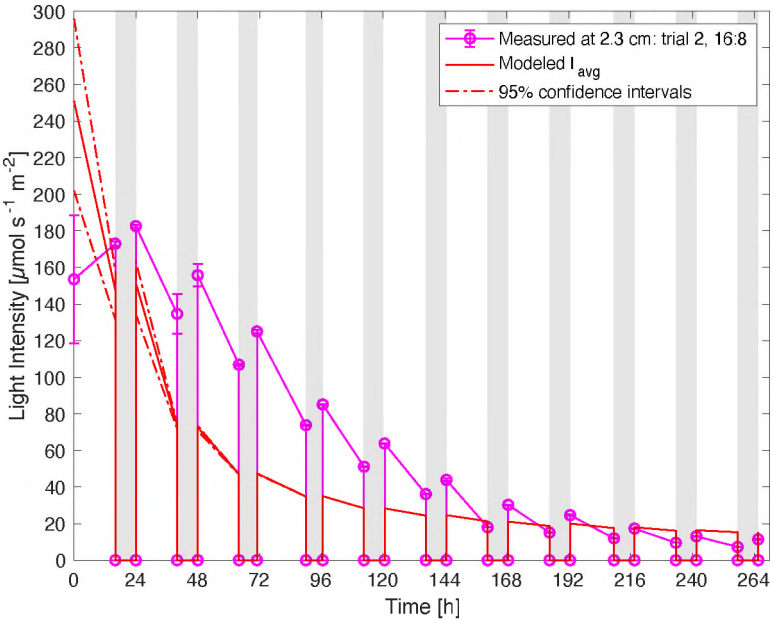

Figure 7-9: Light profile for experiment 16:8, trial 2.

J. pH Profiles

pH profiles for both trials of all experiments are presented in the following figures.

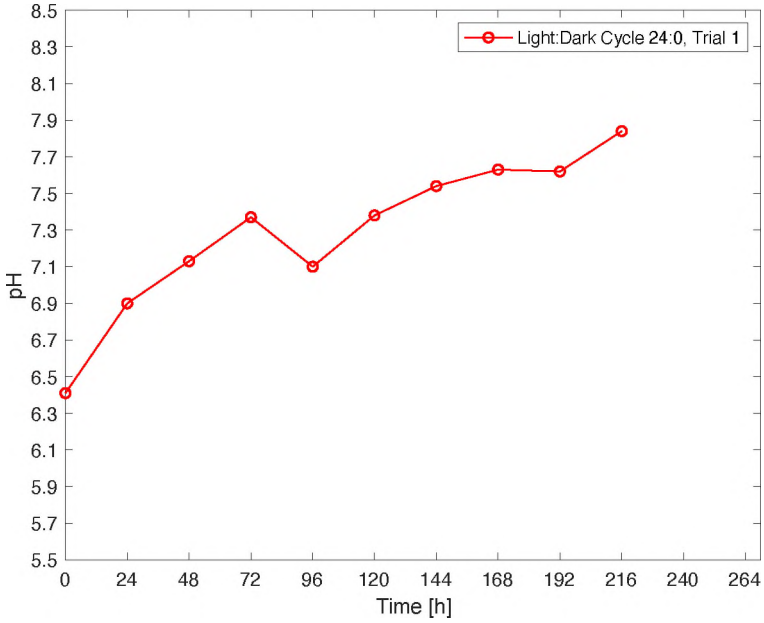

Figure 7-10: pH profile of experiment 24:0, trial 1.

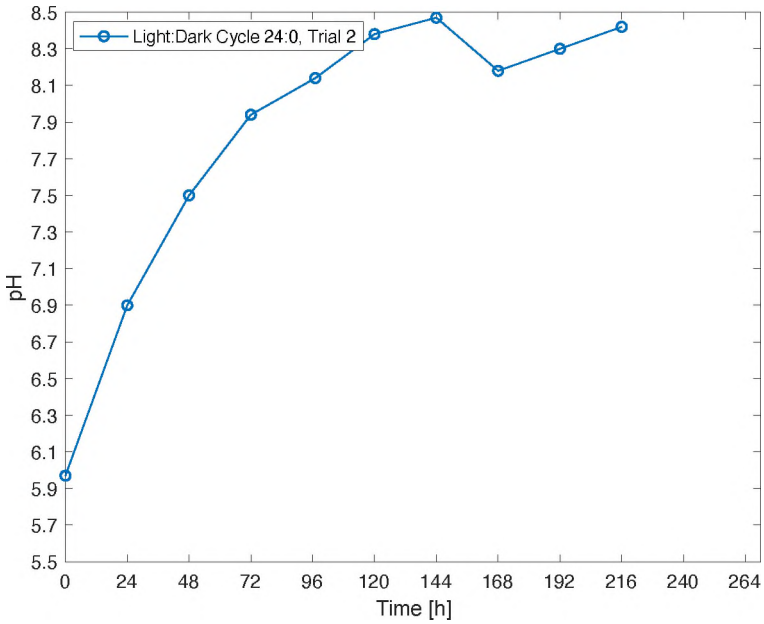

Figure 7-11:pH profile of experiment 24:0, trial 2.

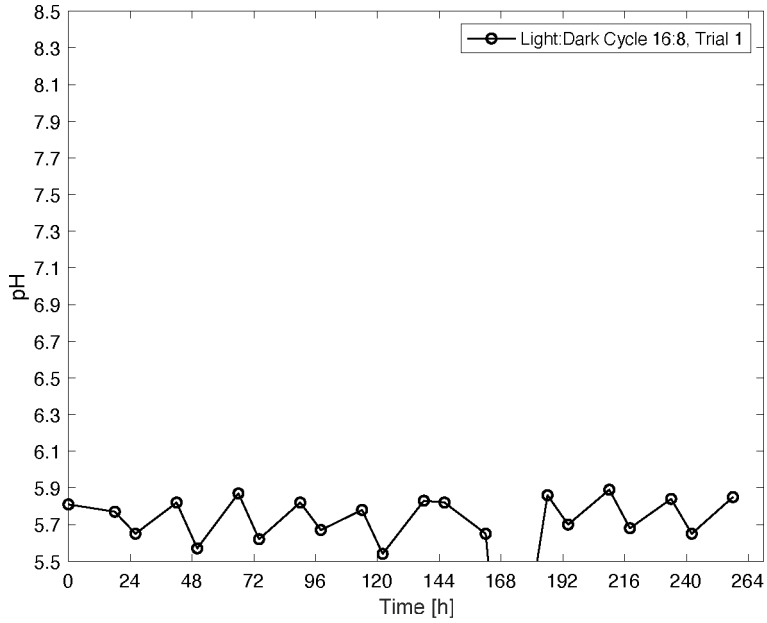

Figure 7-12: pH profile of experiment 16:8, trial 1.

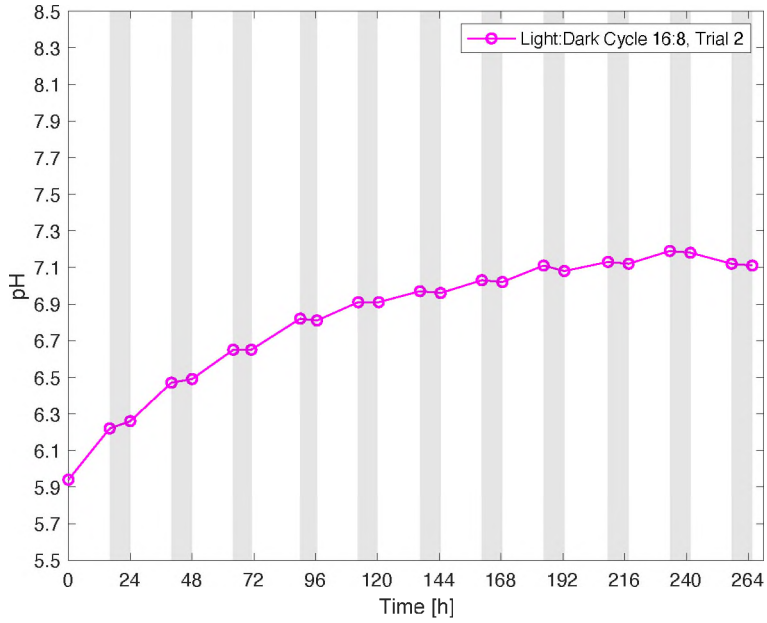

Figure 7-13: pH profile of experiment 16:8, trial 2.

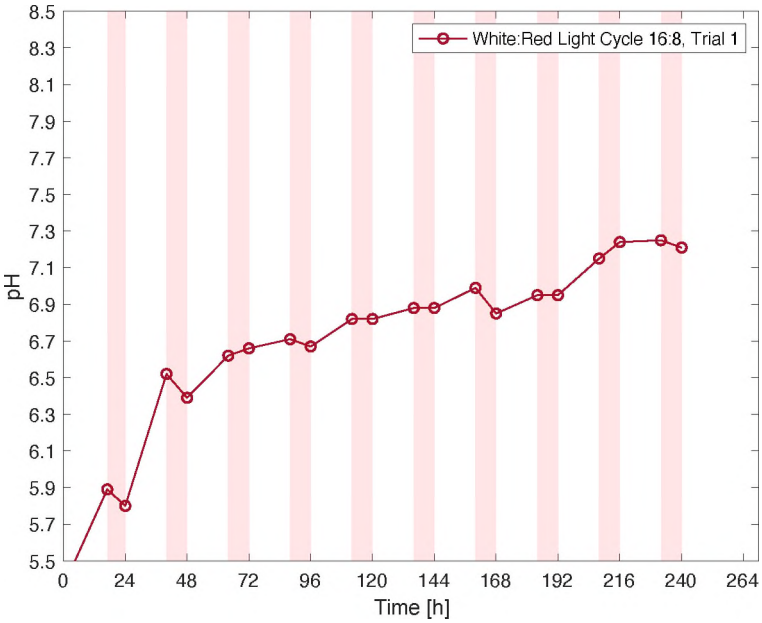

Figure 7-14: pH profile of experiment 16:8red, trial 1.

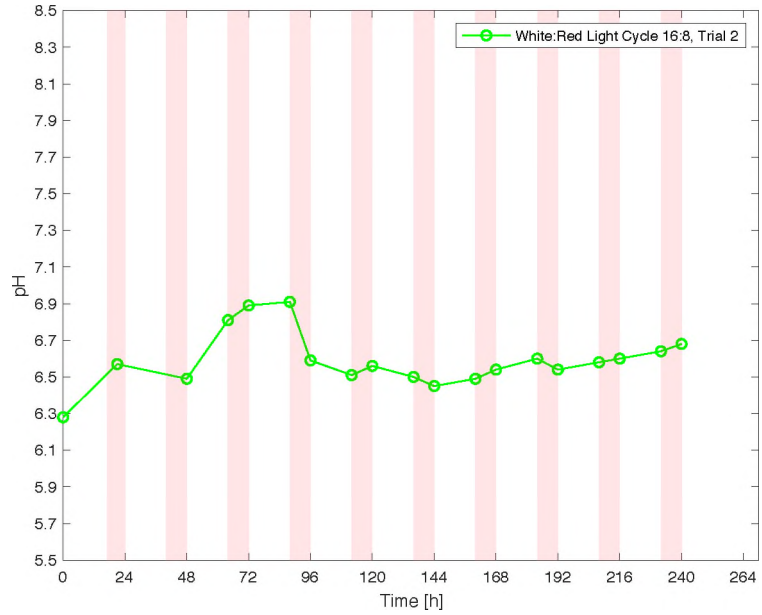

Figure 7-15: pH profile of experiment 16:8red, trial 2.

K. Nitrate Ion Profiles

Nitrate concentration was only measured for the 16:8red experiments, shown in the following figures.

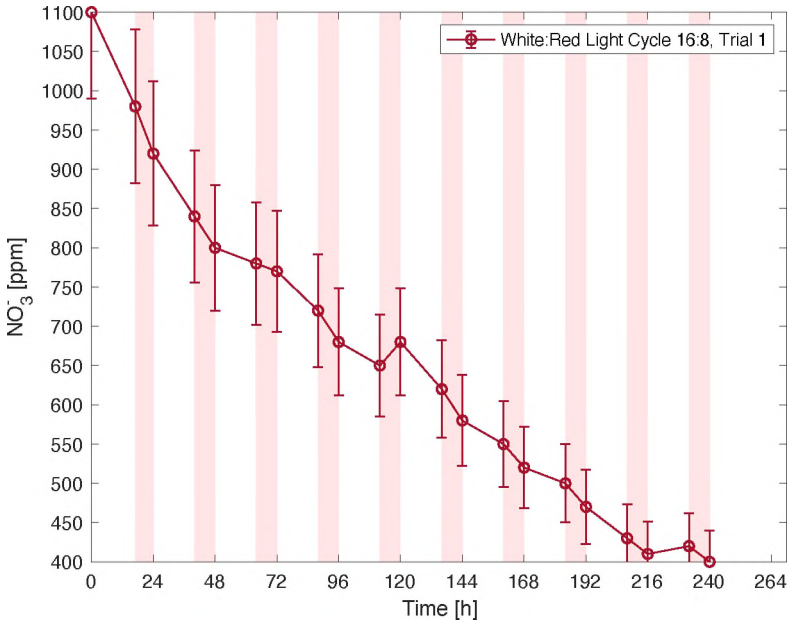

Figure 7-16: Nitrate concentration profile for experiment 16:8red, trial 1.

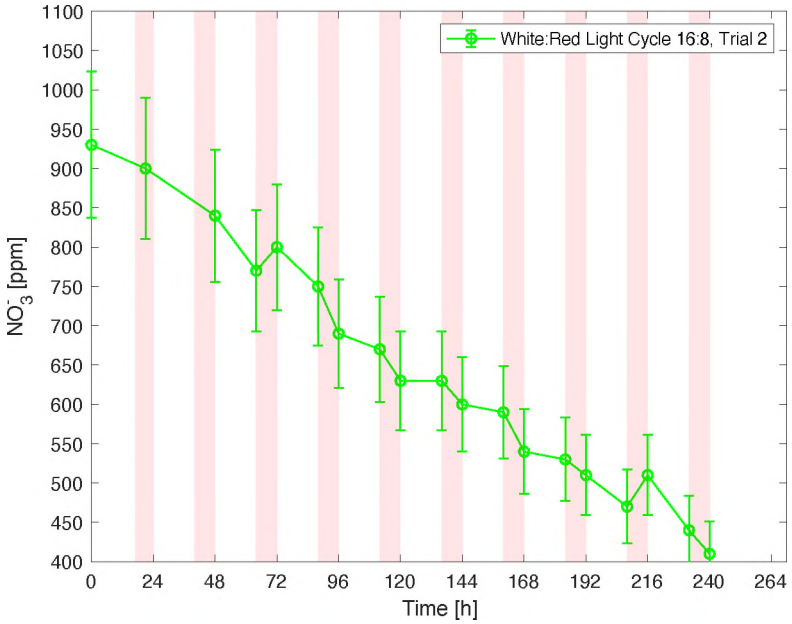

Figure 7-17: Nitrate concentration profile for experiment 16:8red, trial 2.

L. Parameters Sensitivity Analysis

Simulink sensitivity analysis toolbox was used to quantify the effect of the model parameters on the model output. In this sensitivity study, the model parameters ($K_g, \mu_m, and\ k_L$) were varied within a range of the estimated values, and the effect on the final value of the model output (biomass concentration [g/L]) was recorded. One thousand combinations of the three parameters were randomly generated using Monte Carlo method and a uniform probability for a ±10% range around the estimated value of each parameter. The final value of the output of the model followed a normal distribution with a mean of 1.4 [g/L] and a standard deviation of 0.1 [g/L]. In other words, assuming a 10% error in the estimated model parameters, the model predicts, with 95% confidence, that the final biomass concentration will fall in the range of 1.2 - 1.6 [g/L] after nine days of cultivation under a continuous illumination condition (300 μmol s^{-1} m^{-2} surface intensity). The model is not very sensitive to small changes in parameters values, from which we can infer a robust model. Figure 7-18 shows scatter plots for the values of the varied parameters $K_g, k_L,$ $and\ \mu_m$ (x-axis) from left to right, and their effect on the model output (y-axis). The histogram illustrates the probability distribution of the model outcome with the density on the x-axis and the model final value in [g/L] on the y-axis.

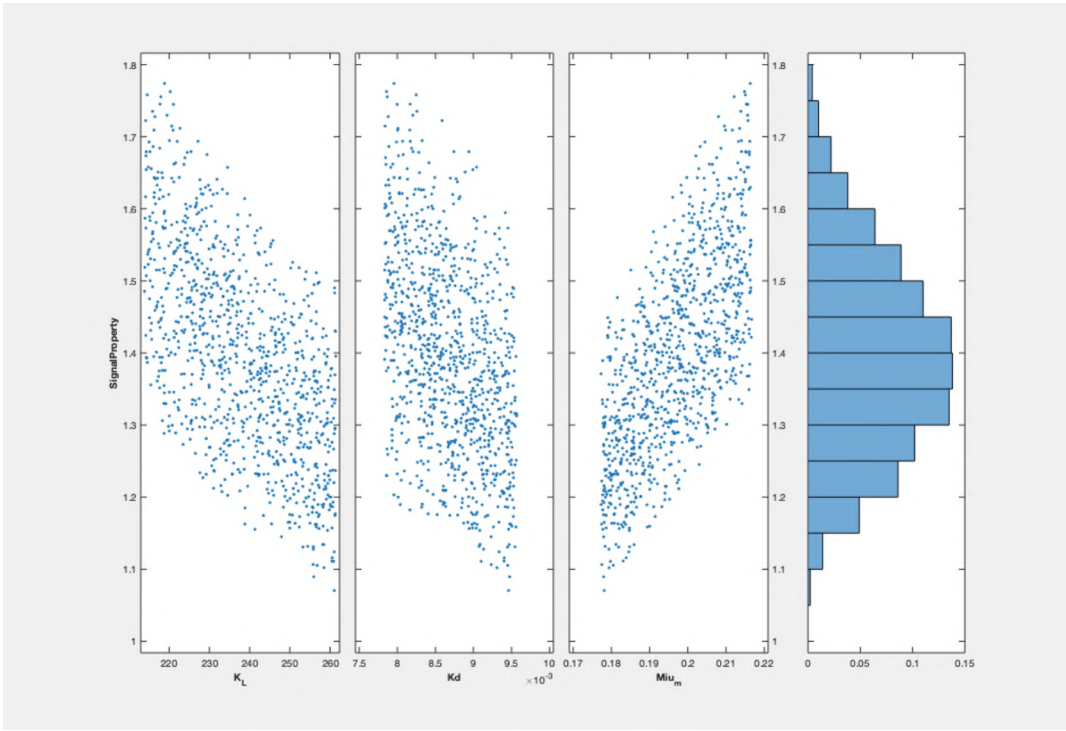

Figure 7-18: Sensitivity analysis illustrates parameter influence on the model output.